Aus der Abteilung für Neonatologie und pädiatrische Intensivmedizin
(Leiter Univ. - Prof. Dr. Matthias Heckmann)
der Klinik und Poliklinik für Kinder- und Jugendmedizin
(Geschäftsführender Direktor: Univ.- Prof. Dr. Holger Lode)
der Universitätsmedizin der Ernst-Moritz-Arndt-Universität Greifswald

A sex based study on hyperoxia induced white matter damage in the developing brain: Effect of estrogen and Fetal Zone Steroids on oligodendrocyte precursor cells.

Inaugural – Dissertation

zur

Erlangung des akademischen

Grades

**Doktor der Wissenschaften in der Medizin
(Dr. rer. med.)**

der
Universitätsmedizin
der
Ernst-Moritz-Arndt-Universität
Greifswald

2019

vorgelegt von:
Donna Elizabeth Sunny
geb. am: 19.03.1986
in: Neeloor, Kerala, India

Dekan: Prof. Dr. med. Karlhans Endlich

1. Gutachter: Prof. Dr. M. Heckmann

2. Gutachter: Frau Prof. Dr. G. Rune

Ort, Raum: Greifswald, Conference Room - Department of Neurology/Neurosurgery.

Tag der Disputation: 23.03.2020

If you have faith as a grain of mustard seed, you will say to your mountain, "MOVE!" and it WILL move... and NOTHING will be impossible for YOU!

- Matthew 17:20

TABLE OF CONTENTS

LIST OF FIGURES

LIST OF TABLES

ABBREVIATIONS

°C	Degree Celsius
µg	Microgram = 10^{-6} Gram
µl	Microliter = 10^{-6} Liter
16OH-DHEA	5-Androsten-3β, 16α-diol-17-on; 16α-Hydroxy Dehydroepiandrosterone
Adiol	5-Androsten-3β, 17β-diol; Androstendiol
Androstentetrol	5-Androsten-3β,16α,17β,18-tetrol
APS	Ammonium persulfate
bFGF	Basic Fibroblast growth factor
BSA	Bovine serum albumin
cDNA	Complementary DNA
CNPase	2',3'-Cyclic-nucleotide 3'-phosphodiesterase
DAPI	4'6-diamidino-2-phenylindile
DHEA	Dehydroepiandrosterone
DHEAS	Dehydroepiandrosterone- Sulfate
DMEM	Dulbecco's Modified Eagle Medium
DMSO	Dimethylsulfoxide
DNA	Deoxyribonucleic acid
E2	17β-Estradiol
EDTA	Ethylenediamine tetraacetate
EGF	Epidermal growth factor
ER	Estrogen receptor
FACS	Flow associated cell sorting
FCS	Fetal calf serum
G	Gravitation force g (9,897 m/s2)
GAPDH	Glyceraldehyde 3-phosphate dehydrogenase
H	hours
HBSS	Hank's Balanced Salt Solution
HEPES	Hydroxyethyl piperazine N'-2-ethane sulfonic acid
HRP	Horse radish peroxidase
HSA	Human Serum Albumin
ICI	ICI 182,780 (Fulvestrant)
kDa	Kilo Dalton = 10^3 Dalton
M	Molar
MAG	Myelin associated glycoprotein
Mg	Milligram = 10^{-3} Gram
Min	Minutes
Ml	Milliliter = 10^{-3} Liter
mM	Millimolar
mRNA	Messenger RNA
MW	Molecular weight
Ng	Nanogram = 10^{-9} Gram
Nm	Nanometer = 10^{-9} Meter
NGS	Normal Goat Serum
OL	Oligodendrocyte
OPC	Oligodendrocyte Precursor Cell
PBS	Phosphate buffered saline
PCR	Polymerase chain reaction

PDGFRα+	Platelet-derived growth factor receptor α-positive
PFA	Paraformaldehyde
PI	Propidiumiodide
PMSF	Phenylmethylsulphonyl fluoride
PVL	Periventricular Leukomalacia
RNA	Ribonucleic acid
ROS	Reactive oxygen species
Rpm	Revolutions per minute
RT	Room temperature
SD	Standard deviation
SDS	Sodium deodecyl sulfate
SEM	Standard error of mean
siRNA	Small interfering RNA
SRY	Sex-determining region Y
TBS	Tris buffer saline
TBST	Tris buffer saline Tween 20
TEMED	Tetramethylethylenediamine
Tris	Trishydroxymethylaminomethane
V	Volt
v/v	Volume/volume
w/v	Weight/volume

1. INTRODUCTION

Oxygen, which is widely used in the neonatal intensive care, has a tremendous impact on the developing brain and is a major factor contributing to white matter damage in the preterm brain[1-4]. This is associated with a clear distinction in the outcome between both the sexes[5, 6]. Male sex has been identified as a major risk factor for poor neurological outcome across multiple studies and steroid hormones have been speculated to be contributing to this difference[7, 8]. Sex is therefore being widely considered as one of the major decisive factors for prognosis and treatment of these infants. But unfortunately we still lack a clear view of the molecular mechanisms that lead to such a profound difference. We have been keenly monitoring these aspects of preterm birth and investigating the adverse effects of hyperoxia on immature glia and other brain cells along with changes in urinary steroid profiles in preterm infants[9-12]. Even though a few recent studies have addressed preterm brain injury in both the sexes separately, studies explaining the effect of oxygen on the development of male and female brains and the effect of steroid hormones are extremely limited. We thought that an understanding of the mechanisms that proceed as a response to oxidative stress and the influence of steroid hormones on these mechanisms, especially in the progenitor cells in the male and female brain will be necessary to design new effective neuroprotective strategies.

In this project, mouse derived primary oligodendrocyte precursor cells isolated and cultured separately from male and female littermates were used. Different concentrations and time regimes of treatment with high oxygen (corresponding to those used in the neonatal intensive care) were tested in order to find an optimum regime that would show the first affected proteins and pathways due to oxidative stress in both the populations. Later, this determined optimum treatment regime was used to treat the cells and monitor the effect on their maturation.

The experimental results showing inhibition of maturation in male cells as an effect of high oxygen along with drastic changes observed in mitochondrial and stress response proteins strongly indicate the need to study cellular responses in both the sexes separately. Regardless of the cell type investigated or the type of insult, the fact that male and female cells can respond differently makes this study important. The presence of inherent differences between the sexes should not be ignored while decoding any cellular mechanism.

The functional finding of Nup133 being a direct upstream regulator of nuclear respiratory factor-1 (Nrf1) reveals a completely novel function of this nucleoporin protein. Nrf1 is an important transcription activator involved in regulating a number of mitochondrial and stress response functions. The involvement of Nup133 in mediating such a response has broad implications because in humans Nup133 is a constitutive cellular protein expressed in a lot of different cell types including a number of cancers. Other than being just a transporter protein, its role in other cellular processes still needs to be studied in detail.

This study also reveals a direct interaction between the estrogen receptor alpha (ERα) and Nup133, opening up another novel regulation that leads to extending the female cells with resistance towards oxidative stress via Nrf1 regulation. Experiments with estradiol and some of the clinically relevant hormone precursor molecules (fetal zone steroids) showed how the estrogen receptor alpha (ERα) along with Nup133 mediates this protective effect in the female cells. Considering that hormone regulations are critical for fetal brain development, we believe that by means of our experimental data we have put forward an explanation to the changes in urinary steroid profiles observed in human preterm infants and their implications.

Taken together, by means of this study we put forward the need for detailed investigations into sex based differences in the steroid hormone profile during fetal development and the role of nucleoporin proteins not only in normal brain development but also under various stress/disease conditions. We believe that changes in these essential cell components could be reasons to some of the observed long term neurological effects in preterm infants.

2. THEORETICAL BACKGROUND

2.1. Preterm birth and PVL

Preterm birth (<37 weeks' gestation) is one of the leading causes of neonatal morbidity and mortality in the world. During the past years, although the incidence of preterm birth has not reduced, the care of preterm neonates has drastically improved so that the survival of those born at even 23 weeks' gestation is now becoming common. However, these babies are at a high risk of severe developmental disability and cerebral palsy. Extreme prematurity is associated with neurological consequences ranging from mild behavioural and cognitive defects to severe disability [13]. Preterm brain injury occurs during a phase of rapid brain development leading to delays in normal maturation. This delay in development after premature birth may arise from a broad range of injuries that can cause significant disruption to ongoing endogenous developmental events in the brain thereby affecting fetal and/or postnatal developmental programs and their normal physiological timing [14]. The main cell types of the brain that are injured by premature birth are oligodendrocytes and oligodendroglial progenitor cells which form the white matter. These cells are particularly sensitive to injury between 24 and 32 weeks' gestation, resulting in white matter injury [15]. The predominant stages of oligodendrocyte lineage cells present in the human brain during this period are the pre-oligodendrocytes and the immature oligodendrocytes, as the mature oligodendrocytes become abundant only after term [16]. The progenitor cells are present in the subventricular zone and from there they migrate into the intermediate zone and cortical plate where they then differentiate into immature and later mature oligodendrocytes, which eventually myelinate axons [17].
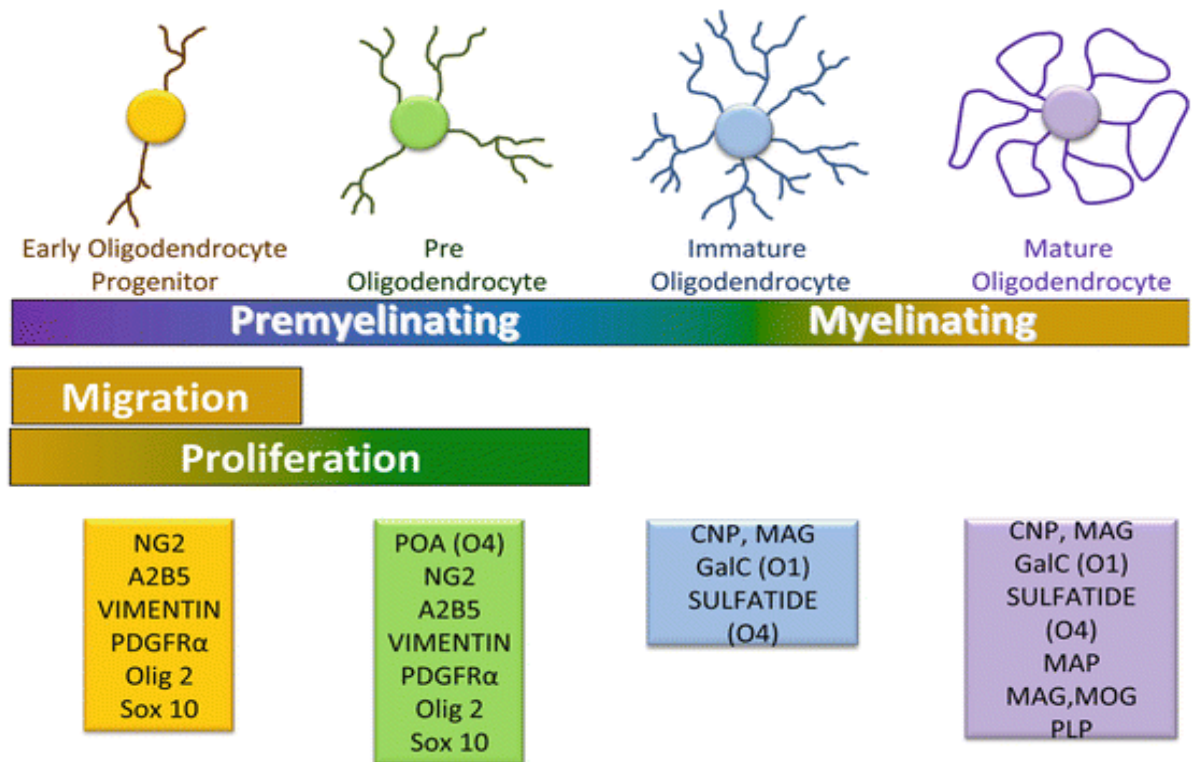
Figure 1.Stages of oligodendrocyte maturation. Figure adopted from Ballabh P. (2014) [150].

Periventricular leukomalacia (PVL) is the predominant underlying pathology of cerebral palsy and cognitive impairment in premature infants and is the most common form of white matter injury in preterm infants resulting in a chronic disturbance of myelination. PVL has its peak incidence in premature infants during 23–32 weeks postconceptional age which is a critical period in human brain development, characterized by extensive oligodendrocyte migration and maturation [18]. It is characterized by mainly two components: a focal necrotic component with loss of all cellular elements in the deep periventricular white matter leading to cystic PVL and a diffused cell-specific lesion with acute loss of developing oligodendrocytes accompanied by astrogliosis, and microgliosis leading to diffused white matter injury.
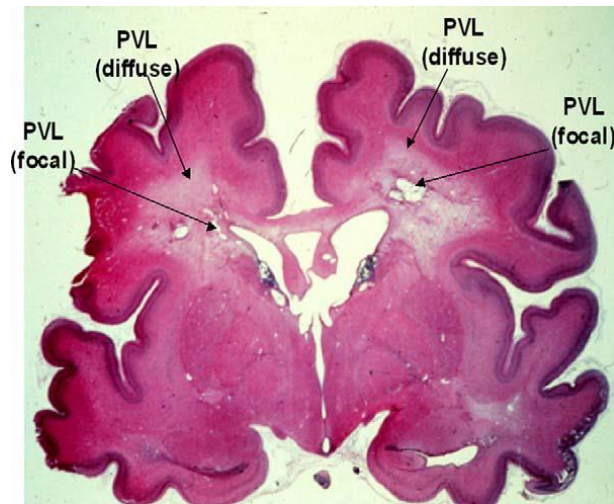
Figure 2. Periventricular leukomalacia. Coronal section of cerebrum (H + E stain) in a premature infant who died several weeks after a cardiac arrest. Note the two components of the lesion (i.e., deep focal areas of cystic necrosis and more diffuse cerebral white matter injury). Figure adopted from Volpe, J. J et al 2011.

Non-cystic periventricular leukomalacia has been now reported in most infants born with a birth weight under 1500 g whereas the incidence of cystic periventricular leukomalacia has decreased over the years [19]. Various studies in postmortem human brain have thrown light into the cellular and anatomical abnormalities associated with diffuse WMI. These studies observed hypomyelination in premature WMI which was associated with a delayed or disrupted developmental program of oligodendrocyte (OL) lineage cells; in particular OL progenitor cells (OPCs) [20]. Under normal developmental conditions, OPCs give rise to the mature oligodendrocytes that myelinate axons. In postmortem human brain, arrested maturation of O4+ preOLs was observed, together with expansion of the cellular pool of early OL progenitors and preOLs [21].

2.2. Hyperoxia and PVL

Preterm infants are in most cases born with immature lungs. They are therefore, frequently exposed to increased oxidative stress as they need supplemental oxygen often for a long period of time [22]. Hence, oxygen is widely used in resuscitation and treatment of neonatal lung diseases. Apart from oxygen being used in the neonatal intensive care, preterm birth itself leads to an exposure to relative hyperoxia resulting from a dramatic rise of oxygen tissue tension at a much earlier developmental phase when compared to intrauterine conditions [4]. It is now known that hyperoxia may induce damage in immature lungs and retina

5

and it has been implicated in the pathogenesis of bronchopulmonary dysplasia and retinopathy of prematurity [22].

Animal and cell culture studies have shown that hyperoxia is a powerful trigger for widespread apoptotic neuronal death in the developing brain. An increase in the density of degenerating cells was observed in various brain regions of 7-day-old Wistar rats and C57/BL6 mice such as the caudate nucleus, layers II and IV of the frontal, parietal, cingulate, and retrosplenial cortices, as well as white matter tracts and the periventricular region after hyperoxia [2]. This cell death was observed to be associated with oxidative stress, decreased expression of neurotrophins, decreased activation of neurotrophin-regulated pathways, and increased levels of proinflammatory cytokines [23]. Hyperoxia also initiated the apoptotic cascade in immature OLs and preoligodendroglial cells, but not in mature OLs in vitro. Vulnerability to oxygen-induced cell death has been found to be age dependent with a maximum during the first week of life in both OL cell cultures and animals [24].
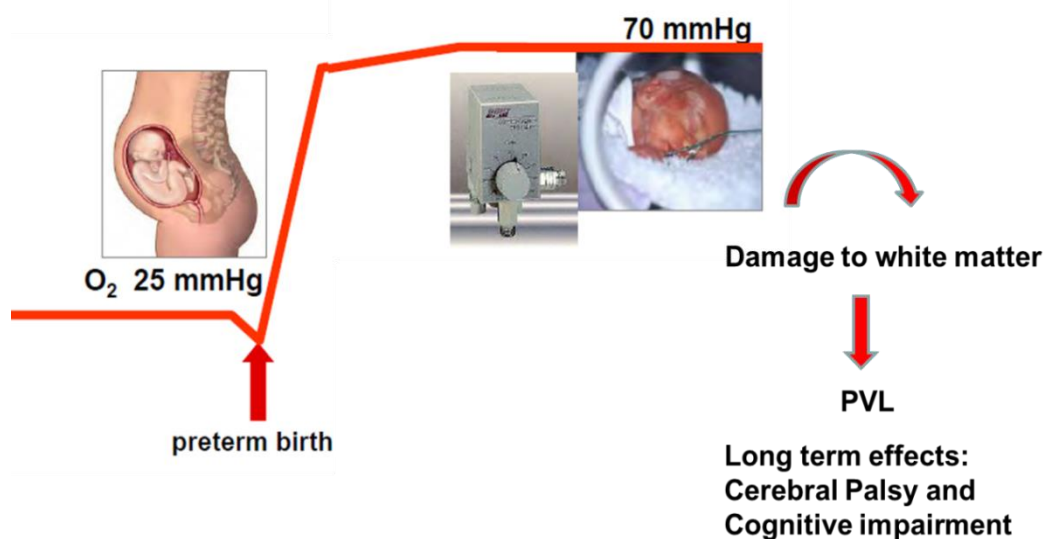
Figure 3. Showing the effect of hyperoxia on preterm infants. Figure adopted and modified from Collins MP, 2001

However, the influence of oxygen on the human brain is still not completely understood. Previous reports have mentioned that even a hyperoxic exposure during a few minutes after birth may increase the oxidative stress for weeks. Because oxidative stress influences apoptosis and cell death, this may have long-term consequences on growth and development [25].

2.3. Sex difference in clinical outcome

It has been a general belief based on observations that females have a better outcome after preterm birth. However, now there are accumulating evidences that females indeed have an advantage over males with a better outcome in the perinatal period, particularly after preterm birth. As a result of various studies focused on gender differences, it is now well known that there is a higher death rate of male foetuses, an increase of about 30% in chromosomally normal spontaneous abortions (i.e. significantly higher than at birth) as compared to female foetuses. The gender difference seems to persist throughout life, especially regarding age-related degenerative changes in the brain. A statistical analysis from Sweden showed that boys are more likely to be delivered prematurely, accounting for 55–60% of all new-borns between 23 and 32 gestational weeks. Also, neonatal deaths in these gestational weeks were observed to be more common among boys. The difference in infant mortality (within 1 year) was found to be the most pronounced at extremely early birth (23–24 gestational weeks), being 60% for boys compared with 38% for girls [6]. Extremely preterm and extremely low birth weight (ELBW) boys appear to be born with a higher constitutional risk for major adverse neurodevelopmental outcomes than girls. Previous studies of mortality, in-hospital morbidity, and neurodevelopmental outcomes have established a distinct male disadvantage for extremely-low-birthweight (ELBW) and extremely preterm infants. However, male gender remains an independent risk factor for adverse neurodevelopmental outcomes [5]. Another study that evaluated the effects of intrauterine growth restriction (IUGR) and very preterm birth on cognitive outcomes, found that children born very preterm after IUGR have an increased risk of cognitive impairment compared with children delivered very preterm and that the differences in cognitive outcome were restricted to boys who may have been especially vulnerable to the influence of IUGR and very preterm birth. It was however not clear why gender may influence cognitive outcome in very preterm infants with IUGR [26].

Taken together, it can be said that the explanation for neurodevelopmental differences between males and females is unknown. Although, gender differences originate from a very early period after conception, the exact mechanisms responsible for the continued differences later in life remain still to be determined. As it is very evident, risk factors for poor neurological outcomes have been identified across multiple studies and the increased risk has been found to be independently associated with male sex. Hyperoxia being one of the major risk factors for poor neurodevelopmental outcome as a result of preterm birth and combining this with the fact that it is in turn associated with male susceptibility, it becomes utmost

important to identify the underlying mechanisms and biology. Male susceptibility arouses interest particularly because it implies that there may be hormonal factors that, if better understood, might open up new avenues in neuroprotective strategies [7].

2.4. Steroid hormones and Fetal Zone Steroids

2.4.1 Estrogen

During pregnancy, due to the placental aromatization of C-19 steroids produced by fetal adrenal glands, the levels of maternal 17β-estradiol (E2) levels in the plasma increases up to 100-fold (15,000pg/mL, approximately 55nM) as compared to the plasma estrogen concentrations in non-pregnant females [27, 28]. The foetus is also exposed to the increasing hormone levels during its development. But at the time of birth, after the umbilical cord is clamped, E2 level decreases by a factor of 100 (5–35pg/mL, or 20–130pM) within 24 hours. Since premature birth happens at a much earlier stage of development, these infants experience this hormone deprivation and simultaneous increase of the oxygen tissue tension much earlier than infants born at term [29].

The presence of high amounts of estrogen is considered to be critical for normal brain development and several studies have even highlighted that the female sex hormones represent potential neuroprotective agents against acute and chronic injuries in the adult brain. The neuroprotective effects of E2 has been observed in the mature brain in several models of neurotoxicity involving hypoxia-ischemia and excitotoxicity such as Parkinson's and Alzheimer's diseases, as well as cerebral ischemia. It is known that the female steroid hormones can influence the apoptotic cascade at different stages. Estrogens have also been shown to promote survival and differentiation of several neuronal populations maintained in culture [30] and to reduce cell death associated with excitotoxicity [31], oxidative stress [32] or exposure to beta-amyloid [33]. It also has profound effects on the function and plasticity of the brain and proliferation, differentiation, and migration of neurons [24].

E2 and the estrogen receptors (ER) are known to play important roles in the development and function of the central nervous system. Both the estrogen receptors, ER alpha and ER beta are found in various regions of the human and rodent brain, which includes the hypothalamus, hippocampus, cerebral cortex, midbrain, brain-stem, and forebrain. They show specific distributions with high densities especially around the ventricles where the brain cell

progenitors are generated. Therefore, it was intriguing to investigate the role of E2 and its receptors on OPC differentiation, especially under hyperoxia.

2.4.2 Fetal Zone Steroids

In humans, estrogen synthesis during pregnency is largely dependent on androgens from fetal and maternal adrenal glands because the placenta lacks the cytochrome P450 enzyme CYP17 (17a-hydroxylase) which is essential for de novo estrogen synthesis from acetate or cholesterol. The human fetal adrenal cortex is an active endocrine organ that produces steroid hormones, which regulate intrauterine homeostasis and the maturation of the fetal organ system. An active steroidogenic specialized compartment of the fetal adrenal cortex is called the fetal zone whose mass increases in utero up to term and then declines rapidly after birth. During pregnancy, there is a continuous exchange of steroid molecules between the placenta and the fetus as a result of which huge amounts of androgens produced by the fetal zone are used by the placenta for estrogen biosynthesis and therefore, this functional association is termed as the "feto-placental unit" [9, 34, 35].

As a result of preterm birth, the feto-placental unit is disrupted and the synthesis of estrogen and progesterone in the placenta stops. However, the fetal zone of the preterm infant continues to synthesize DHEA which is the main precursor molecule for estrogen synthesis. This DHEA gets converted into more hydrophilic metabolites and these are eventually excreted from the body through urine. Studies have shown that the fetal zone shrinks much slowly in preterm infants as compared to term infants where it rapidly shrinks after birth [36]. Consistent with this observation, it was found that the urinary excretion of 3b-OH-5-ene steroids in preterm born infants was significantly higher for a longer period of time and did not approach that of term infants before 40 weeks postmenstrual age [11]. Additionally, a persistent higher plasma concentration of DHEAS was found in preterm infants from the day of birth until 10 month of age when compared to that of term infants [37].

However, a gender difference does not seem to exist in FZ regression/involution in humans, at least in terms of hormone secretion, given the testicular secretion of androgens in male infants. In one of the studies [38], it was shown that the serum levels of cortisol, dehydroepiandrosterone (DHEA) sulfate (DHEAS), and androstenedione sharply decreased during the first week of life. However, only in males, the androstenedione levels increased as of day 21. Another study reported that the plasma levels of adrenal steroids, with the exception of cortisol, decreased progressively from birth to 6 months of age. The plasma

levels of 17-hydroxyprogesterone, 11-desoxycortisol, and cortisol did not reveal gender differences, whereas testosterone and androstenedione levels were higher in males and DHEAS levels were higher in females [35].

Since, preterm birth is accompanied by a drop in estrogen level and an increase in the levels of these precursor molecules to which the developing brain is normally exposed to, the precise role of these precursor molecules in brain development need to be addressed. If investigated in detail, they might as well prove to be novel neuroprotective agents that can promote cell survival and maturation.
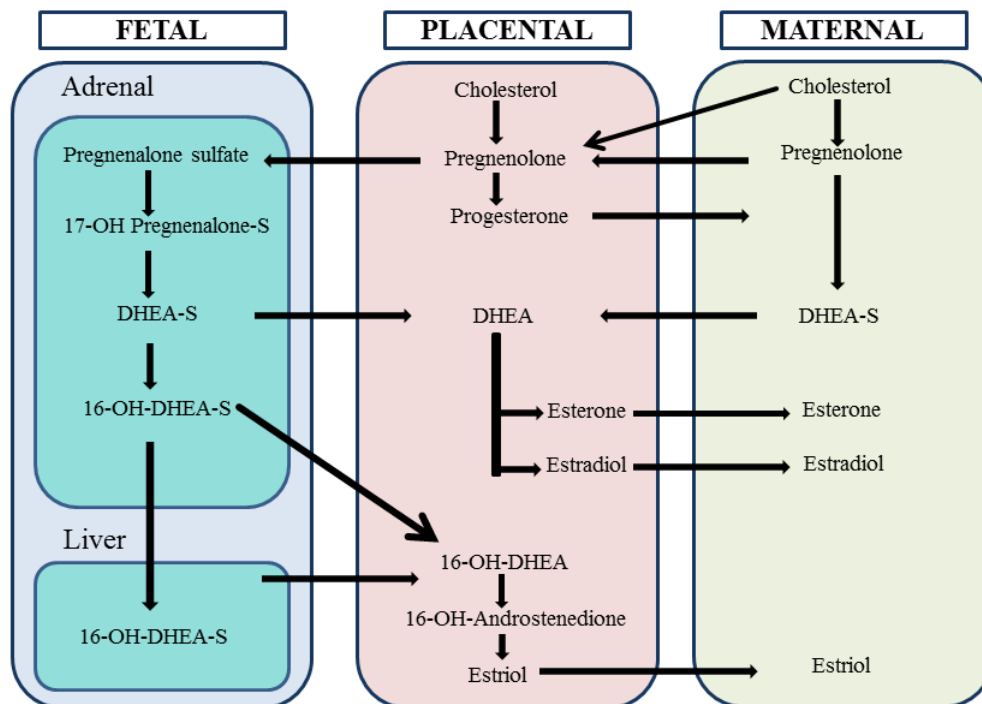
Figure 4. Estrogen and progesterone synthesis in the fetal, placental and maternal compartments.

a) 16a-OH-DHEA

Dehydroepiandrosterone sulfate (DHEAS) is the main steroid molecule produced by the fetal zone. Its production starts at around 8–10 weeks of gestation and later it increases to 100–200 mg per day until term. In the fetal lever, a part of the fetal DHEAS produced is hydroxylated to form 16a-hydroxy-dehydroepiandrosterone sulfate (16a-OH-DHEAS) and both these compounds are required for estrogen synthesis in the placenta. Being the precursors for placental estrogen synthesis, FZSs are structurally related to estrogens and thus can interact with the ERs [39]. For example, dehydroepiandrosterone (DHEA) and DHEAS and its

metabolites, 5-androsten-3b, 17b-diol [androstenediol (Adiol)], and 5-androsten-3b, 16a-diol-17-one [16ahydroxy- DHEA (16OH-DHEA)] are potent activators or agonists of ER-alpha and/or ER-beta. [10]. Regarding the presence of DHEA in the brain, previous reports have mentioned that higher concentrations of DHEA is found in the brain as compared to plasma and that the brain is capable of de novo synthesis of DHEA and DHEAS [40]. However, the precise role of 16a-OH-DHEA in oligodendrocyte differentiation has not been addressed so far.

b) Allopregnanalone

During pregnancy, in addition to estrogen, progesterone (PROG) is synthesized in increasing concentrations in the placenta until term which then dramatically reduces to neonatal serum levels after birth. Allopregnanolone (ALLO) is a progesterone derivative that has been studied in the greatest detail. It is initially produced by the placenta and later the brain. It has been reported that ALLO reduces cell death, increases cell proliferation and promotes myelination [41-43], making it an excellent candidate for treating preterm brain injury. As a consequence of preterm birth, infants are withdrawn prematurely from placentally-derived steroids such as ALLO, which may enhance the risk for cerebral injury. Since the levels of ALLO peaks just prior to delivery, it has been suggested to possibly play a role as an endogenous neuroprotective agent for the developing brain [44]. Studies in several animal models have reported that ALLO reduces apoptosis following in utero hypoxia–ischemia [45-47], it also limits apoptosis and neurite outgrowth while promoting myelination [48] and that it can protect developing neurons and glia from injury [48, 49]. However, the underlying mechanisms are largely unknown. Despite these pre-clinical findings, there is not much data available regarding the ALLO levels in human new-borns and data correlating ALLO levels with neurological outcomes, especially in the most preterm infants (<28 weeks gestation) who are deprived of ALLO much earlier than normal [14].

c) Adiol

5-Androstene-3β, 17β-diol (Adiol) is a major natural metabolite of dehydroepiandrosterone (DHEA) that acts as an intermediate in testosterone and estrogen synthesis. It is a member of the 5-androstene family of endogenous steroids and can activate ER-α and/or ER-ß [50-52]. Additionally, intracellular aromatases (CYP19) present in the brain can convert it into more estrogenic molecules exerting an even stronger effect on ERs. It is reported to bind to the androgen receptor (AR) and to influence sexual development and behaviour in several mammals. A number of studies have reported various therapeutic properties of Adiol,

including anti-inflammatory [53-56], anti-apoptotic [57] and neuroprotective activities in an experimental auto-immune encephalomyelitis model of multiple sclerosis [58, 59]. Adiol is also capable of modulating the action of gamma-amino butyric acid A (GABAA) receptors in the brain and is reported to have anticonvulsant and analgesic properties. It has also been suggested to affect memory and learning. In addition, some investigators have proposed that Adiol may increase intracellular cAMP levels through binding to the sex hormone binding globulin [60].

2.5. Nucleoporins

In eukaryotes, the nuclear and cytoplasmic compartments are separated by the nuclear envelope (NE). It is a double lipid bilayer system consisting of two concentric membranes, the inner nuclear membrane (INM) which stays directly in contact with chromatin and Lamin filaments and the outer nuclear membrane (ONM), which is contiguous with the endoplasmic reticulum and studded with ribosomes on the outer side. The space between these membranes is called the perinuclear space (PNS) which is interrupted by nuclear pore complexes (NPCs) spanning the nuclear envelope through pores formed by the fusion of inner and outer nuclear envelope membranes. NPCs are large multi-component protein assemblies that function as mediators of selective bidirectional exchange between the nucleoplasmic and cytoplasmic compartments, thus allowing communication between the nucleus and the cytoplasm [61, 62]. They show a broad degree of compositional and structural conservation among all eukaryotes and are estimated to be the largest protein complexes in the cell, ∼90–120 MDa in human cells. The NPC has a highly conserved doughnut shaped structure with an eight fold rotational symmetry which is composed of multiple copies of ∼30 individual components, termed as Nucleoporins (Nups). Its core consists of two outer rings of membrane-embedded scaffold sub- complexes at the nucleoplasmic and cytoplasmic periphery and two adjacent inner rings built around a central transport channel. The central channel has a diameter of ~38nm, corresponding to the maximum size of known transported particles [63]. Its component nucleoporins (Nups) can be subdivided into two major classes. The first class represents the structural scaffold of the NPC which is stably embedded into the NE and it includes the NUP107/160 complex and the NUP205/188/93 complex. They are remarkably stable once assembled into the NPC and have longer residence times exceeding one cell cycle. The second class represents the peripheral components of the NPC consisting of approximately 15 Nups, most of them containing phenylalanine-glycine (FG) repeat motifs, which bind directly to soluble transport receptors and facilitate transport through the nuclear pore [64]. Interestingly,

many nucleoporins of this group are mobile and display highly variable rates of association with the nuclear pore [65]. Many of them are highly dynamic, being able to move on and off the pore with kinetics of seconds to a few hours [66].
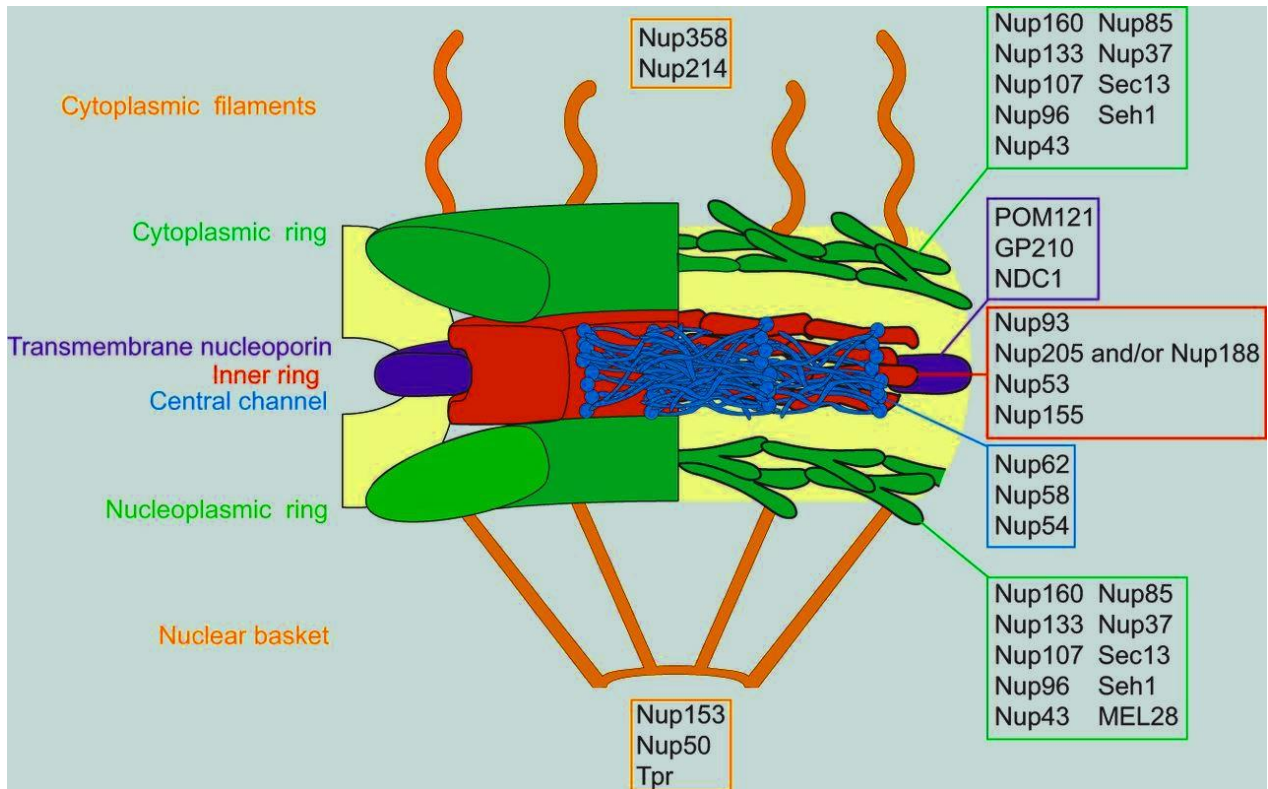
Figure 5. General organization of NPC. Figure adopted from (Marion Weberruss et al. 2016)[67].

Only recently, it has become evident that the NE and its associated proteins play a major role in cellular organization, gene expression and the regulation of development [68-70]. The NPC plays an obvious role in gene regulation by controlling the export of generated RNA and import of transcription and signalling factors. However, in addition to its role in transport, the NPC and its individual Nups have been shown to play a major role in genome organization and gene expression by direct binding to specific genomic locations [71-80]. Multiple studies in a number of organisms have identified the presence of specific Nups at active and silent gene loci, and have also revealed a functional requirement of NPC components in the execution or maintenance of selective transcriptional programs and chromatin states. It has been observed that a gradual deterioration of NPCs leads to accumulation of cytoplasmic tubulin inside the nuclei of aged rat neurons which is a characteristic of neurological disorders including Parkinson's disease [81]. Hence implying that, an intact NPC is important to avert pathological progression of neurodegenerative diseases in the brain [82]. Additionally, a number of Nups

have been demonstrated to be critical for tissue specific differentiation. These observations indicate that the NPC is capable of integrating its transport and genome-binding activities, for example, by bridging the nuclear import of developmental transcription factors to their activating functional target promoters. Hence, emerging as a new scaffold for genome organization, and may play a role as a nexus of developmental signalling, being able to coordinate transport, spatial genome organization and gene expression [66].

2.5.1 Nup133

Nup133 is a component of the evolutionarily conserved Nup107-160 complex. It consists of nine polypeptides in total (Nup160, Nup133, Nup107, Nup96, Nup85, Nup43, Nup37, Seh1 and Sec13) which are assembled in a Y-shaped complex [151]. This complex extends on both sides of the nuclear envelope and is one of the major NPC structural subunits [63, 83]. Several studies have illustrated the role of Nup107-160 complex in interphase nuclei as a NPC component and in mitosis for spindle assembly and proper kinetochore function [84-89]. Nup133 was initially thought to be essential for NPC assembly in vertebrates [85, 88] but later studies in whole organisms including mouse demonstrated that it is dispensable for any essential structural function of the Nup107-160 complex. It was found that Nup133 was not ubiquitously transcribed in all cell types in mouse during development and that it was not critical for cell survival. Nup133 doesn't seem to have a significant contribution to mRNA export but is capable of regulating protein transport via NLS-independent nuclear transport pathways similar to those uncovered for a number of transcriptional regulators [90]. It has also been observed that a perturbation of Nup133 function can contribute to oncogenesis.

The functions of Nup133 were specifically interesting in this study because it was reported to be essential for neuronal differentiation during mouse development. A study revealed that neuronal differentiation was dependent upon the activities of Nup133 at the time of differentiation and/or even at earlier steps in the neural lineage. They also found that the neural progenitor cells lacking Nup133 abnormally retained features of pluripotency and differentiated inefficiently along the neural lineage, both in embryonic stem cell culture and in the developing embryo. Thus, pointing towards an important role of Nup133 in establishing the neural lineage. [91].

Moreover, it's position at the periphery of the Nup107-160 complex, with its NH2-terminal β-propeller domain free for interaction, makes it prone to interact with other proteins and protein complexes or even protein-RNA complexes in the nucleus though which it could

mediate its role in cell differentiation and development [92]. Thus, in addition to participating in nuclear transport and mitosis, Nup133 might also bind to components of chromatin remodeling complexes and repressor/activator complexes with histone-modifying activities in the nucleus to mediate as yet unknown functions of the NPC in vertebrate cells [93].

2.5.2 Nup210

Nup210 is a large transmembrane nucleoporin with a long luminal domain, a single transmembrane segment with a small C-terminal region facing the NPC, and a large, well-conserved N-terminal domain that protrudes into the perinuclear space between the inner and outer nuclear membranes [94]. It was the first transmembrane nucleoporin to be discovered and was initially thought to be involved in anchoring the NPC to the NE and initiating nuclear membrane fusion during nuclear pore assembly [95-97]. However, it was later observed that Nup210 was recruited at a later stage during the nuclear pore assembly suggesting that it is not required for NPC formation and that it also exhibits a tissue specific expression with higher levels in brain, kidney, skin, lung, gut and pancreas [98, 99].

The possibility of a potential role of Nup210 in regulating cell differentiation was first proposed when it was observed that it had a differential expression in the kidney during mesenchymal to epithelial transition [99, 100]. Later, it was identified to play a pivotal role during myogenic and neuronal differentiation. When the expression pattern of Nup210 was studied in an embryonic stem cell (ESC) to neuroprogenitor (NP) cell differentiation system, it was seen to be absent in ES cells but was strongly expressed in neuroprogenitors. Nup210 was found to be important for the induction of genes essential for cell differentiation via recruitment of transcription or mRNA export factors to the NPC and hence, essential for neural differentiation and the maintenance of the neuroprogenitor state [82, 101].

2.5.3 Nup50

Nup50, a component of the nuclear basket in the NPC structure, was initially noticed as it undergoes unusual changes in localization during male germ cell differentiation[102]. It is a mobile Nup that shuttles between the NPC and the nucleoplasm with very short residence times of seconds at the NPC. This dynamic behaviour of Nup50 is dependent on active transcription by RNA polymerase II and is achieved through the N-terminal half of the protein, which contains importin α and Nup153-binding domains. It attaches to the NPC by interacting with Nup153 and is uniformly distributed in the nucleoplasm with a general exclusion from nucleoli. However, it has been observed that the dynamic nature of Nup50 is

independent of importin α, Nup153, and Nup98, even though the latter two proteins also exhibit transcription-dependent mobility. It is a ubiquitously expressed NPC protein in adult and embryonic tissues with the highest expression in the developing neural tube and adult testes [103].

It mainly functions as a soluble cofactor in nuclear protein import by actively displacing NLSs from importin-alpha and facilitating disassembly of the importin-alpha:beta-cargo complex and also in importin recycling. Apart from its role in protein transport, Nup50 has been shown to perform additional functions related to chromatin biology within the nucleoplasm and away from the NPC. It was observed that a targeted disruption of Nup50 caused severe neural tube and CNS abnormalities and growth retardation in mouse embryos, indicating its important role in CNS development. Another study in C2C12 myoblasts showed that the depletion of Nup50 did not affect cell proliferation but inhibited their differentiation into myotubes. These studies point towards the possibility of Nup50's interaction with developmental genes that might be functionally required for developmental and differentiation processes such as the formation of terminally differentiated myotubes [103, 104].

2.6. Lamins

Lamins are prominent 60 to 80 kDa intermediate filament (class V) proteins of the nuclear lamina. They are the major structural proteins of the animal cell nucleus forming a meshwork lining the inner nuclear membrane (INM) [105]. They have a tripartite structure with two globular head and tail domains flanking a central α-helical rod domain. This structure enables them to form high-order polymers and a framework to support multi-protein complexes that are involved in several nuclear functions, hence, serving as a scaffold for spatial genome organization.

The lamina is mainly composed of two types of Lamins; type A and B which are encoded by three lamin genes, LMNA, LMNB1 and LMNB2. Lamin A and C are the two major splice variants produced by LMNA gene along with two minor isoforms, while Lamin B1 and B2 are transcribed from the LMNB1 and LMNB2 genes respectively[106]. Lamins undergo a number of different post-translational modifications and are spliced alternatively to create multiple isoforms. For example, pre-Lamin A undergoes enzymatic cleavage to become mature Lamin A [107, 108]. What connects Lamins to their role in regulating gene expression is that the various isoforms are differentially expressed in different cell types and at specific developmental stages. For instance, B-type lamins (B1 and B2) are constitutively expressed in

most cell types, whereas the expression of A and C type lamins are cell type and developmental stage specific, Lamin A being predominantly expressed in the most differentiated cell types [109, 110]. Studies in mouse have shown that a depletion of Lamin A accelerated the transition to pluripotency in somatic cells, whereas cells overexpressing Lamin A took longer to reprogram to form iPC (induced pluripotent cells) [111]. Also, mutations in the human Lamin A (LMNA) gene has shown to be responsible for an array of serious diseases called laminopathies, including cardiomyopathy, musculardystrophy, lipodystropy, neuropathy and progeria [108]. Moreover, latest studies have established that the Lamin proteins tether heterochromatin and developmentally silenced domains to the nuclear periphery [112-115], and that they interact with a number of proteins affecting chromatin organization, condensation and DNA replication, which include transcription factors and chromatin re-modellers [106, 116-120]. Taken together, these studies demonstrate that the Lamins are expressed in a tissue specific manner and form unique territories in the lamina which likely contributes to a cell type specific NE composition and even though the mechanistic details are largely unknown, these studies establish a pivotal role of Lamins cellular organization, chromatin and gene regulation necessary for the determination and manifestation of cell fate [121, 122].

The role of Lamins in regulating differentiation-specific gene expression programs specifically in CNS development and differentiation has been studied in Lamin B knockout mouse models that displayed an array of organogenesis defects in the brain while the self-renewal and pluripotency properties of mouse ESCs remained intact [123].

Genome wide studies of Lamin B1 Associated Chromatin Domains (LADs) during neuronal differentiation in mice showed that while ESCs and terminally differentiated cells share a broad LAD structure, smaller subregions of gene clusters undergo rearrangements corresponding to steps of the differentiation process [124, 125]. For example, genes associated with "stem- ness," as well as cell cycle related genes, become lamina-associated during differentiation. Conversely, cell type or lineage specific genes were released from the lamina and de-repressed or "unlocked" for expression at a subsequent step in differentiation [115].

In Drosophila, the gene encoding a critical transcriptional factor hunchback was shown to move to the nuclear lamina during differentiation of neuroblast cells to neurons [126]. This gene repositioning correlated with a loss of progenitor cell competence and was found to be dependent on the B type Lamin Dm0. Depletion of Lamin Dm0 extended neuroblast competence, presumably through disruption of targeting the hunchback locus to the nuclear

lamina. These studies indicate the nuclear lamina is extensively utilized throughout metazoan to stably silence differentiation-specific genes [66].

3. HYPOTHESIS

Based on previous reports and clinical observations we hypothesized that hyperoxia has differential effects on the developing male and female brains and that it brings about profound changes in the intricate cellular machinery of male OPCs that possibly affects their capability to differentiate. Hence, we developed a mouse primary OPC cell culture model to find answers to the following questions:
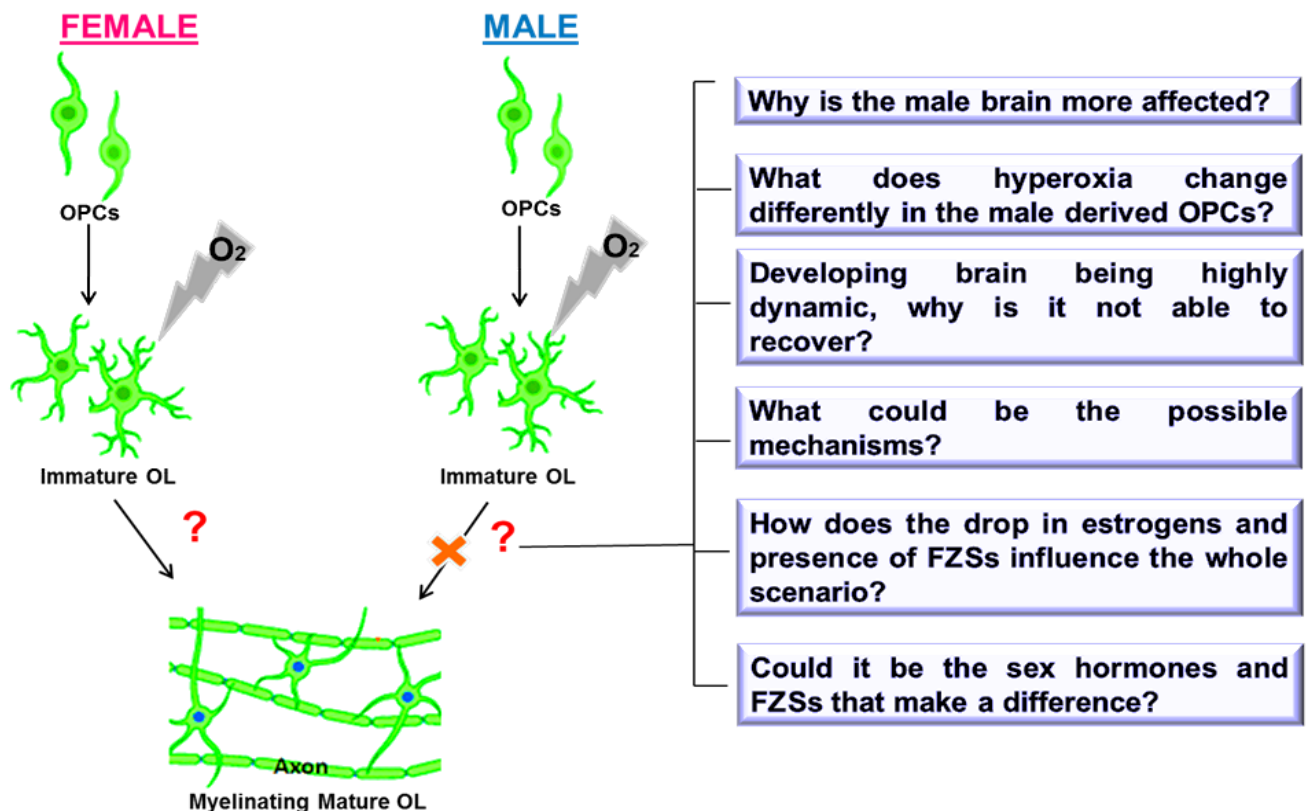
We believe that hyperoxia brings about an imbalance of important proteins in the male OPCs that can result in altered cell division capability producing an abnormal pool of OPCs compromised on their ability to give rise to mature oligodendrocytes. Thereby, leaving the brain unable to recover after hyperoxic injury even though it is known that there is an apparent replenishment of OPCs post injury; leading to long term effects especially in the male subjects.

We also wanted to investigate how the drop in estrogen concentration and the presence of FZSs influence these hyperoxia induced mechanisms. We hypothesised that the presence of the female sex hormone (17β-estradiol) and the FZSs positively affect the OPCs in females but not males.

4. MATERIALS AND METHODS

4.1. Materials

All materials used including details of chemicals, kits, antibodies, labwares, machines, softwares and details of preparing cell culture medium, buffers and other solutions are listed in Appendix I.

4.2. Methods

4.2.1 Animal strains

Mouse protocols were approved by the Veterinary and Food Control Office, State Department of Agriculture, Food Safety and Fisheries Mecklenburg-Vorpommern, Germany (Permit Number: ZSF3936/11/17). Animal colonies were housed and maintained following the international FELASA, national GVsolas and local University of Greifswald animal research guidelines. Animal care and breeding was performed at the Central Core & Research Facility of Laboratory Animals, Medical School of Greifswald. Experimental procedures were performed under specific pathogen free conditions in accordance with established institutional ethical guidance and approved protocols from the animal facility. The PLP-GFP transgenic mouse line, in which expression of the GFP reporter gene is driven by the plp regulatory sequences in a C57BL/6J background mouse strain, was obtained as a kind gift from Prof. Bernard Zalc (Centre de Recherche de l'Institut du Cerveau et de la Moelle epiniere UPMC-Paris6, UMR_S 975; Inserm U 975; CNRS UMR 7225, Paris) [127]. Transgenic mice did not display any obvious developmental defects. Crl:CD-1 (ICR) mice were received from Charles River Company and breed for maximal two generations at the facility to get the donor mice. Both strains were used to generate oligodendrocyte precursor cells.

4.2.2 Isolation and cultivation of mouse primary OPCs

Hypoxia is particularly important for the central nervous system, where oxygen (O_2) levels range from 8% at the pia to 0.5% in the midbrain [152]. Traditionally, all in vitro stem cell systems have used oxygen tensions that are far removed from the in vivo situation (21% O_2). This has shown to affect the survival of cells particularly in transplantation experiments due to the stress caused by switch in the oxygen tension [153-156].

Hence, we tested the protocol on cells derived from three different wild type mouse strains (Balb/C, B6NAlbino and CD1) and used 3% and 21% O_2 conditions to cultivate the cells. Later, the purity of the culture was analyzed using FACS.
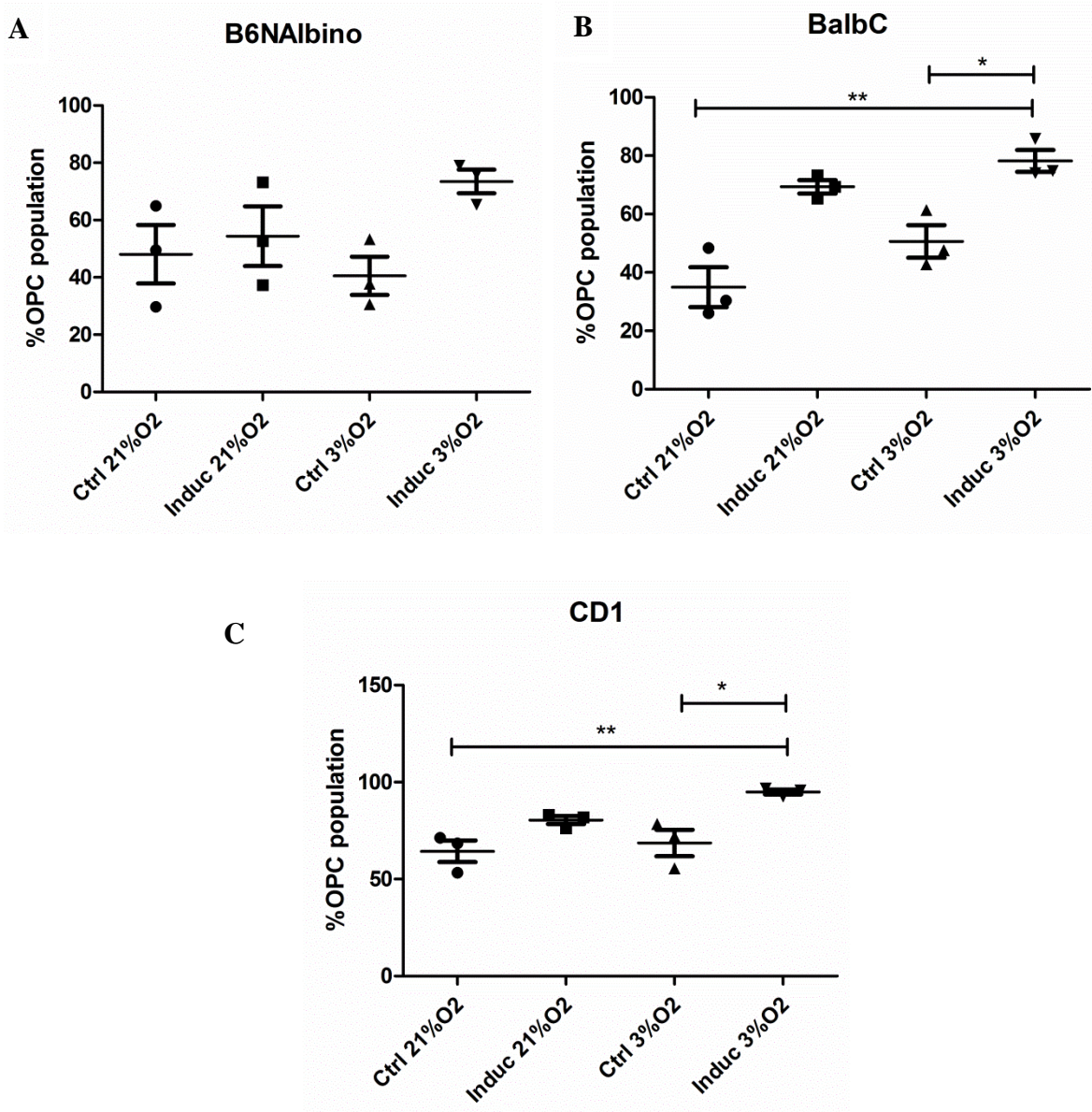
Figure 6. FACS data showing the difference between the percentage population of OPCs in different mouse strains.
FACS staining was performed using Anti-A2B5-APC antibody (Miltenyi Biotec) and PE-anti-mouse CD140a antibody (Biolegend). Control cells were kept in neurosphere growth medium containing EGF/FGF throughout while the induction group was fed with the OPC medium containing B104 conditioned medium. (A) Shows the results from B6NAlbino strain, (B) from the BalbC strain and (C) from CD1 strain.
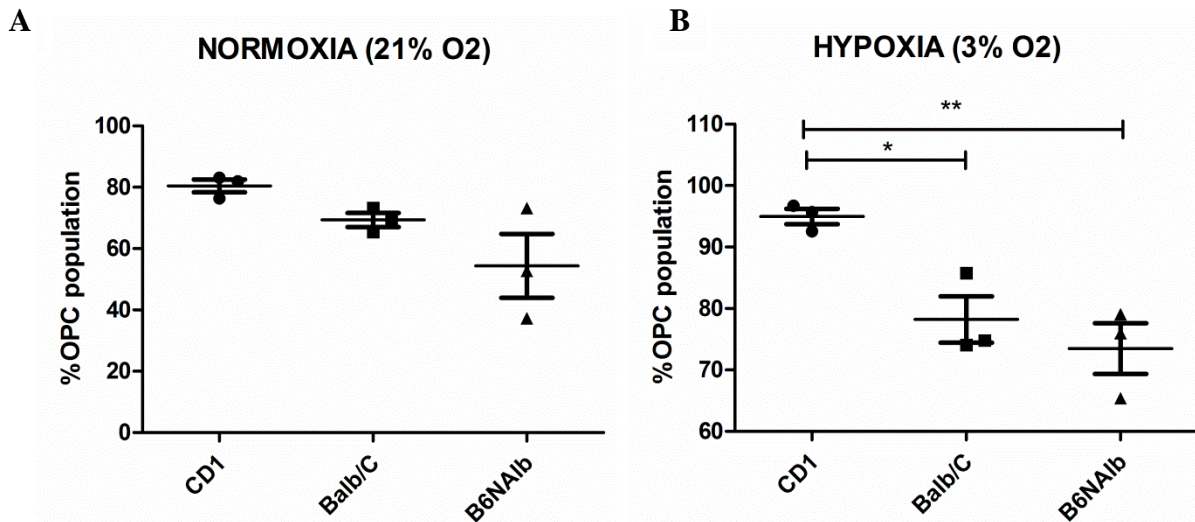
Figure 7. FACS data showing the difference between the percentage population of OPCs under 3% and 21%O$_2$ conditions.
The graphs show a comparison between the percentage of OPC yeild from the three strains when cultured under (A) normoxic (21% O$_2$) and (B) hypoxic (3% O$_2$) conditions. The CD1 wild type strain showed the maximum yeild of approximately 95% OPCs when cultured at 3% O$_2$. While the yeild of OPCs was boosted from approx. 50% to 75% in the B6Nalbino strain, the BalbC cells did not show any considerable difference. This clearly shows that the primary cells derived from different wild type mouse strains respond differently towards the protocol.

The results (Figure 6) showed that the different wild type strains responded differently to the protocol and that the CD1 wild type strain could yield more than 95% pure OPCs under hypoxia. Furthermore, hypoxic conditioning could increase the yield of OPCs by an average of 10% in all the three strains (Figure 7).

The PLP-GFP strain derived OPCs were validated using immunoflourescence. Cells were isloated and cultured as per the same protocol. The images (Figure 8) showed more than 90% of all cells PLP positive with cells at different stages of maturation.
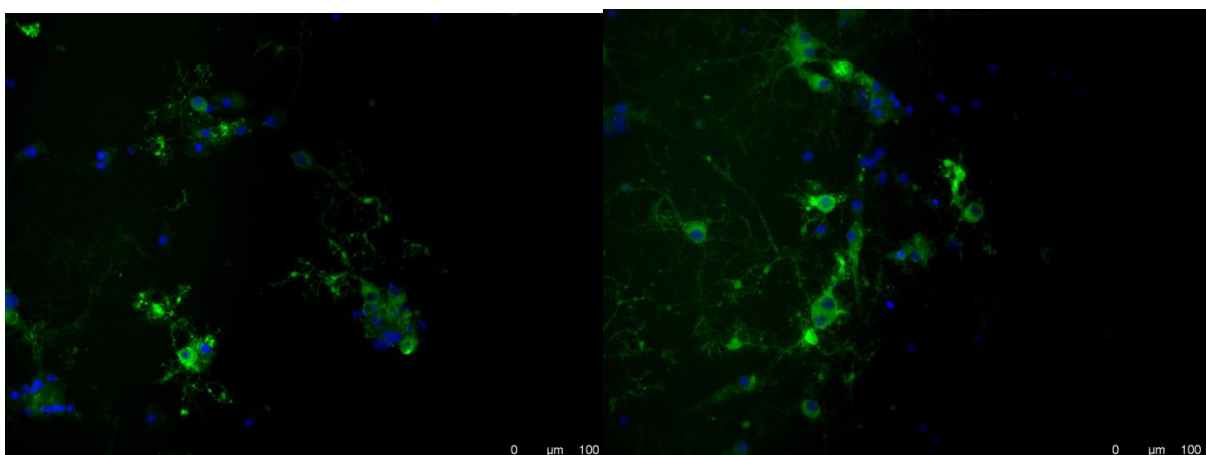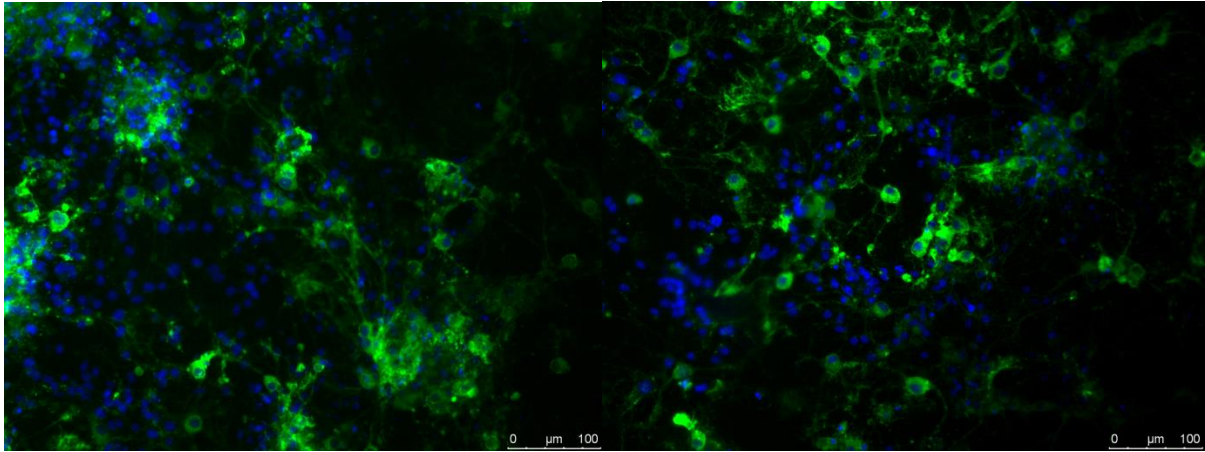
Figure 8. Flouresence microscopy images of OPCs derived from PLP-GFP strain that were plated on poly-ornithine coated coverslips and stained with DAPI (blue) showing OPCs (green) in different maturation stages. Scale bar 0-100μm.

Hence, OPCs were isolated from postnatal day 2 to postnatal day 4 old CD-1 (Wild type strain) mice. For each isolation, tissue from the mid brain region comprising the sub ventricular zone from 3 male and 3 female (from the same litter) brains were pooled separately. The sex of the pups was determined visually with occasional genotyping to confirm. Animal care and breeding was performed at the Zentralen Service- und Forschungseinrichtung für Versuchstiere der Universitätsmedizin Greifswald. All animal usage for cell isolation was performed according to the institutional regulation regarding animal ethics and applicable laws.

A) Isolation and Neurosphere expansion

Before starting the isolation, 4 sets of sterile dissection instruments were prepared in order to reduce the chances of contamination: separate sets for the skin, skull, for removal of the brain and to cut out the desired region of the tissue. After decapitation, the brain was isolated intact and transferred to a petridish containing sterile ice-cold dissection solution. The brains were rinsed in cold dissection solution once to wash off any remaining blood. The meninges was stripped off from the surface of the brain by looking under a dissection microscope and then the SVZ region was carefully isolated from each brain of both the sexes separately. The tissue from both the groups was then subjected to enzyme digestion at 37°C for 10-15mins. The reaction was stopped using trypsin inhibitor solution. The resultant single cell solution was resuspened in 1ml Neurosphere growth medium and seeded in equal densities into 5 T-75 suspension culture flasks each (for male and female) containing 15ml neurosphere growth medium. The flasks were kept at 3%O_2, 5%CO_2 and 37°C incubator. After 24hrs the flasks were first inspected for any signs of contamination before the cells were allowed to expand

further. After 2 days, 5 ml of neurosphere growth medium was added to each flask and the cells were allowed to divide and form spherical aggregates (neurospheres) for at least 2 more days so that considerable amount of neurospheres were formed.

B) Oligosphere formation

In order to program these neural progenitor cells to become OPCs, after ~5-6 days when the neurospheres were around 100μm in diameter, gradually the neurosphere growth medium was replaced by the B104CM containing oligosphere medium every alternate day for 2 weeks. After this time period, the cells were trypsinized and used for experiment.
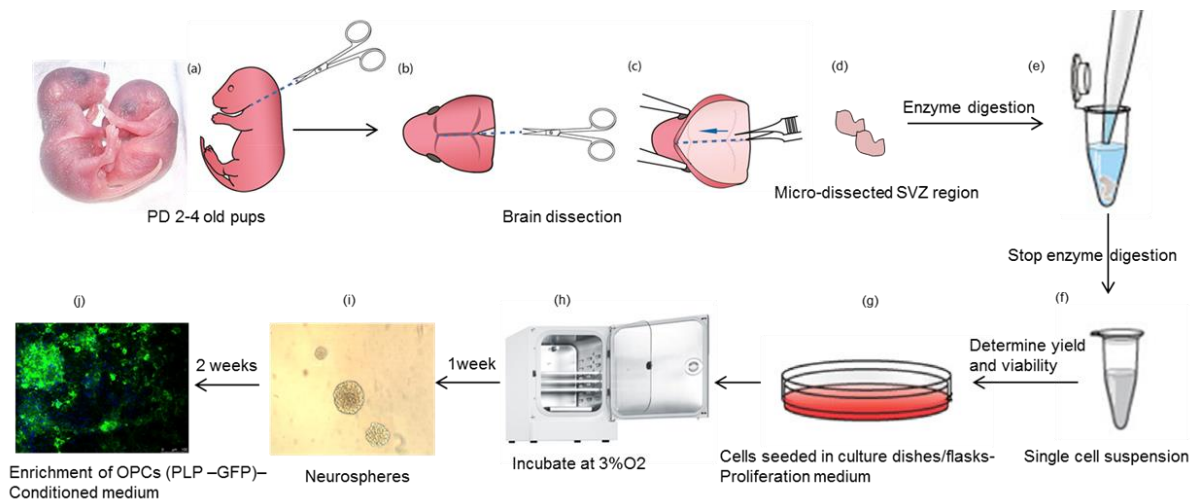
Figure 9. Flow diagram for tissue isolation and culture of OPCs.

C) B104 Neuroblastoma cell culture and Conditioned Media preparation

B104 Neuroblastoma cell line was purchased from ATCC. The cells were grown in T-75 flasks for adherent cells with 18ml growth medium.

For preparing conditioned medium, the B104 cells were allowed to grow till the flasks were completely confluent. The culture media was then removed and the cells were washed once with Puck's BSS or 1xPBS (sterile). Then the cells were fed with 20ml N2 supplement containing medium per flask and kept in the incubator at 37°C and 5% CO_2 for 4 days.

After 4 days, the medium was collected and PMSF was added to a final conc. of 1ug/ml. It was then centrifuged immediately at 2000g for 30min at 4°C. The supernatant was filter sterilized, aliquoted and stored at -80°C.

*Note: Detailed protocol is published online [128].

4.2.3 OLN93 cell culture

The OLN93 cell line was obtained from Prof. Dr. Christiane Richter-Landsberg (Universität Oldenburg, Germany). It is a rat derived, pre-OL adherent cell line derived from spontaneously transformed cells in primary rat brain glial cultures[129].

A) Thawing and cultivating

The cells were cultured as per the protocol mentioned by Gerstner et al. [4], in Dulbecco's modified Eagle's medium (DMEM) (with 3,7g/l $NaHCO_3$, 25mM HEPES, 4,5g/l D-Glucose, 4,4 g/l NaCl; Biochrom), supplemented with 10% heat inactivated Fetal Calf Serum (FCS, Biochrom), 0,01% Human Serum Albumin (HSA, Grifols) and 1% Penicillin-Streptomycin solution. In order to initiate a culture, the cells were first taken out from liquid nitrogen and for example, one vial of cells was kept in a 37°C waterbath with continuous shaking for aprroximately 1-2mins and was then transferred immediatedly to 9ml warm culture medium. The cells were then centrifuged for 7 mins at 300g and the pellet was resuspened in 1 ml medium. The resusupended cells were then transferred completely to a fresh T-75 adherent cell culture flask containing 18ml culture media. The flask was then kept in a humidified cell culture incubator at 37°C and 5% CO_2 with normal air (21% O_2, Normoxia). Medium changes (9ml media exchange) were done every 2-3 days. Cells were passaged after every 5-7 days depending upon the cell density. Cells upto only 10 passages were used for the experiments, after which the culture was discarded and new frozen vials were thawed.

B) Passage and Plating cells for Experiment

The cells were passaged when they were around 80-90% confluent. For passaging, the cells were first washed with 1x Dulbecco's phosphate-buffered saline (DPBS, PAN Biotech) and then trypsinized using 2ml TrypLE (TrypLE Express, Life Technologies) solution until all the cells were detached from the surface. TrypLE was deactivated (to stop the enzyme reaction) by adding 8 ml of PBS and the complete 10ml cell suspension was transferred to a 50ml Falcon tube. The flask was the washed 2 times again with 10 ml PBS each to recover all the cells and then centrifuged at 300g for 7 mins. The pellet was resuspended in 1 ml medium and appropriate volume from this suspension was diluted to count the cells using a hemocytometer. Required amount of cells were then seeded into new T-75 flasks for cultivation.

For hyperoxia experiments, 200,000 cells per well were seeded into 6-well plates (Cell+, Sarstedt) containing 1ml media in each well (to improve oxygen diffusion). Once the cells

were seeded, they were given the respective treatments (steroids, blockers and 80%O_2 hyperoxia) immediately. The cells were kept under the treatment conditions for 24-48 hrs depending upon the experiment.

C) Freezing

Cells from the earliest passages were always forzen in liquid nitrogen to maintain the cell repository. For freezing, after trypsinization, the cell pellet was resuspended in FCS and the cells were counted and diluted in FCS in such a way to obtain 10^6 cells per 900µl FCS. 900ul each of this cell suspension was distributed into labelled Cryotubes (Carl Roth) and then mixed with 100ul Dimethylsulfoxid (DMSO, Sigma-Aldrich) to get a final volume of 1ml. Since, DMSO is cytotoxic, the tubes were transferred immediately into pre cooled, isopropanol (Carl Roth) filled Cryoboxes (Cryo 1°C Freezing Container, Thermo Fisher) and kept at -80°C. After 48hrs the cryotubes were transferred to liquid nitrogen (ARPEGE, Air Liquide) or kept at -80°C for maximum 6 months.

4.2.4 Treatment strategies

A) OPCs

For each experiment, the oligoshperes in suspension from all the 5 flasks of each sex were pooled into falcon tubes separately, centrifuged at 3000 rpm for 10 mins and the pellet was trypsinized using TrypLE^{TM} (Thermo Fischer). After trypsinization, the cells were counted and seeded in equal densities into 6 well plates for adherent cells (without any coating; Cell+, Sarstedt) containing 1ml respective treatment media per well (Table 1). The plates were then kept at 80%O_2, 5%CO_2 and 37°C (hyperoxia) and 3%O_2, 5%CO_2 and 37°C (normoxia) incubators respectively, for 24-48 hrs depending on the experiment.

For differentiation experiments, the cells were first given 80%O_2 shock for 24hrs with or without steroid treatment in 1ml treatment media and later 1ml fresh respective treatment media was added to each well and all plates were returned to 3%O_2 (normoxia) condition. The cells were then allowed to differentiate for 4 days with 1ml media (respective treatment media) change every alternate day.

The hormones and other substances used were all reconstituted in DMSO and diluted accordingly (as shown in Table 2) to be used as working stock solutions. All control samples were treated with 1µl/ml (1:1000) DMSO.

Table 1: Treatment media.

Experiment	Media composition
Differentiation	Oligosphere medium
24/48h Treatments	DMEM/F12 (without NaHCO$_3$) + 45% glucose solution (666 µl for 50ml DMEM/F12)

Table 2: Steroid hormones, Agonists, Antagonists and Inhibitor concentrations.

Substance	Abbreviation	Function	Working stock conc.	Final conc.
17β-Estradiol	E2	ER-α/ER-β-Agonist	100µM	100nM
4,4',4''-(4-Propyl-[1*H*]-pyrazole-1,3,5-triyl)trsiphenol	PPT	ER-α Agonist	100µM	100nM
5-Androsten-3β, 16α-diol-17-on	16αOH-DHEA	FZS	100µM	100nM
5-Androsten-3β, 17β-diol	Adiol	FZS	100µM	100nM
ICI 182,780	ICI	ER-α/ER-β-Antagonist, GPER-Agonist	1mM	1µM
(3α,5α)-3-Hydroxy-pregnan-20-one	Allopregnanolone	FZS	100µM	100nM

B) OLN93 cells

The OLN93 cells were trypsinized, counted and seeded in equal densities into 6 well plates for adherent cells (without any coating; Cell+, Sarstedt) in 2ml reduced serum medium (5% FCS). The cells were then allowed to recover for 24hrs under normal oxygen conditions, after which the medium volume was reduced to half, the respective steroid treatments were administered and the cells were kept at 80%O$_2$ for 48hrs.

After 48hrs, the plates were taken out, complete media was aspirated from the wells and the cells were washed once with 1x DPBS. The plates were kept on ice and the cells were then lysed directly in the plate using 300-500µl M-PER lysis buffer (M-PER Mammalian Protein Extraction Reagent, Thermo Fischer) containing protease & phosphatase inhibitors (Halt Protease & Phosphatase Single-use inhibitor cocktail 100x, Thermo Fischer). The cell lysate was centrifuged at 10,000xg for 6 mins at 4°C and the supernatant was quantified on the spectrophotometer.

4.2.5 Preparation of protein extracts for Mass Spectrometry

Cells were harvested in 8M urea/2M thiourea and proteins extracted by 5 cycles with 10 min incubations at 37°C at 1400 rpm and freezing in liquid nitrogen for 5 min. Nucleic acids were fragmented by sonification and insoluble cell compartments pelleted via centrifugation (1h, 15600g, 20°C). The supernatant was stored at -80°C. Bradford protein assay was used to determine the protein concentration. A volume equivalent to 4 µg of protein was filled up to a total volume of 20µL with 20mM ammonium bicarbonate (ABC); 1µL DTT (25mM) was added and samples were incubated at 60°C for 1 h. 7µL ABC were added and released thiol groups were alkylated with 2µL of 100mM iodoacetamide (15 min at 37°C in darkness). Samples were digested with trypsin in a ratio of 1: 50 (protease: protein) overnight at 37°C. The digestion was stopped via addition of acetic acid in a final concentration of 1%. Resulting peptide extracts were purified at C18 material (ZipTip, Merck Millipore, Darmstadt, Germany).

Analysis was carried out on an LC-coupled ESI-tandem mass spectrometer as described earlier (Murr et al. J.Prot. Res., 2017). Separation of peptides was achieved on a reverse phase nano-Acquity UPLC column (1.7µm, 100µm i.d. × 100mm, Waters GmbH, Eschborn, Germany) using a 90 min non-linear gradient ranging from 2 to 60% ACN in 0.1% acetic acid at a flow rate of 400 nl/min. The detection was carried out with a LTQ-Orbitrap-Velos mass spectrometer (Thermo Electron, Bremen, Germany) in data-dependent mode selecting 20 precursor ions with the highest intensities for CID fragmentation per cycle. Once measured masses were excluded 60s from a new fragmentation. Proteins were identified by searching in a forward-reverse UniProt/SwissProt database with a restriction on Mus musculus (and using the SorcererTM software platform with sequest algorithm implemented in Rosetta Elucidator software suite (Ceiba Solutions, Boston, MA, USA). A statistical evaluation of the results was performed by analysis in peptide/protein prophet and the annotation of peptides was carried out at a false-positive rate of <1% that is equivalent to a peptide probability >0.87. Only

proteins with a probability >0.8 and a peptide count ≥ 2 were used for statistical analysis carried out in Analyst (Genedata, Basel, Switzerland). For functional categorization of differentially abundant proteins (p-value<0.05) Ingenuity Pathway analysis, STRING and Go annotation as provided by UNIPROT database were used.

4.2.6 Western blotting

A) Protein extraction and sample preparation

Protein extracts were prepared either from freshly treated cells or from frozen cell pellets. Cells were first scraped off using cell scraper while still in the medium and then centrifuged at 3000rpm for 10 mins at room temperature. The pellet was then washed once with 1x DPBS, centrifuged again and then lysed using M-PER lysis buffer. For lysis, the cells were incubated on ice for 30mins with repeated vortexing. Then the lysate was centrifuged at 10,000g for 6 mins at 4°C and the supernatant was quantified on the spectrophotometer.

Samples were prepared for western blot using the quantified protein extracts as shown in Table 3.

Table 3: Sample preparation calculation for western blot.

A	B	C	D	E	F	G
Sample	Protein conc. ($\mu g/\mu l$)	Volume for 40μg protein (μl)	H_2O (μl)	Sample loading dye (4x) (μl)	Sample reducing agent (10x) (μl)	Total volume (μl)
Formula		40/B	G-C-E-F			
M 3%O$_2$ CTRL	22,42	1,78	19,42	8,5	3,3	33
M 80%O$_2$ CTRL	32,65	1,23	19,97	8,5	3,3	33
F 3%O$_2$ CTRL	30,54	1,31	19,89	8,5	3,3	33
F 80%O$_2$ CTRL	32,57	1,23	19,97	8,5	3,3	33

B) SDS-PAGE

For gel electrophoresis, 12% or 8% gels were prepared as mentioned in the solution preparation section (appendix I). The gels were cast using the Mini-Gel module for

electrophoresis (BioRad) and 1x Running buffer (Rotiphorese, 10x SDS Page buffer, Roth) was used for filling the tank during PAGE. Before loading, the samples were cooked at 80°C for 10 mins with continuous shaking, cooled and spun down. After loading, the gels were allowed to run at 100V (PowerPac1000, Bio-Rad Laboratories) for 15-20mins till the samples were stacked and then the voltage was increased to 120V. The samples were allowed to migrate till the end of the glass plate, after which the electrophoresis was stopped and the separated proteins were transferred onto nitrocellulose membrane.

C) Transfer

The Wet-Tank transfer method was used to transfer the proteins onto a membrane. For transfer, 1x transfer buffer was first prepared as mentioned in the solution preparation section (appendix I) and chilled shortly in a -20°C freezer before use. The transfer cassette was assembled while immersed in chilled transfer buffer by putting the sponge (Bio-Rad Laboratories), filter paper (Criterion blotter Filter paper, Bio-Rad Laboratories), the gel, nitrocellulose membrane (Amersham Protran 0.45µm NC Western Blotting Membrane, GE Healthcare), filter paper and sponge in the same order as mentioned. Once the cassettes were prepared, they were inserted into the transfer apparatus filled with 1x chilled transfer buffer. It was allowed to run for 3hrs at 75V on ice.

D) Immunodetection

After the transfer was complete, the membrane was retrieved from the cassette and stained with Ponceau S solution to check the transfer efficiency and protein loading. The membrane was then washed 3-5 times with 1x TBST to de-stain, after which it was blocked for 1hr in blocking solution (Pierce™ Protein-Free (TBS) Blocking Buffer, Thermo Fischer) at room temperature (RT) on a rocking platform. After blocking, the membrane was incubated with the respective primary antibody solution overnight at 4°C on a rocking platform.

*Primary antibody solutions were prepared by directly diluting the antibody in the Pierce™ Protein-Free (TBS) Blocking Buffer. The solutions were always stored at -20°C and reused as long as it gave good bands (minimum 30 times). Once the prepared antibody solution was exhausted, it was discarded and a fresh dilution was prepared. For all Cell Signaling Technology antibodies, a 1:1000 dilution was used. For all other antibodies, 1.5:1000 dilution was used.

The next day, the primary antibody solutions were retrieved; the blots were washed once with 1xTBS and then incubated with secondary antibody for 1hr at RT on a rocking platform. After the incubation, the blots were washed with 1xTBST, 3 times for 5 mins each on a rocking platform at RT. Then washed once with 1xTBS for 5 mins at RT and developed. For developing, SuperSignal™ West Femto Maximum Sensitivity Substrate was used. The substrate was poured directly on the membrane and the chemiluminisence was detected using a Gel Doc system (Gel Doc System, Bio-Rad Laboratories). Images were taken at 3-4 different exposure times for each membrane.

*A 1:10000 dilution was used for all secondary antibodies.

After developing, the blots were washed again 2 times with 1xTBS and re-probed directly with another primary antibody (if the proteins to be detected were of different molecular weights) or stripped using the stripping buffer and then re-probed. For stripping, the blots were incubated with stripping buffer for 10-20 mins on a rocking platform with the highest speed and then washed 2 times with 1xTBS for 5 mins each. They were washed again 2 times with 1x TBST for 10 mins each and then 1 time with 1xTBS for 5 mins. The membrane was blocked for 1hr at RT and then incubated with primary antibody overnight at 4°C.

E) Analysis

The chemiluminescent images were analyzed using the Image Lab software from Bio-Rad. Densitometric analysis was done by calculating the intensities of individual bands and then normalizing with the house keeping control for each condition. Relative quantification was then performed by calculating the ratios between different conditions.

4.2.7 Immunofluorescence staining

A) CNPase staining (Differentiation Experiment)

For IF staining, the cells were trypsinized and plated in equal densities into 8-well chamber slides (8-well on PCA detachable, Sarstedt) designed for microscopy. The cells were given $80\%O_2$ treatment in 100µl differentiation treatment media (as mentioned in Table. 1) per well containing the respective steroids or vehicle control for 24hrs. The normoxia control slides were also treated exactly the same way but kept at $3\%O_2$ with reduced medium for 24hrs. After 24hrs, the slides were taken out and 100µl respective treatment media was added to all wells and all slides were returned to $3\%O_2$ (normoxia) incubator. The cells were then allowed to differentiate for 4 days with 100µl media change every alternate day. After 4 days, the cells

were fixed and processed for IF with CNPase Antibody (Mouse Anti-CNPase (Clone 11-5B), Abcam) as mentioned below in the general protocol.

B) NUP133 staining

For the NUP133 staining, the cells were trypsinized and plated in equal densities into 8-well chamber slides (8-well on PCA detachable, Sarstedt) designed for microscopy. The cells were given $80\%O_2$ treatment in 100µl of the normal treatment media (as mentioned in Table. 1) per well containing the respective steroids or vehicle control for 24hrs. The normoxia control slides were also treated exactly the same way but kept at $3\%O_2$ with reduced medium for 24hrs. After 24hrs, the cells were fixed and processed for IF with NUP133 Antibody (Anti-Rabbit NUP133 Polyclonal, Proteintech) as mentioned below in the general protocol.

C) General protocol

After treatment, slides were taken out from the incubator and the media in each well was aspirated off. The cells were then washed once with 1xDPBS (200 µl per well) and then incubated with 200 µl per well of cold 4% PFA at 4°C for 30mins to fix the cells. After fixation, the wells were washed 2 times for 10 mins each with 1x DPBS (200 µl per well) and the cells were blocked with freshly prepared blocking solution (200 µl per well, prepared as mentioned in the solutions section) for 2hrs at RT. Meanwhile, the primary antibody solution was prepared. For both CNPase and NUP133 staining, a dilution of 1:500 was used to prepare the primary antibody solution in 3% NGS in 1x PBS + 0.3% Triton x100 and was stored at 4°C until used. After the 2 hr incubation, blocking solution was removed and 50 µl of the prepared primary antibody solution was added to each well. The slides were then incubated overnight at 4°C.

Secondary antibody preparation: Alexa Fluor 594 antibodies (Goat Anti-Mouse IgG (H+L) Alexa Fluor 594 Conjugate or Goat Anti-Rabbit IgG (H+L) Alexa Fluor 594 Conjugate, Life Technologies) that were originally diluted 1:1 in glycerol were used in a dilution of 1:250 in 3% NGS in 1x PBS + 0.3% Triton x100 for preparing the secondary antibody solution. The total amount of antibody required was calculated according to 200 µl per well. Being light sensitive, the secondary antibody solutions were always prepared and stored in dark at 4°C till use.

After the primary antibody incubation, the wells were washed 3 times with 1x PBS for 10 mins each and then 100 µl of the prepared secondary antibody solution was added to each

well and incubated at RT for 2hrs in dark. Later, the wells were washed 3 times again with 1x PBS for 10 mins each. After the last wash, complete PBS was aspirated from the wells and the detachable wells were carefully removed. The slide was then mounted with Vectashield Mounting Medium with Dapi (Vector Laboratories) over a thin glass coverslip and allowed to dry overnight at 4°C in dark after which they were ready for microscopy.

4.2.8 Real time PCR

A) RNA isolation

RNA isolation was performed from the 24hr treated OPCs using TRIzol reagent (Life Technologies). The cell pellet was directly homogenized in 1ml TRIzol and incubated at RT for 5mins to allow complete dissociation of the nucleoprotein complex. Later, the protocol was followed as mentioned by the manufacturer to obtain the phase separation. After the phase separation, RNA was precipitated with 0.5ml of 100% isopropanol and for this step an incubation of 30mins at RT was performed instead of 10mins mentioned in the protocol. After precipitation, the RNA pellet was washed as mentioned in the protocol and resuspended in 30μl of DEPEC water and stored at -80°C without heating at 60°C. The isolated RNA was quantified on a Nano drop before freezing.

B) cDNA preparation

For cDNA preparation, the QuantiTect Reverse Transcription Kit from QIAGEN was used. The kit protocol was followed as such without any changes. An initial RNA amount of 1μg was used for each reaction. All steps were performed on the Bio-Rad MyiQTM Single Color Real-Time PCR Detection system. The prepared cDNA was then stored at -20°C.

C) qPCR

For qPCR, the PowerUp™ SYBR™ Green Master Mix from Thermo Fischer was used. A total reaction volume of 10μl containing the master mix, primers and cDNA template was prepared by adding the components as mentioned below.

Component	Concentration/Dilution	Volume per well
SYBER green master mix	2x	5μl
Primer forward	5μmol/l	0.5μl
Primer reverse	5μmol/l	0.5μl
cDNA template	1:10/1:15	4μl

*A cDNA dilution of 1:15 was used for the house keeping genes (Gapdh and Hprt1), for all other genes 1:10 dilution was used.
All primers used are listed in appendix II.

The qPCR reaction was set up on a 96 well PCR plate (MicroAmp Fast 96-well Reaction plate (0.1ml), Thermo Fischer) by pipetting 6µl of the master mix for each gene per well and then adding 4µl of the diluted cDNA template to each well. Once the plate was prepared, it was sealed with an optical adhesive cover (Optical Adhesive covers, Thermo Fischer) and mixed on a shaker for 1 min at 800 rpm. The plate was then spun down and inserted into the Step-One Plus Real-Time PCR-System from Applied Biosystems. The PCR cycling program was set up in the software as mentioned below.

Step	Temperature	Duration	Comment
Initial activation/Amplification	95°C	5 mins	DNA polymerase is activated
Denaturation	95°C	30 sec	Melting of dsDNA
Annealing	58°C	30 sec	Annealing of primers
Extension	72°C	30 sec	Synthesis of new strands/measurement of fluorescent signal
Melting curve	65 - 95°C	10 sec	In 1°C steps
Total number of cycles = 45			

D) Analysis

After the run was completed, the raw data files including all the Ct values were exported as Excel sheets from the PCR machine. The data was then analyzed manually by the ΔΔCt method. Data from 3 bio-replicates were then analyzed together using the Graphpad Prism software to calculate the standard deviation, significance and mean standard error.

4.2.9 Immunoprecipitation (IP)/Co-IP

A) OPCs

Immunoprecipitation was performed using the Pierce™ Direct Magnetic IP/Co-IP Kit from Thermo Fischer. In order to identify the proteins interacting with Nup133, IP was performed on the 24hr treated OPC cell lysates using the Anti-Rabbit NUP133 Polyclonal antibody from

Proteintech. For each IP reaction, 5µg of Nup133 antibody was used for coupling with 30µl of bead solution and 1mg protein lysate was used for the antigen immunoprecipitation step.

The protocol supplied by the manufacturer was followed as such except that the bead-antibody coupling reaction was incubated for 1hr at 4°C and the quenching reaction was carried out with incubation at 4°C for 30 mins. The cell lysate was incubated with the antibody-bead complex overnight at 4°C and the final elution step was performed with 30µl of Elution buffer instead of 100µl mentioned in the protocol. The eluted protein was first neutralized and then frozen directly at -80°C (to be analyzed by western blotting later).

B) OLN93 cells

IP was performed exactly as mentioned above using the OLN93, 24hr treated cell lysates with Anti-Rabbit NUP133 Polyclonal antibody from Proteintech. But in this case, after the antigen was immunoprecipitated, the complex was washed as mentioned in the protocol and then the precipitated proteins were directly digested on the beads and were prepared for Mass Spectromertic analysis.

4.2.10 Chromatin Immunoprecipitation – Next generation sequencing

A) ChIP

Chromatin immunoprecipitation was performed using the MAGnifyTM Chromatin Immunoprecipitation System kit from Thermo Fischer. The manufacturers' protocol provided with the kit was followed to perform the experiments except for the below mentioned changes:

Step 1 - For the immunoprecipitation, 20µl of Dynabeads Protein A/G was used for each reaction and an antibody (Anti-Rabbit NUP133 Polyclonal antibody, Proteintech) concentration of 10µg was used for the bead-antibody coupling step. The volume of dilution buffer used in the subsequent step was also scaled up accordingly. The coupling reaction was carried on for 2 hrs instead of 1hr mentioned in the protocol. For positive control, 5µg of Mouse Anti-Estrogen receptor alpha (33) mAb from Thermo Fischer was used and the respective negative control antibodies provided in the kit were used for the negative control samples.

Step 2 - For each experiment; male and female derived OPCs were trypsinized and directly fixed with 37% Formaldehyde solution for 15 mins. The reaction was stopped by adding Glycine as mentioned in the manufacturers' protocol. The cell pellet was then washed 2 times

with 1xPBS (cold) and then lysed using 100µl of lysis buffer (provided in the kit) per tube. Cells were kept on ice and incubated for 15 mins with intermittent vortexing (3-5 times) to ensure that the cells were lysed properly. The lysate was then frozen at -80°C till the chromatin shearing was performed.

Step 3 - Mechanical shearing of the chromatin was performed by sonicating the samples on ice using a Bandelin Probe Sonicator for 35 sec, 9 cycles and at a power of 40%. The samples were then centrifuged at 14,000rpm for 5mins at 4°C and the supernatant was collected and stored in labelled tubes at -80°C. To check the DNA fragmentation, 5µl of the supernatant was loaded onto 2% agarose gel and electrophoresed at 75V for about an hour. O' gene Low range DNA ruler was used to determine the fragment size on the gel.

Step 4 - For diluting the chromatin, a 1:1 dilution was used for all experimental samples including the input controls and the positive and negative controls. The dilutions were performed exactly as mentioned in the protocol.

Step 8 - For purifying the DNA, 80µl of DNA purification magnetic beads diluted in DNA purification buffer was used for each reaction. The samples were incubated with the purification beads for 10 mins at RT. Finally, the purified DNA was eluted in 30µl of DNA elution buffer.

The eluted ChIP output DNA was quantified on a Nano drop and stored at -20°C.

B) Illumina NextSeq sequencing and data processing

The prepared ChIP output DNA form 4 individual bio-replicates, along with an Input Control for each sample was outsourced for NGS. The Illumina NextSeq 500 platform and a high-output v2 1x75bp cycles kit were used to sequence the Illumina TruSeq ChIP libraries. The produced single-end reads which passed Illumina's chastity filter were subjected to de-multiplexing and trimming of Illumina adaptor residues using Illumina's real time analysis software (no further refinement or selection was done). The quality of the reads was checked with the software FastQC (version 0.11.7). Subsequently, the reads were mapped to the mm10 reference genome using the software BWA-MEM (version 0.7.17). PCR and optical read duplicates were removed from the mapping files using the software Picard (version 2.9.0). Peak calling, annotation (e.g., distance to nearest transcription starting site), motif search and pathway analysis was done with the software HOMER (version 4.9). Librarie preparation, sequencing and data analysis described in this section were performed by Microsynth AG

(Balgach, Switzerland). Integrated Genome Viewer (IGV) software was used for further analysis.

C) ChIP-qPCR (NGS Validation)

Validation of the NGS results was performed using ChIP-qPCR. Three independent ChIP experiments were performed using exactly the same protocol described above for ChIP-Seq and the data was generated from separate qPCR runs. The identified peaks of the genes of interest were overlaid on the reference genome using the USCS genome browser to identify the specific regions of the target genes to which the detected peak sequence aligned. Primers were then designed using these specific regions of the gene to yield a maximum product size of not more than 100bp. The NCBI Primer design tool, primer-BLAST (https://www. ncbi.nlm.nih.gov/tools/primer-blast/) was used to design the primers using RefSeq mRNA for reference to flank each targeted peak site. Primer pairs were cross-checked for spurious hybridization potential using UCSC *In-Silico* PCR web server (https://genome.ucsc.edu/cgi-bin/hgPcr?db=mm10) against the mouse (mm10) reference genome to minimize spurious hybridization. The primers used for validation are as listed in appendix II.

4.2.11 Genotyping

Genotyping was performed for the sex-determining region Y (SRY) gene of mouse by PCR using DNA isolated from CD1 mouse (pups) tissue in order to determine the gender.

DNA isolation – DNA was isolated from tail tip or a part of the brain tissue using the QIAamp DNA Kit Mini from QIAGEN. The protocol was followed exactly as mentioned by the manufacturer. In the final step, DNA was eluted from the column using 50µl of elution buffer, was quantified on the Spectrophotometer (Genesys 10S UV-Vis, Thermo Fisher) and stored at -20°C.

PCR – The primer sequence for the SRY primer used is as follows:

Forward Primer 5′-GTGAGAGGCACAAGTTGGC-3′ and Reverse Primer 5′-TCTTAAACTCTGAAGAAGAGAC-3′ (Eurofins). The primer was diluted to obtain a 5µM/l working concentration. For amplification, the DreamTaq DNA-Polymerase (Thermo Fisher) was used. The reaction mixture was prepared with a total volume of 20µl per reaction as shown below:

Component	Volume	Final concentration
DNA	500ng	25ng/µl
10x Buffer	2µl	1x
dNTPs	0,4µl	200nM
Primer *F*	0,1µl	100nM
Primer *R*	0,1µl	100nM
Polymerase	0,1µl	0,5U
DEPC-ddH$_2$O	Fill upto 20µl	-

A master mix was prepared first with the 10x buffer, dNTPs and primers calculated together for all samples. At first, DEPC-ddH2O was pipetted into 8-Tube PCR strips followed by 2.7µl of the master mix per tube and the DNA template was added at the end. PCR was run on the Bio-Rad MyiQTM Single Color Real-Time PCR Detection system. The PCR amplification program was as follows:

Phase	Temperature	Duration	
Initiation	95°C	3min	
Denaturation	95°C	30sec	
Annealing	57°C	30sec	40 cycles
Elongation	72°C	1min	
Final Phase	72°C	7min	

After the reaction was finished, the samples were loaded on a 2% agarose gel and electrophoresed at 100V. The bands were visualized under UV light using a Gel Doc system (ChemiDoc, Bio-Rad Laboratories) and images were captured.

4.2.12 Flow cytometry (FACS)

A) Primary OPC culture characterization

Flow cytometric analysis was performed initially during establishment of the primary OPC cell culture method, for identifying the percentage population of cells in male and female derived cultures that expressed the OPC markers A2B5 and PDGFRα after culturing with B104 conditioned media for 2 weeks. For this characterization, FACS measurements were performed with cells cultured at 21%O$_2$ and 3%O$_2$ simultaneously and also from different wild type mouse strains to identify the best conditions that could yield the highest amount of A2B5 and PDGFRα positive OPCs.

Cells were pooled from male and female flasks separately (only the spheres in suspension were used) into 50 ml falcon tubes, centrifuged at 2000rpm for 10 mins and the supernatant was discarded. The cell pellet was then trypsinized with 2ml TrpLE^{TM} solution by incubating at 37°C for 10 mins. After trypsinization, the pellet was resuspended in 5 ml cold FACS buffer and the cell suspension was passed through a 40µm Cell strainer (BD Bioscience). The resultant suspension was centrifuged at 2000rpm for 10 mins and the pellet was then resuspended in 1ml cold FACS buffer. Cells were then counted using a hemocytometer and the dilution was adjusted in such a way as to obtain approximately $1x10^6$ cells per 100µl volume. A total volume of 100µl was dispensed into each FACS tube and the antibodies (Anti-A2B5-APC mAb conjugate (Clone- 105-HB29), Miltenyi Biotec; Mouse IgM-APC Isotype control antibody, Miltenyi Biotec; PE Anti-Mouse CD140a (Clone- APA5), Biolegend; PE Rat IgG2a, k Isotype Ctrl (Clone- RTK2758), Biolegend) were added directly to the tubes to obtain a final dilution of 1:50. Tubes were mixed shortly and incubated in dark at RT for 1hr. After the incubation, the cells were washed 2 times by adding 2ml of FACS buffer to each tube and centrifuging at 1500rpm for 5 mins each. After washing, the stained pellet was resuspended in 300µl FACS buffer and the tubes were kept in dark on ice until they were measured.

Measurement was done on a BD FACS Canto machine. For compensation, the compensation beads (Comp Beads, BD Bioscience) coupled with PE and Alexa Fluor 647 (for APC) was used. After the compensation, using the isotype controls, the gates were set and the samples were measured with 100000 events per sample. Data was later analysed using the FlowJo software.

B) Apoptosis detection

In order to determine the extent of apoptosis in the male and female derived OPCs after 24-48hrs 80%O_2 treatment, the CellEventTM Caspase-3/7 Green Flow Cytometry Assay kit was used. For each test, staurosporin treated cells (in a concentration of 0.5µM) for 24/48hrs were used as positive control. The staining protocol was performed exactly as mentioned in the manufacturer's protocol with $1x10^6$ cells in each tube.

Measurement was done on a BD FACS Canto machine. For compensation, the compensation beads (Comp Beads, BD Bioscience) coupled with PE (for Caspase) and Alexa Fluor 647 (for SYTOX) was used. After the compensation, using the controls, the gates were set and the

samples were measured with 100000 events per sample. Data was later analysed using the FlowJo software.

4.2.13 *In silico* molecular docking

The chemical structures of the FZSs (ligands) were downloaded from PubChem (https://pubchem.ncbi.nlm.nih.gov/) and the structures of the receptor molecules including the ligand binding sites were downloaded from the RCSB Protein Data Bank (http://www.rcsb.org/). Downloaded structures were loaded onto the Maestro 10.4 software where the structures were modified. For example, the ligands already attached to the receptors were removed making the binding sites free for the test ligands. The modified ligand and receptor structures were then loaded onto the UCSF Chimera (1.10.2) software and docking was performed using the Autodock Vina function.

4.2.14 siRNA transfection

Transfection experiments were performed using Lipofectamine RNAiMAX Transfection Reagent (13778-150, Thermo Fischer Scientific) according to the manufacturer's protocol. Reverse transfection was the chosen method used for performing the experiments. For each experiment, cultures of OLN93 cells (passage 25-32) were trypsinized, counted (2 x 10^6) and seeded into standard 6-well plates into which the siRNA-Lipofectamine complexes were directly added at the same time. A final siRNA concentration of 50pm per well was used. Stealth RNAi™ siRNA Negative Control, Med GC (12935300, Thermo Fischer Scientific) was used as the negative control. Cells were incubated at 37℃, 5%CO_2 and normal room air for 48h. The cells were then subjected to RNA (with Trizol) and protein isolation.

Table 4. siRNA sequences

siRNA sequence	Company	Catalog no.
siRNA sequence (5'-3') : Nup133 #1: GAUUGCUUCCUGGACAGCUACGUUU AAACGUAGCUGUCCAGGAAGCAGUC	Thermo Fischer Scientific	Cat # 1330001; Assay ID# RSS307530
siRNA sequence (5'-3') : Nup133 #2: GCACCACAGCUCAUCAGUCUGUAUA UAUACAGACUGAUGAGCUGUGGUGC	Thermo Fischer Scientific	Cat # 1330001; Assay ID# RSS307532

4.2.15 Human infant urine study

This study was approved by the Ethics Committee of the Justus Liebig University of Giessen (reference number 04/02) and confirm to the Declaration of Helsinki regulatory standards and was performed in Giessen. A written informed parental consent was obtained from all the subjects included in this study.

Preterm infants with a gestational age of less than 30 weeks 11 and more than 30 weeks 130, who had no family history of adrenal illnesses and who had no major congenital anomalies, were eligible for the study. Postnatal steroid therapy was considered as a criterion for exclusion. Gestational age was determined using the expanded Ballard score and/or obstetrical dating.

Preterm infants were classified as being well according to previously described criteria [131]. Well infants had no signs of infection and did not receive treatment with surfactant or inotropes. Ill preterm infants suffered from one or more of the following diseases: respiratory-distress syndrome treated with surfactant, infection at birth (C-reactive protein > 10 mg/liter and symptoms of an infection during the first 72 h of life), hospital infection (C-reactive protein > 10 mg/liter and symptoms of an infection after the first 72 h of life), ventricular hemorrhage more than II° according to the criteria described by Papile et al. [132].

Twenty-four-hour urine collections were made frequently in the first week after birth, i.e. on the first, second, third, and fifth day. Only the data from the first three days after birth was considered to generate the data as the severity of illness was expected to be highest in this period. The urine-collection procedure was performed as described previously 133. Urinary steroid profiles were determined by GC-MS analysis according to the procedure previously described[133]. A total of 17 C21-steroids/metabolites were determined by selected ion monitoring as listed in Table 5.

Table 5: List of 3ß-hydroxy-5-ene-steroids identified in human infant urine samples.

	Metabolites	
1	A5-3ß17a	5-androstene-3ß,17adiol
2	DHEA	5-androstene-3 β,OH-17-one
3	16a-OH-DHEA	5-androstene-3 β,16a-diol-17-one
4	16ß-OH-DHEA	5-androstene-3ß,16ß-diol-17-one
5	15ß16a-OH-DHEA	5-androstene-3ß, 15ß, 16a-triol-17-one

6	16-O-A5D	5-androstene-3β, 17ß-diol-16-one
7	A5T-16a	5-androstene-3ß,16a,17ß-triol
8	A5T-16ß	5-androstene-3ß,16ß,17ß-triol
9	16a18-OH-DHEA	5-androstene-3β, 16α, 18-triol-17-one
10	15ß17a-OH-P5-olon	5-pregnene-3ß,15ß,17a-triol-20-one
11	16a-OH-P5-olon	5-pregnene-3ß,16a-diol-20-one
12	A53b16a17b18tetrol	5-androstene-3ß,16a,17ß,18-tetrole
13	A53b15b16a17btetrol	5-androstene-3ß,15ß,16a,17ß-tetrole
14	15ß-OH-P5-tetrol	5-pregnene-3 β, 15ß, 17a,20a-tetrol
15	21-OH-P5-olon	5-pregnene-3ß,21-diol-20-one
16	P5-3ß20a21-triol	5-pregnene-3ß,20a,21-triol
17	P5-tetrol	5-pregnene-3ß,16a,20a,21-tetrole

To assess the overall secretion, these 17 major urinary metabolites were quantified (peak-area integration) and summed. Daily urinary excretion rates of the metabolites were corrected for body weight per micromoles creatinine to take into account changes in glomerular filtration rate [133].

Differences in fetal zone steroid concentrations between healthy terms and healthy preterms were visualized by box plots. Associations between groups of infants (sick preterms, healthy preterms and terms) with fetal zone steroid concentrations were analyzed by linear regression models in the whole population as well as stratified by sex. The beta coefficients and the belonging 95% confidence intervals were plotted. All analyses were performed using the Stata version 15.1 software (Stata Corporation, College Station, TX, USA).

4.2.16 Statistical analysis

The statistical analysis for western blot and real time PCR were performed using the GraphPad Prism 5 software. Data from all bio-replicates (minimum 3 for each experiment) for each experiment was plotted with the mean value and standard error bars (standard error of mean, SEM). For statistical comparison between two variables, unpaired Student's t-Test was used and One way ANOVA (one-way analysis of variance) with Tukey's/Dunnet's post-hoc Test was applied to compare between multiple treatment groups. A variance with a P value < 0.05 was considered significant. Various levels of significance were depicted as follows: $*p < 0.05$; $**p < 0.01$; $***p < 0.001$.

5. RESULTS

5.1. PART 1 (EFFECT OF HYPEROXIA)

5.1.1 Hyperoxia leads to impairment of differentiation in male OPCs.

To begin with, we tested different concentrations and time periods of oxygen treatment (corresponding to what is used in the neonatal intensive care) to find an optimum that allowed us to identify the initial target proteins affected by hyperoxia whose effect could be otherwise masked by the later response of large number of proteins responding to wide spread severe oxidative stress and cell death. In our model system, experiments were performed with separate male and female derived OPCs simultaneously. The cells were given an optimum treatment regime of 80% oxygen shock for 24h and then were returned back to normal oxygen conditions and were allowed to recover and differentiate for 4 days. It must be noted that at the time point O_2 shock, they are largely immature and vulnerable to oxygen damage. The aim of designing the experiment with a recovery time was to see how this exposure of oxygen to the immature cells affects their maturation capability. After this, the protein expression of CNPase, an early OPC differentiation marker was checked in both male and female cells using western blot (Figure 1-A). We checked CNPase expression as under the given culture conditions we did not use any additional specific factors for inducing advanced myelination. The expression of CNPase was found to be significantly downregulated in the male OPCs (p<0.01). A qualitative assessment using immunofluorescence with CNPase antibody showed a much more severe effect of oxygen on the male cells with very few cells even attached to the surface of the plate. On the other hand, the female cells could adhere to the culture plate and also differentiate. Even though the overall observed number of differentiated cells was relatively less as compared to the normoxia control, the female cells looked much more vital and also differentiated much better than the male cells (Figure 1-B). Concerning cell death, we assessed the cells microscopically using propidium iodide staining and found that after 24h oxygen treatment and recovery, the male cells were only stressed to an extend that they no longer could adhere to the surface but rather floated in the medium with 90% of the cells alive. The cells in suspension were however washed away during the subsequent stages of immunofluresence staining. Even though it is previously known that hyperoxia leads to an impairment of maturation in OPCs [2-4, 134], these results indicate that there exists a sex based difference in this response and that the male cells seem to be more sensitive to hyperoxic treatment.
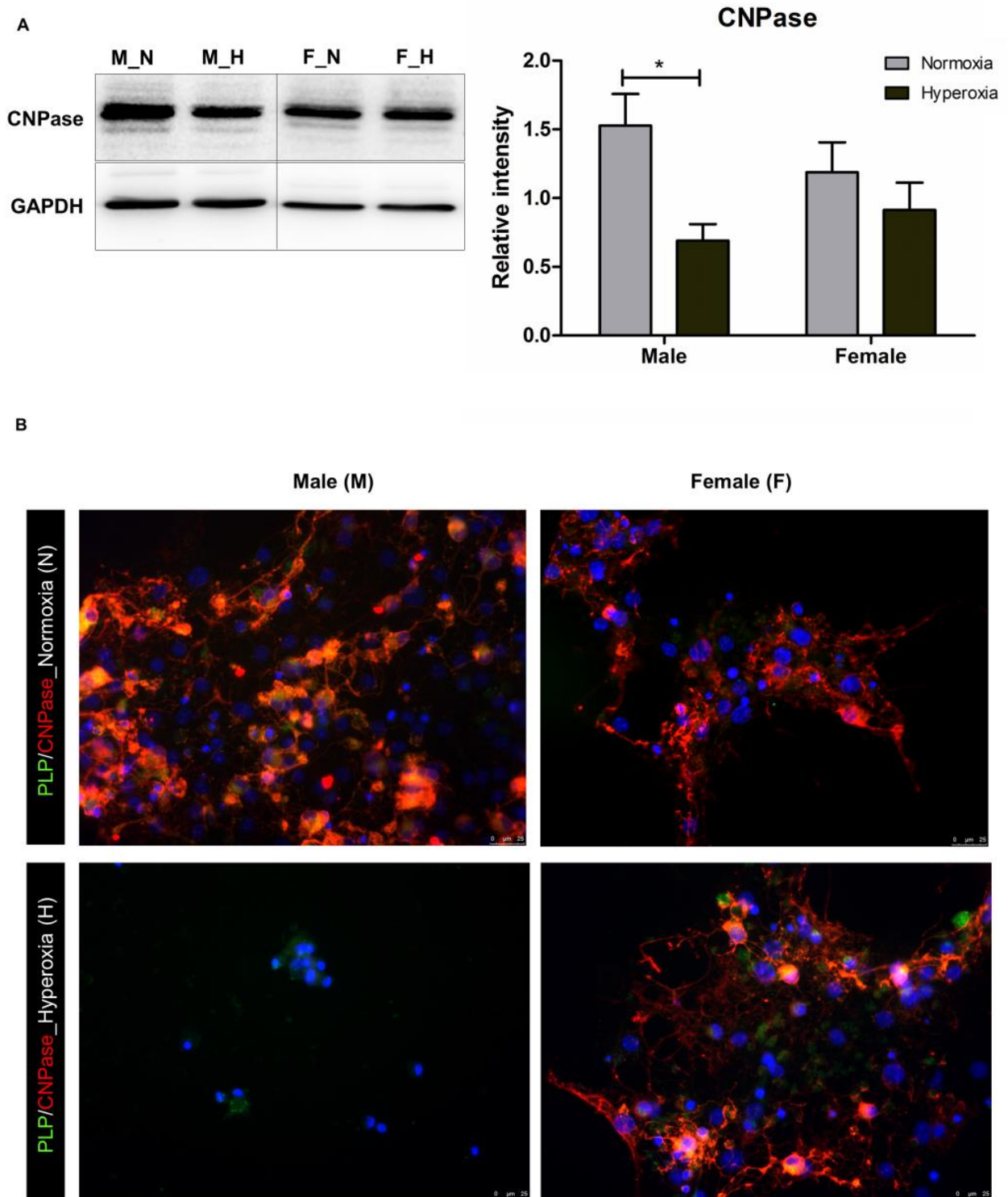
Figure 10. Hyperoxia leads to impairment of maturation in OPCs.
(A) Western blot analysis of male and female OPCs with anti-CNPase antibody at normal
($3\%O_2$) differentiation conditions and 24h post $80\%O_2$ shock, showing a significant decrease
in expression in the male OPCs. (CNPase is usually expressed in two different biological
active isoforms, observed as bands of molecular sizes 46 kD and 48 kD. Since the
representative blot shown in the figure was generated from an 8% resolving gel, the difference
of 2kD is observed as a single thick band. However, when analysed on a 12% gel, 2 bands

were observed. However, for the analysis and results shown here, all blots with 8% resolving gel were used and hence both isoforms were included).

(B) Representative images of male and female OPCs stained for the OPC maturation marker CNPase after differentiation under normal oxygen conditions and post 24h 80%O_2 shock. Scale bar represents 75µm.

Data are representative of three independent experiments. Bars and error represent mean ± SEM of replicate measurements. $*p < 0.05$, $**p < 0.01$, $***p < 0.001$, $****p < 0.0001$ (Student's t test).

Alterations were also observed in the expression of proteins related to cell adhesion and migration in the male derived cells post hyperoxia (Figure 11). Since the ability of cells to adhere is considered one of the essential factors to initiate cell differentiation, this could also be an additional factor affecting differentiation post hyperoxic treatment.
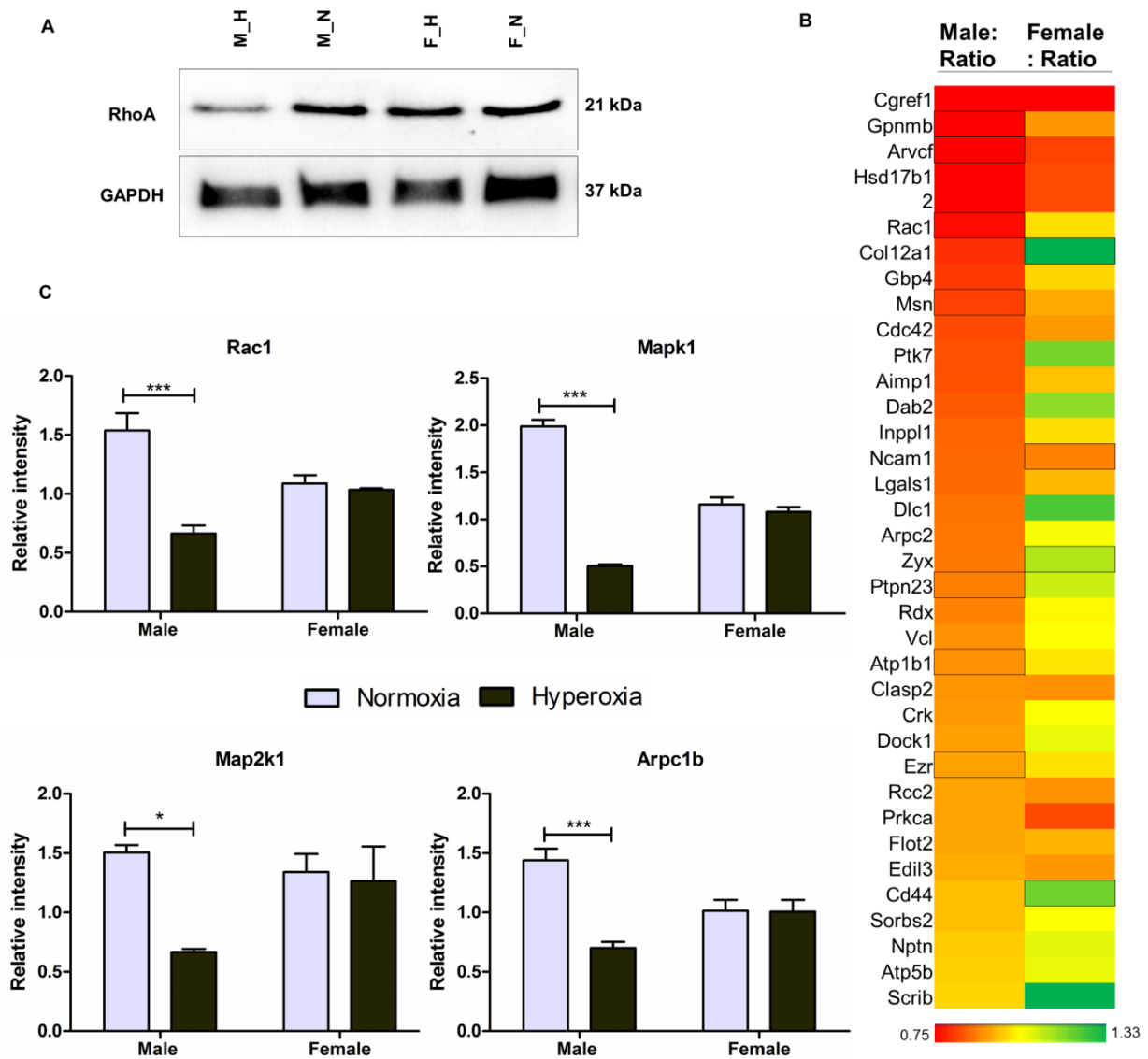

Figure 11. Proteins involved in cell adhesion and migration downregulated in male OPCs.

(A) Immunoblot analysis of RhoA protein showing downregulation in male OPCs post 24h 80%O_2 treatment.

(B) Heat-map representation of adhesion proteins that were dysregulated in male and female derived OPCs post 24 h 80%O_2 treatment in comparison to 3%O_2 (normoxia) controls. Mapped expression ratios are depicted with a color scale as shown in the figure, such that highly downregulated proteins are indicated in red, intermediate in yellow, and highly upregulated proteins in green. Proteins are sorted according to Gene ontology (biological process). Dark outlined cells represent the significant proteins in each group. The cut off p value being 0.07. Data are representative of five independent experiments.

(C) Independent intensities of Rac1, Mapk1, Map2k1 and Arpc1b plotted from MS results showing a significant downregulation in male OPCs post hyperoxia.

Data are representative of three experiments. Bars and error represent mean ± SEM of replicate measurements. *p < 0.05, **p < 0.01, ***p < 0.001 (Student's t test).

5.1.2 Hyperoxia leads to downregulation of lamins and nucleoporins.

In order to further assess the actual reasons behind such a pronounced effect of oxygen in the male cells, a global proteome analysis was performed using tandem mass spectrometry (MS). Male and female derived cells were treated with 80% oxygen for 24h; after this time point they were lysed and tryptic peptides were prepared for MS from this cell lysate. Analysis of MS data revealed a higher number of altered proteins in male than in female cells when compared to the respective normoxic control, with a very little overlap between the identified proteins in both the groups (Figure 12-B). This finding strongly supported the previous observation that the male cells were much more sensitive to oxygen than the female counterparts. Gene ontology based cellular function analysis showed that some of the major cellular functions such as protein synthesis, cellular growth and proliferation, and molecular transport were affected to a much greater extent in the male cells (Figure 12-A).
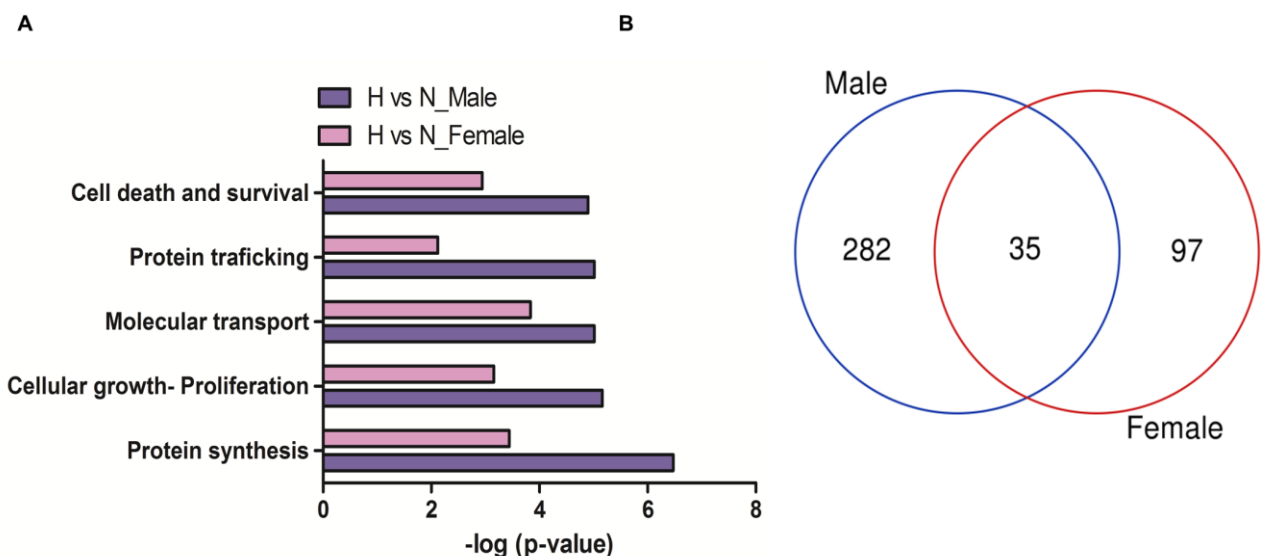
Figure 12. Hyperoxia leads to an overall severe effect on the male OPCs.
(A) Functional categorization of significantly enriched proteins in male OPCs and female OPCs post 24h 80%O_2 treatment using IPA. Bar graphs depict the most extensively enriched biological processes among the altered proteins. Cut off p value < 0.05 (Fisher's exact test). (B) Venn diagram of significantly altered proteins (normalized to the normoxic conditions) in male and female OPCs post 24h 80%O_2 treatment. Cut off p value < 0.05. Data are representative of five independent experiments.

Detailed protein interaction analysis of the significantly altered proteins as a result of hyperoxia in both male and female cells using STRING interaction networks and the independent intensity plots from MS showed a downregulation of all detected types of lamins and many nucleoporin proteins only in the male derived cells (Figure 13 A-B).
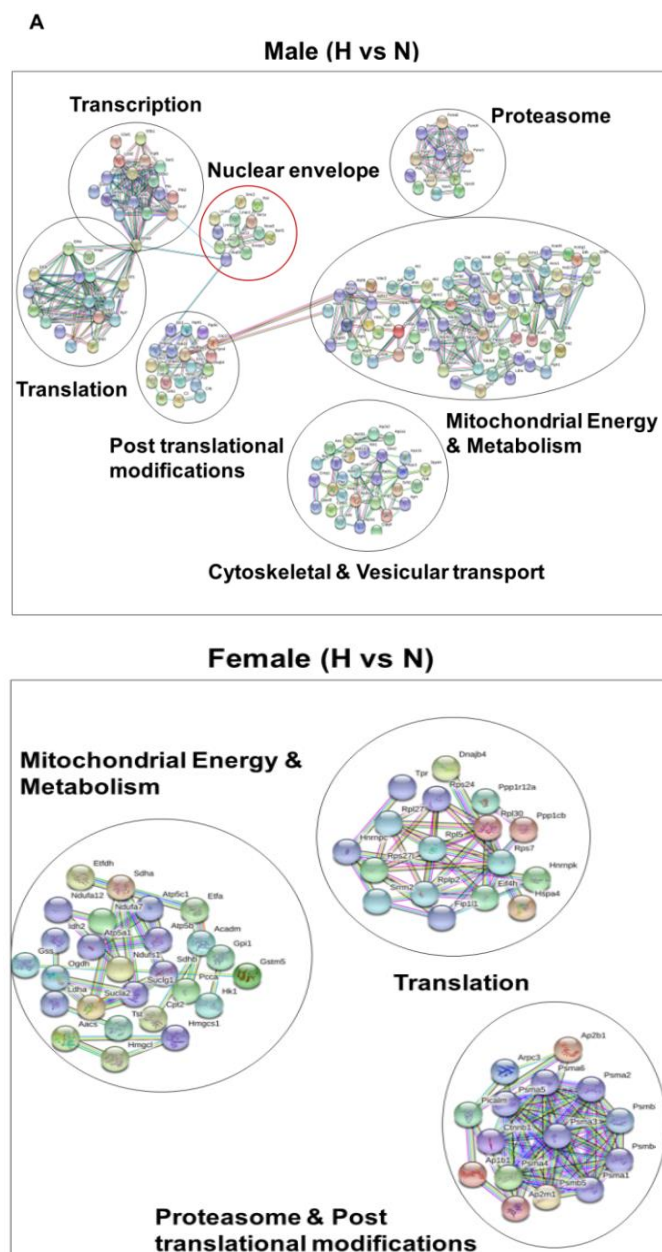
Figure 13. Nuclear envelope (NE) proteins are downregulated in male OPCs as a result of hyperoxia.
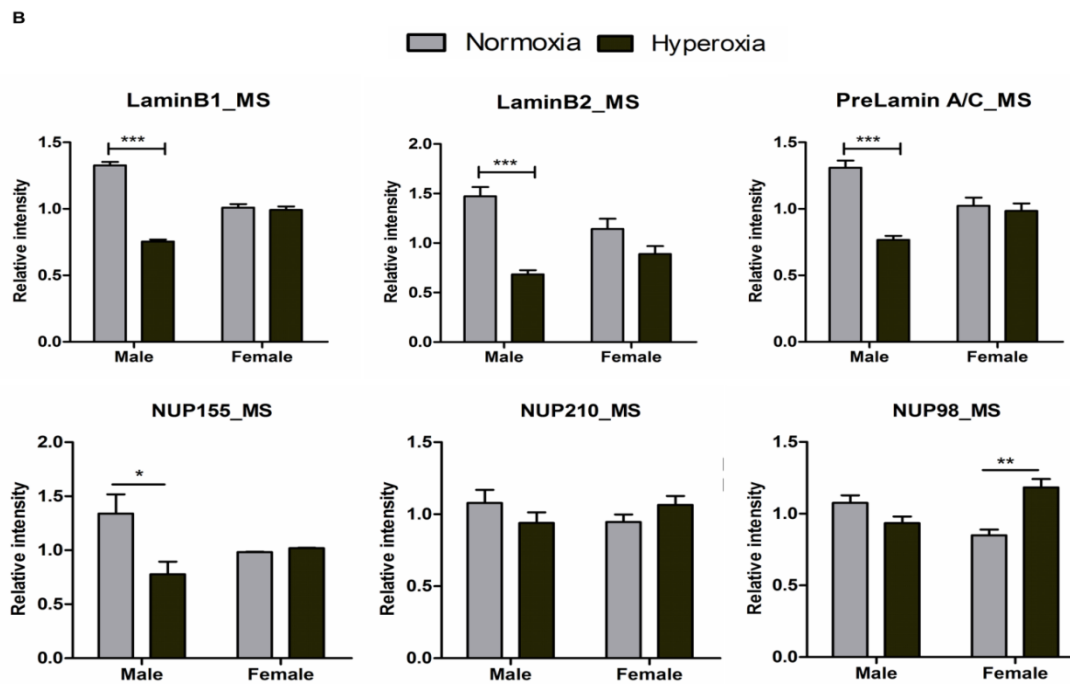
(A) STRING Protein interaction analysis of the significantly altered proteins (p< 0.05) in the male (hyperoxia vs normoxia) and female (hyperoxia vs normoxia) groups, with an interaction score of highest confidence (0.900), showing the nuclear envelope proteins to be altered only in the male group.

(B) Intensities of Lamin B1, Lamin B2, Pre-Lamin A/C, Nup210, Nup155 and Nup98 plotted from the mass spectrometry results show a significant downregulation of Lamin B1, Lamin B2, Nup155 and Prelamin A/C in male derived OPCs post hyperoxia. For Nup210 and Nup98 a similar trend in both cell groups was observed. $*p < 0.05$, $**p < 0.01$, $***p < 0.001$, $****p < 0.0001$ (Student's t test), n=3. Values are means ± SEM.

Independent validations of Nup133, Nup50, Lamin B1, and Nup210 by western blot and qPCR confirmed the downregulation only in the male cells (Figure 14 A-C). The above mentioned proteins were particularly interesting as all of them have been previously identified across different studies to be involved in CNS development.
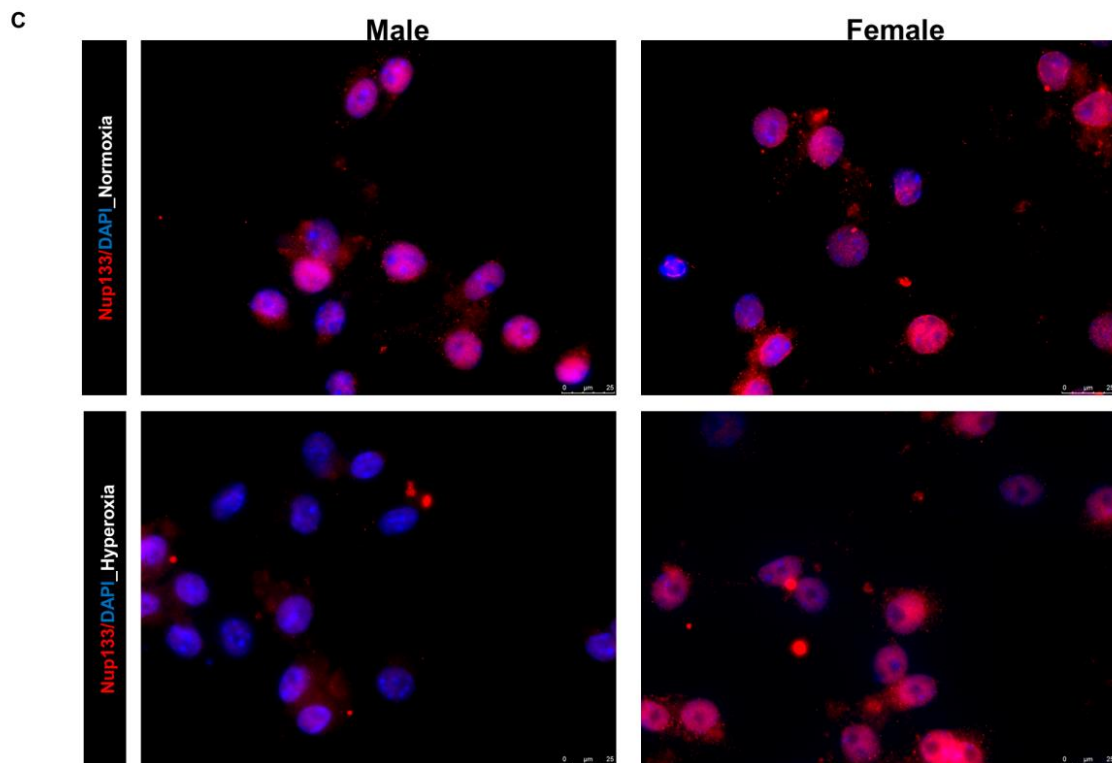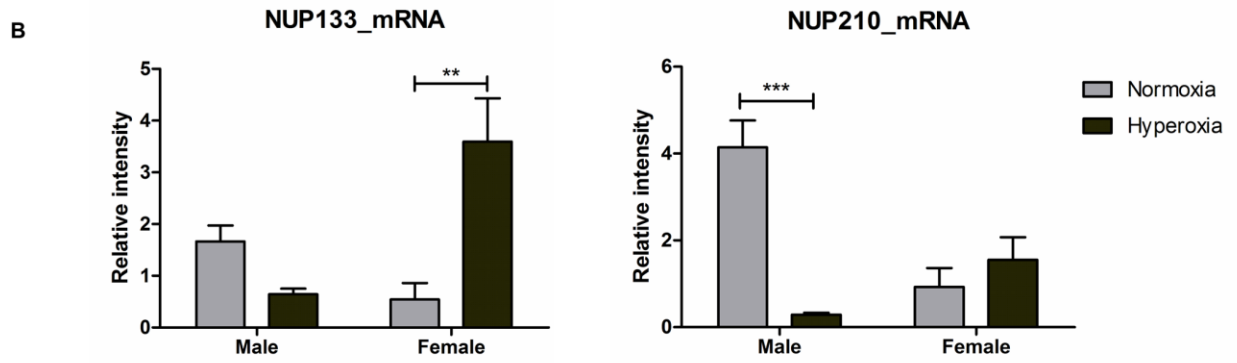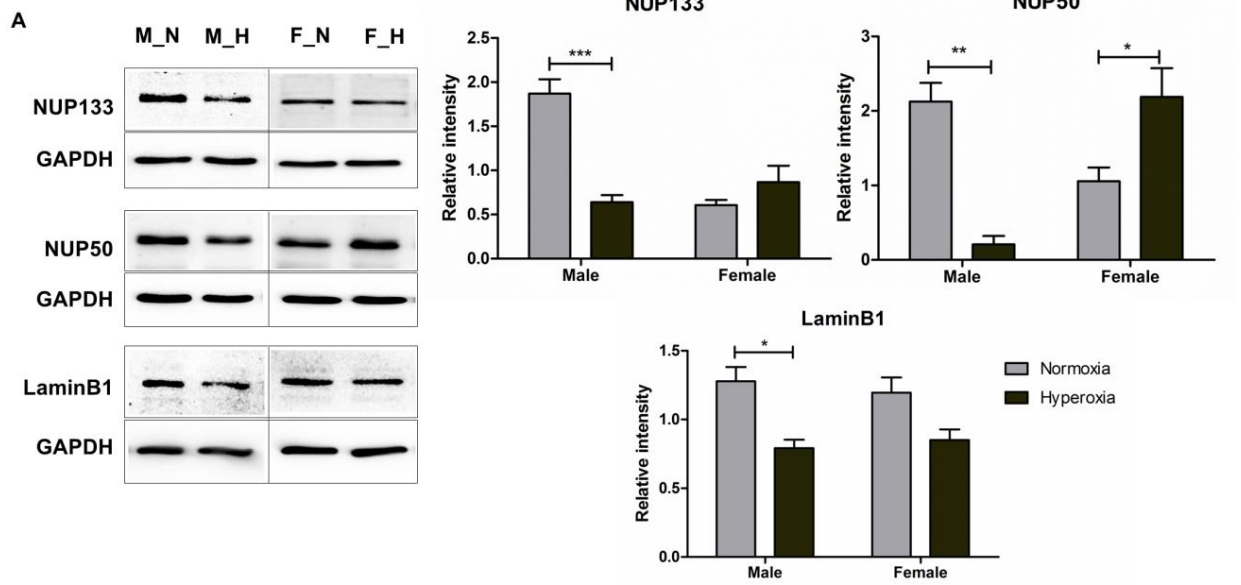
A

B

C

Figure 14. Independent validation of the mass spectrometry results proving that the expression of some of the nuclear envelope (NE) proteins are significantly downregulated in male OPCs as a result of hyperoxia.

(A) Western blot analysis of male and female OPCs with anti-Nup133, anti-Nup-50 and anti-Lamin B1 antibodies under normal ($3\%O_2$) conditions and post 24h $80\%O_2$ treatment, showing a significant decrease in expression in the male OPCs. Whereas in female OPCs, Nup133 protein expression showed a trend towards upregulation and Nup50 showed a significant upregulation post hyperoxia. ***$p<0.001$, **$p<0.01$, *$p<0.05$ (Student's t test), n=3. Values are means ± SEM.

(B) mRNA expression of Nup133 and Nup210 showing downregulation in male OPCs and upregulation in female OPCs post hyperoxia. ***$p<0.001$, **$p<0.01$, *$p<0.05$ (Student's t test), n=3. Values are means ± SEM.

(C) Representative images of mouse male and female OPCs stained for Nup133 after treatment under normal oxygen conditions and post 24h $80\%O_2$ shock. Scale bar represents 25µm.

Hence, all these nuclear proteins that are known to be important for CNS development can be identified as novel targets of oxidative stress leading to extended vulnerability in male cells.

It was notable that in case of all these nuclear proteins, a basal level difference in expression was observed with a higher abundance in the male cells compared to female cells. A similar difference with a slightly higher expression in the male cells was also found in case of CNPase (Fig. 10 A). This could imply that under similar conditions, the male OPCs differentiated more than the female cells. A previous study in rodent model [157] supporting this observation reports that at any given time point, the density of oligodendrocytes present in different parts of the male brain are 20-40% higher than in females. Our results from the proteome analysis also showed that there exists differences between male and female derived cells under normal conditions (Figure 15 A-B). Therefore, a better understanding of such inherent differences between both the sexes might also be helpful to predict cellular behavior.

A
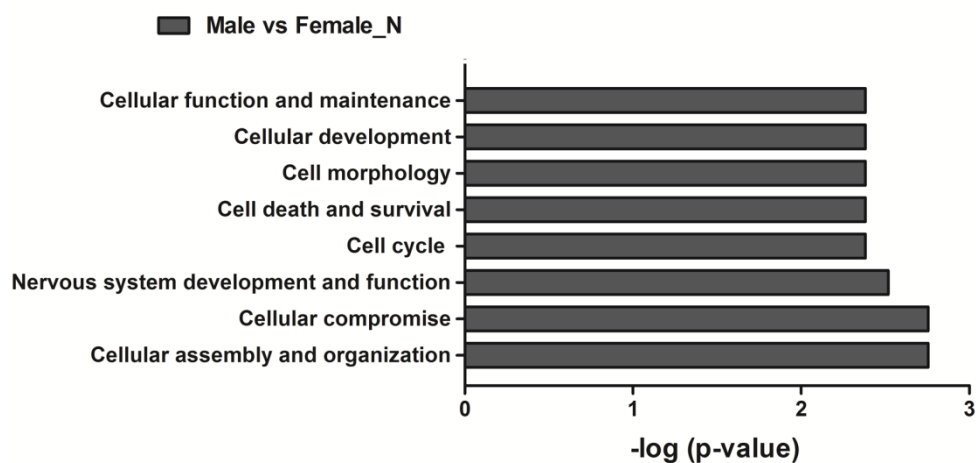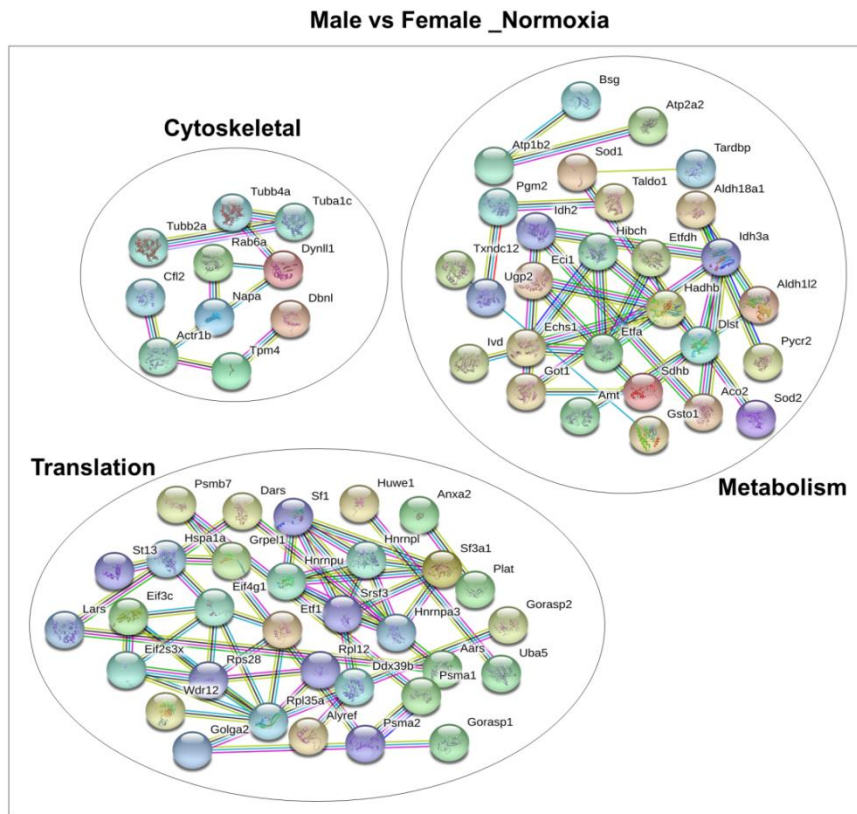
Figure 15. Inherent protein profile differences between male and female OPCs under normal conditions.
(A) Functional categorization of significantly different proteins in male and female OPCs under normal conditions using IPA. Bar graphs depict the most extensively enriched biological processes among the significantly different proteins. Cut off p value being 0.05.
(B) STRING Protein interaction analysis of the proteins detected to be significantly different (p< 0.05) in the male vs female (Normoxia) group from the MS data, with an interaction score of high confidence (0.700), showing proteins related to energy and metabolism, protein synthesis and a few cytoskeletal proteins to be differentially expressed in male and female cells.

5.1.3 Nup133 is involved in actively regulating the expression of differentiation related genes in OPCs.

Nup133 was further chosen to investigate its downstream targets because even though it is known that Nup133 plays a crucial role in neural cell differentiation, the mechanisms of its action are largely unknown. Hence, assuming that Nup133 could bind to the mammalian genome, targeted chromatin immunoprecipitation experiments followed by next generation sequencing were performed to identify its genomic targets. The Nup133 antibody to be used for ChIP-Seq was first validated by immunofluorescence and it was found that it stained intra-nuclear sites and nuclear periphery in both male and female derived cells. Additionally, the

antibody also proved to be efficient and specific in western blot and immunoprecipitation experiments (Figure 16).
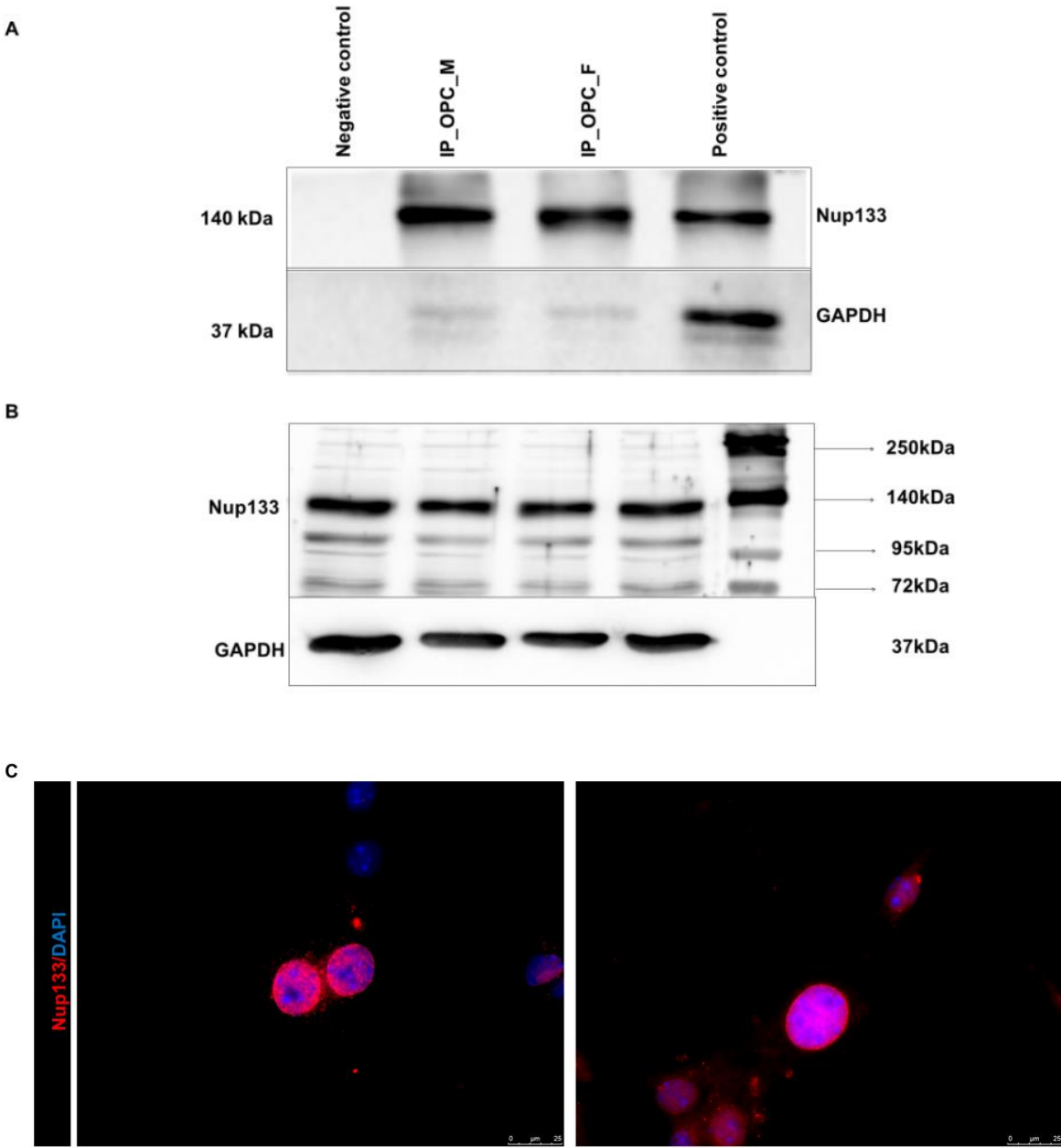
Figure 16. Nup133 antibody validation.
(A) Nup133 immunoprecipitation (IP) detected by immunoblot in male and female derived OPCs without any treatment. Positive control shown here is cell lysate obtained from male OPCs and negative control is the pull down product obtained from IP performed using control IgG antibody.
(B) Western blot detection of Nup133 bands in cell lysates prepared from untreated OPCs.
(C) Representative immunofluorescence images of OPCs stained for Nup133 at different focal plains. Scale bar represents 25µm.

The ChIP-Seq results were further validated by randomly selecting a few NUP133-binding peaks called from the ChIP-Seq experiment and confirming the interaction between NUP133 and these selected regions by ChIP-qPCR on three independently performed ChIP experiments (Figure 17).
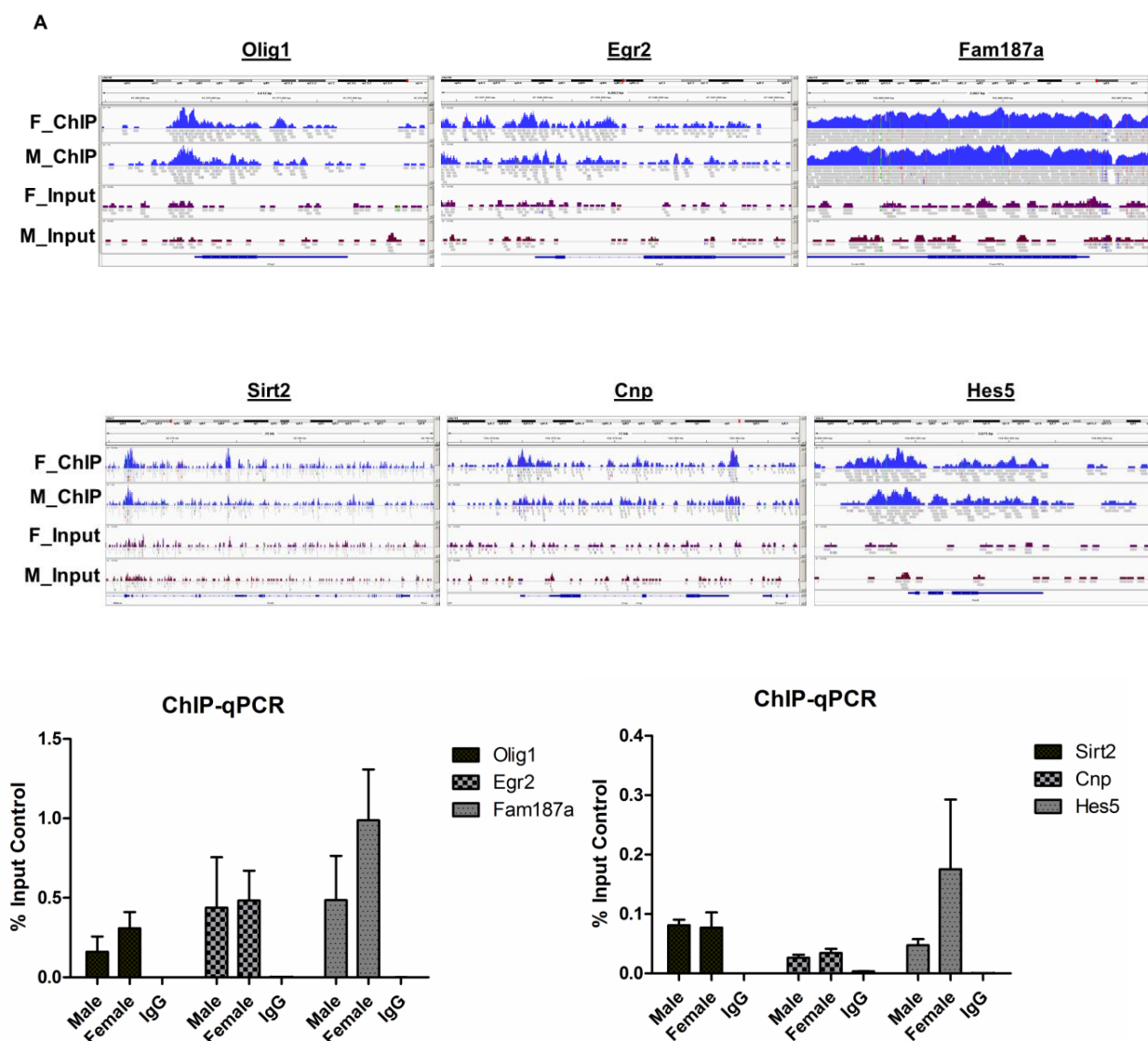
Figure 17. Validation of ChIP-Seq targets by ChIP-qPCR.
(A) IGV genome browser tracks showing enrichment peaks for each respective target. Primers were designed specifically ON-target covering the highest peak areas. Graphs depicting enrichment over total genomic input (%Input) for male, female and mock IgG (IgG) control conditions for 6 chosen gene targets identified by ChIP-Seq. Results for all ChIP-qPCR data were generated from three independent experiments.

Initially, to evaluate the global distribution of Nup133-occupied regions, the identified Nup133 bound sites were plotted against their distance to the nearest transcription start site (TSS). A strong enrichment for Nup133 occupancy within 1 kb of the nearest annotated TSS in both male and female groups (Figure 18-A) was detected, indicating that Nup133 has a

stronger occupancy around target promoters. Further analysis identified 18% of the total identified peaks localized to known (annotated) promoters in male cells and 16% in female cells with the highest occupancy at intron regions in both the populations (male – 40%, female – 41%) (Figure 18-B). Analysis of targets with protein-coding and non-protein-coding designations showed 87% of all identified targets as protein coding in both male and female cells (Figure 18-C). These results signify that Nup133 apart from its role in transportation might actually be involved in actively regulating gene expression. In order to see if there was any notable difference between the targets of Nup133 in male and female derived cells, the peaks identified upstream of promoter regions (1000bp) were analyzed in both the groups and it was found that there was only very little overlap of 17.6% suggesting a greater difference (data not shown). However, further analysis of these targets that were found to be unique in both the groups using Ingenuity Pathway Analysis software did not show any significant difference in the involved canonical pathways (data not shown).
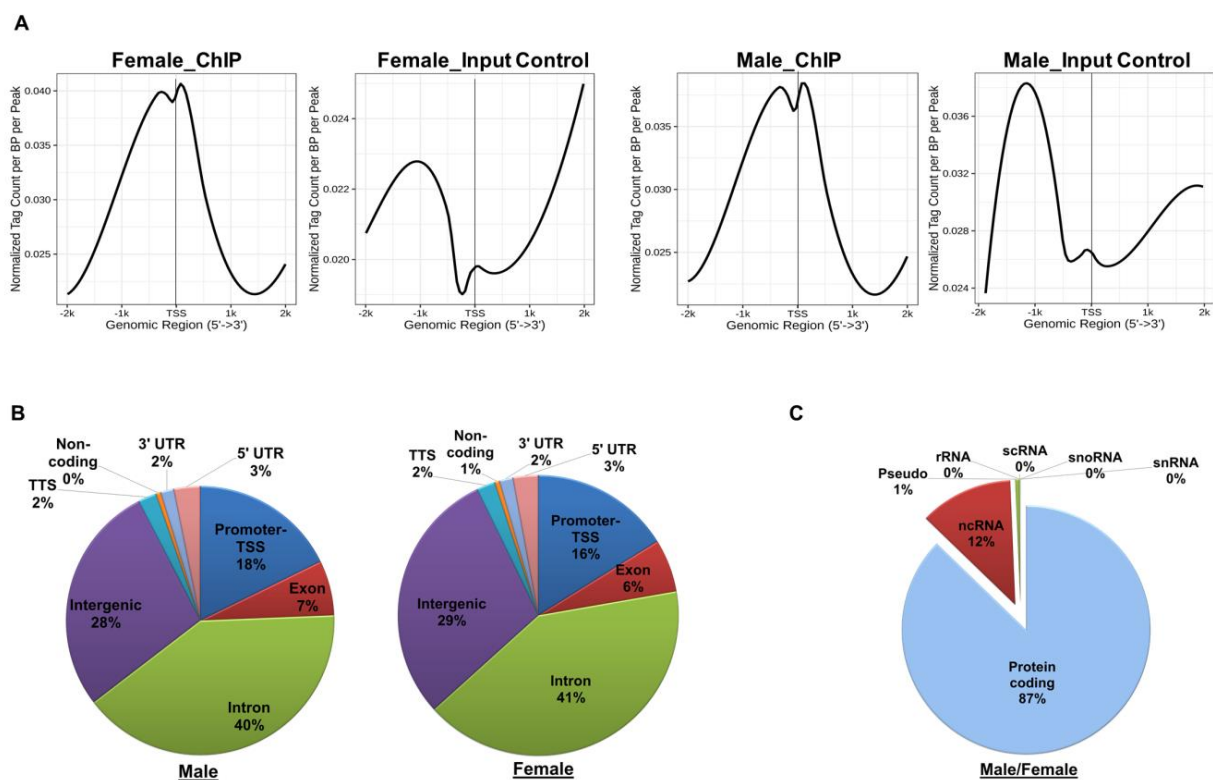
Figure 18. Identification of Nup133 targets in male and female OPCs.
(A) Line plot representation of ChIP-Seq signal density for Nup133 male and female ChIP and Input Controls centered on predicted TSS.
(B) Pie chart showing proportions of genomic landmarks corresponding to Nup133-bound targets.
(C) Pie chart showing proportions of targets with protein-coding or non-protein-coding designation.
ChIP-Seq data are representative of four independent experiments.

Most importantly, Nup133 occupancy was found at the promoter sites of many genes known to be critical for oligodendrocyte differentiation, like Cnp, Olig2, Egr2, Sox8, Id4 etc. (Figure 19). Some of these genes were also validated by qPCR and the results showed a trend exactly fitting into the hypothesis of Nup133 regulating the expression of these genes (Figure 20). Hence, these results show that NUP133 associates with and is actively involved in modulating the expression of developmentally regulated genes in both male and female derived OPCs.
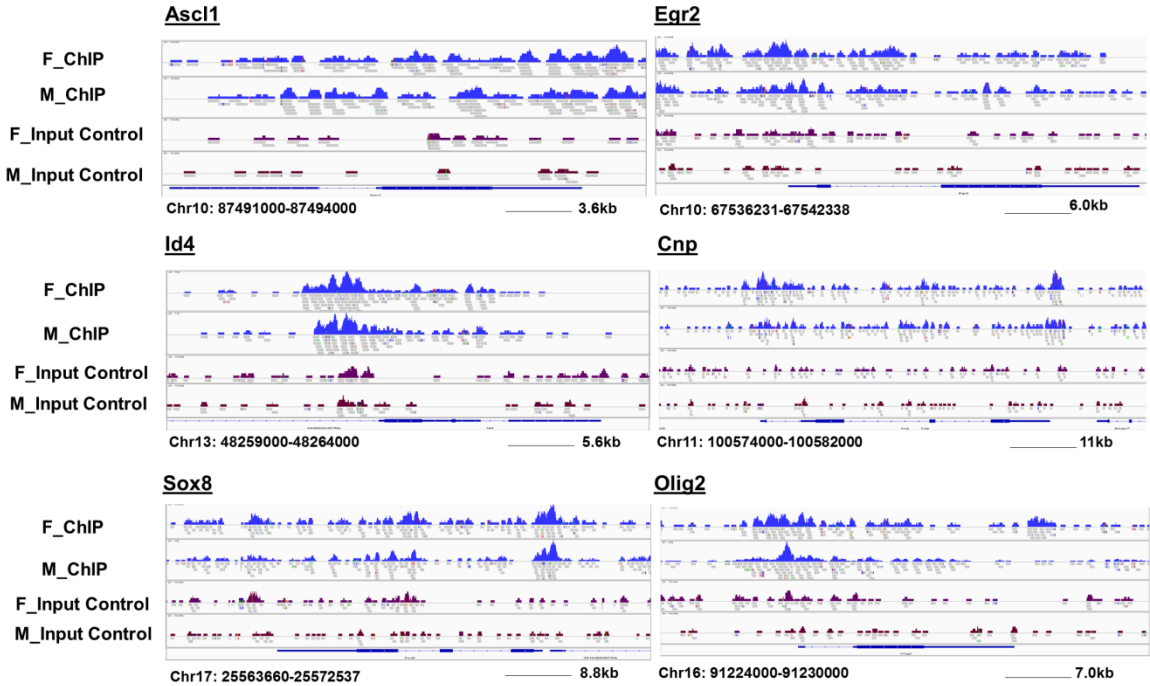
Figure 19. Integrative Genomics Viewer (IGV) visualization of Nup133 occupancy at selected target sites related to oligodendrocyte differentiation.
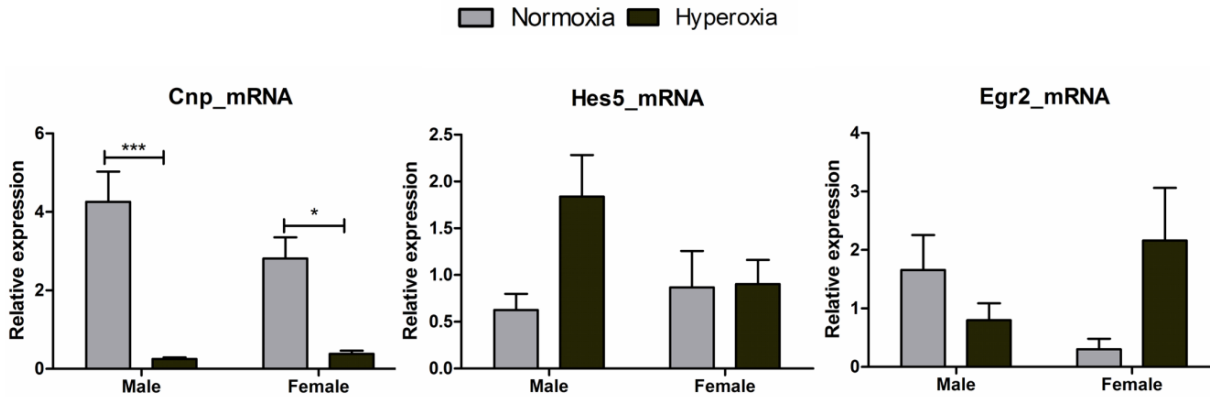
Figure 20. mRNA expression validation of Cnp and Egr2 showing downregulation in male OPCs post hyperoxia. Whereas Hes 5 that acts as a transcription repressor and a negative regulator of oligodendrocyte differentiation is upregulated in male OPCs post hyperoxia.

Data are representative of three independent experiments. Bars and error represent mean ± SEM of replicate measurements. $*p < 0.05$, $**p < 0.01$, $***p < 0.001$, $****p < 0.0001$ (Student's t test).

5.1.4 Nup133 mediates oxidative damage in male derived OPCs through its direct target Nrf1.

Analysis of known motifs using the software HOMER, identified Nuclear respiratory factor-1 (Nrf1) as the highest ranking significant motif common in both male and female cells (Figure 21-A). Nrf1 is an important transcription factor that activates the expression of various key metabolic genes regulating mitochondrial function and oxidative stress response[135, 136]. This finding strongly advocates for Nrf1 being a direct target of Nup133.
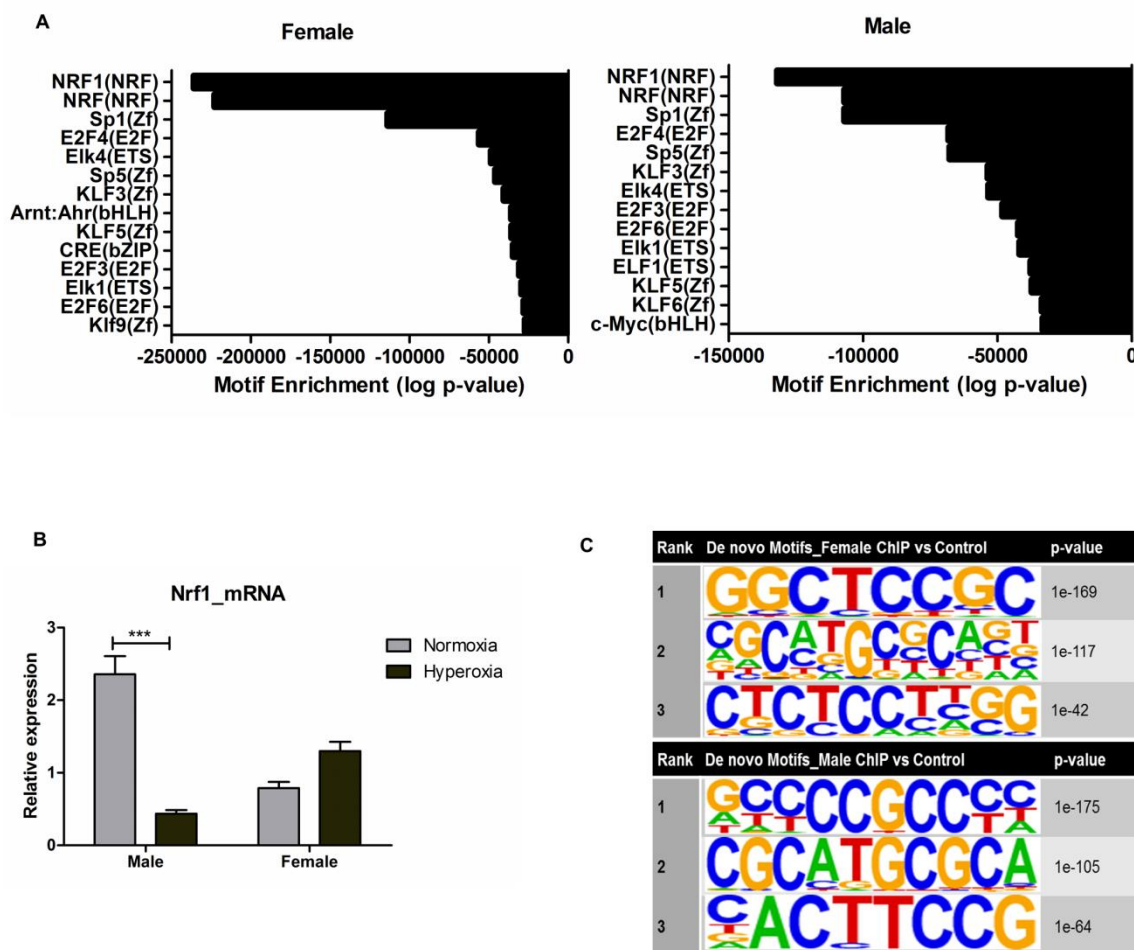
Figure 21. Motif analysis of Nup133 binding regions.
(A) Known motif analysis of Nup133-binding regions identified by the software HOMER. The highest significant motif was identified as Nrf1 and found to be common in both male and female groups. q-value determine by Benjamini correction was 0.0000 for all the represented motifs.

(B) mRNA expression validation of Nrf1 showing downregulation in male OPCs and a slight upregulation in female OPCs post 24h hyperoxia. Real time PCR data is representative of three independent experiments.

(C) De novo motif analysis of Nup133-binding regions identified different motifs with the highest significance ranking in male and female groups. The q-values for all the presented motifs were determined as 0.01.

ChIP-Seq data are representative of four independent experiments.

To confirm if a downregulation of Nup133 resulting from hyperoxia in male OPCs could also lead to a downregulation of Nrf1, we performed independent qPCR experiments using hyperoxia treated male and female OPCs. The results showed a matching pattern of Nrf1 expression change post hyperoxic treatment as was seen in case of Nup133 (Figure 21-B). Nrf1 expression was significantly downregulated in male derived cells, whereas, in case of female cells a slight upregulation was observed. This observation supports possible regulation of Nrf1 expression in OPCs by Nup133. Furthermore, de novo motif analysis also revealed certain novel motifs that were found to be different in both male and female cells and await further investigation in future studies (Figure 21-C).
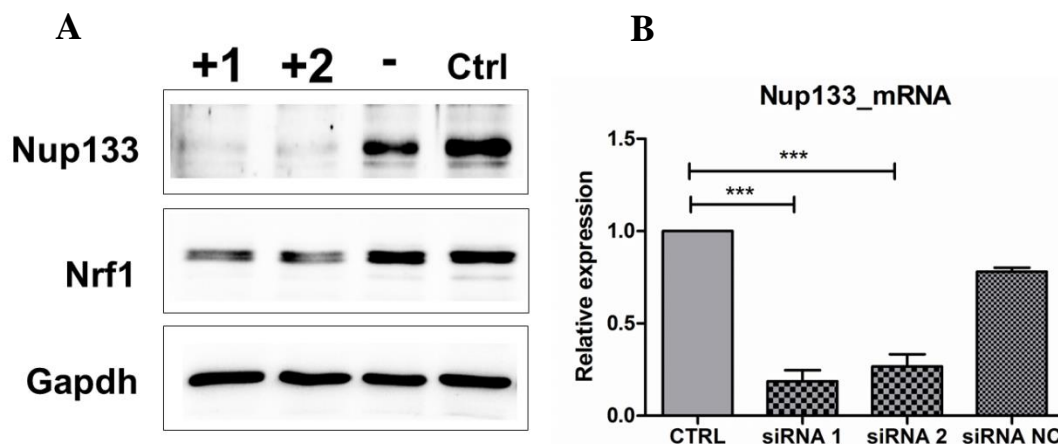
Figure 22. Results of transient knock down of Nup133.
(A) Western blot of Nup133 and NRF1 showing +1 for Nup133 specific siRNA 1, +2 for Nup133 specific siRNA 2, - for scrambled siRNA and Ctrl for non-transfected cell lysate. Transfection was performed in the OLN93 cells with 48h siRNA incubation. Data is representative of three independent experiments.(B) RT-qPCR analysis of Nup133 expression following siRNA transfection for 48h. Scrambled siRNA (siRNA NC) and untreated sample (Ctrl) are used as controls. Data is representative of three independent experiments.

For additional confirmation, small interfering (si) RNA transfection was performed to down-regulate Nup133 expression in the OLN93 (immature oligodendroglia) cell line. We found that Nrf1 expression was also down-regulated along with Nup133 proving the regulation of Nrf1 expression in OPCs by Nup133 (Figure 22). It also explains the drastic effect on

mitochondrial and stress response proteins in the male derived cells that was observed in the proteomic data and sheds light into why the male derived cells have increased susceptibility towards oxidative damage.

5.1.5 Hyperoxia leads to disrupted mitochondrial function and stress response pathways in male OPCs.

Most interestingly, a number of proteins related to mitochondrial function were seen to be significantly downregulated in the male OPCs. Nrf mediated oxidative stress response pathway and some of the fatty acid oxidation pathway proteins were also seen to be significantly affected in the male cells (Figure 23). Giving a very clear picture of the impact of hyperoxia on different molecular functions; these results indicate that the downregulation of these stress response pathways and extensive mitochondrial dysfunction might be the critical reasons behind a stronger negative effect on the male cells. The effect on NRF mediated oxidative stress response provides additional support to the above mentioned regulation of Nrf1 by Nup133.
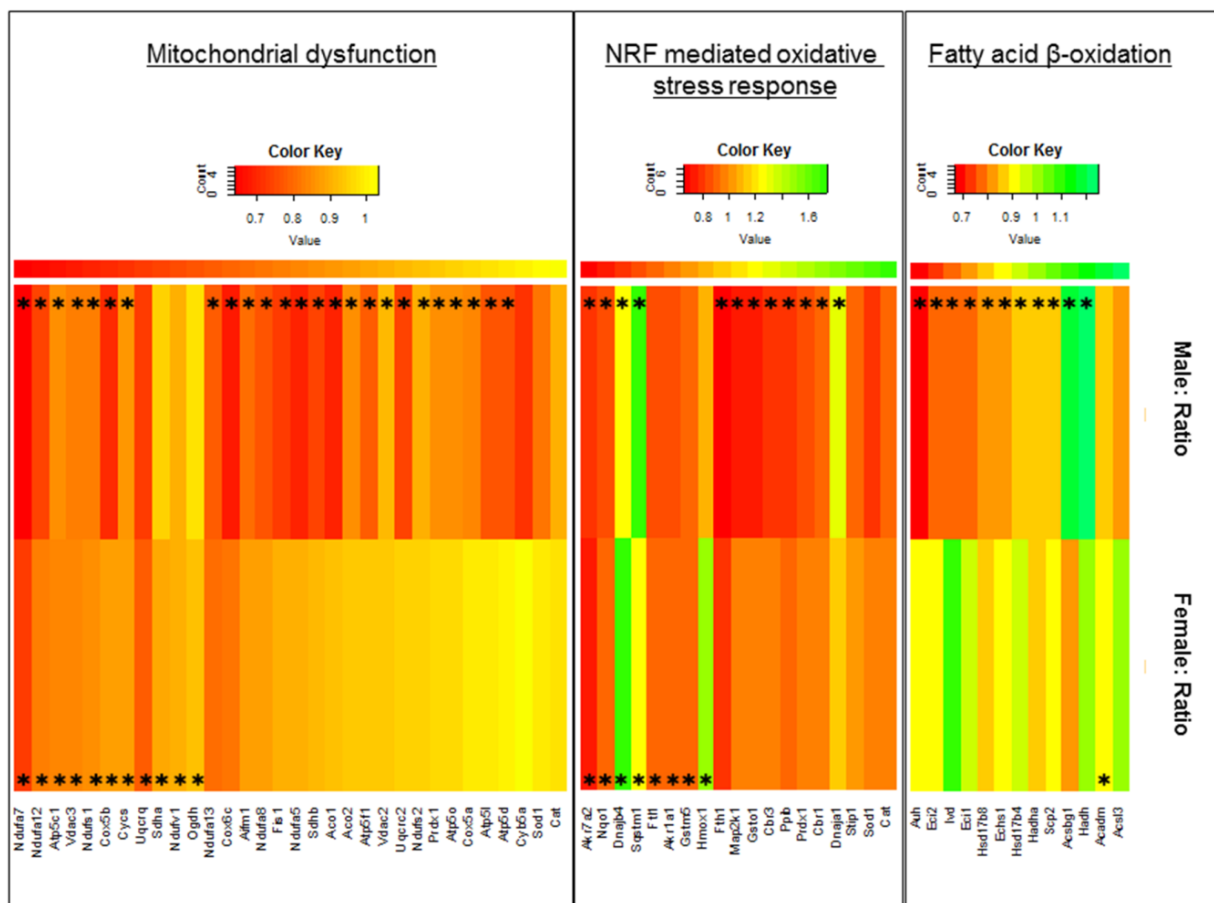
Figure 23. Heat-map representation of mitochondrial and stress response proteins that were dysregulated in male and female derived OPCs post 24 h 80%O_2 treatment in

comparison to 3%O$_2$ (normoxia) controls. Highly downregulated proteins are indicated in red, intermediate in yellow, and highly upregulated proteins in green. Proteins are sorted according to IPA categories. Cells marked with * represent the significantly altered proteins in each group. The cut off p value < 0.07. Data are representative of five independent experiments.

5.1.6 Hyperoxia inhibits mitophagy in male OPCs resulting in elevated stress.

The mass spectrometry results also showed a decrease in Superoxide dismutase [Cu-Zn] (SOD1) and Superoxide dismutase 2, mitochondrial (SOD2) levels in the male OPCs, whereas in the female cells both remained unchanged (Figure 24). Since both these enzymes are well known to play vital roles in regulating mitochondrial and intracellular ROS levels, a downregulation in these proteins would result in excessive increase in intracellular ROS in the male cells which in turn inhibits mitophagy. Mitophagy is a selective autophagy method by which the defective and dysfunctional mitochondria are degraded to maintain a healthy organelle population. This process is particularly important under conditions like oxidative stress that leads to mitochondrial dysfunction.
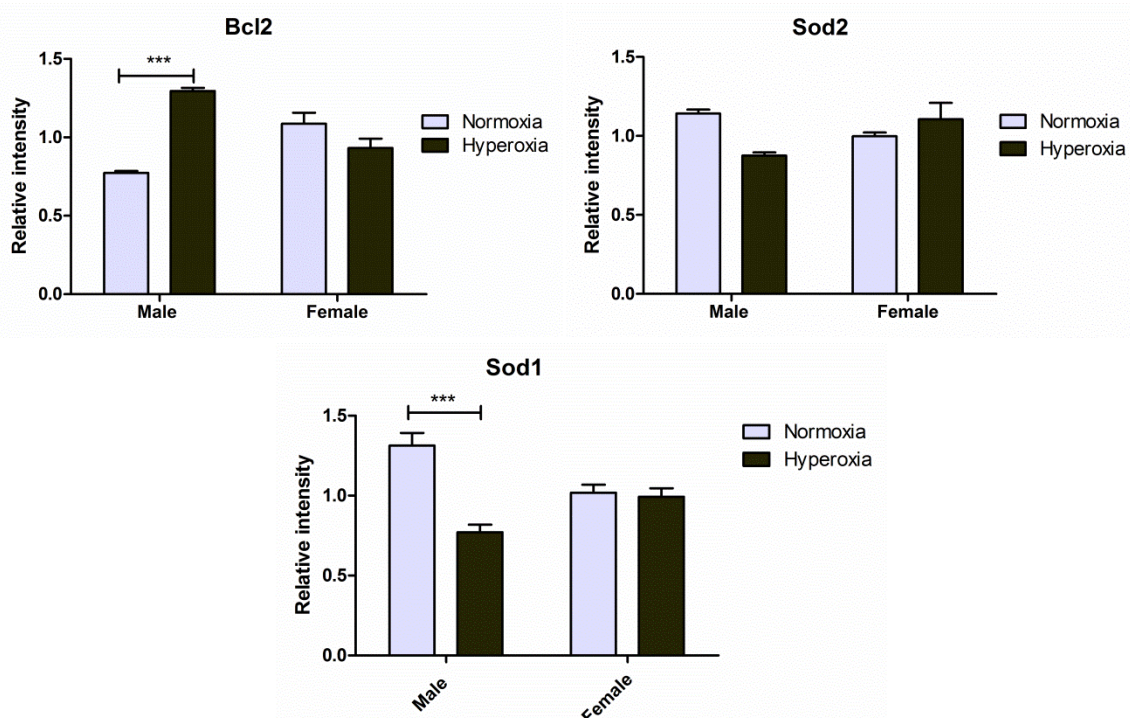
Figure 24. Changes in mitophagy related proteins in male OPCs as a result of hyperoxia. Intensities of Sod1, Sod2 and Bcl2 plotted from the mass spectrometry results. Sod1 and Sod2 show a downregulation in male derived OPCs post hyperoxia while Bcl2 shows a significant upregulation. *p < 0.05, **p < 0.01, ***p < 0.001, ****p < 0.0001 (Student's t test), n=5. Values are means ± SEM.

On looking into the mechanistic details in the male cells, an upregulation in Bcl2, an inhibitor of the autophagic protein Beclin1 and a downregulation of Beclin1 itself was observed. While Park7 (DJ-1) and Atg7 levels remained the same, indicating an inhibition of mitophagy. On the other hand, in female cells, Bcl2 was downregulated and Beclin1, Park7 and Atg7 were all seen to be upregulated, indicating that mitophagy occurs in female cells thereby aiding in their survival (Figure 25).

Figure 25. mRNA expression changes in mitophagy related proteins in male OPCs as a result of hyperoxia. mRNA expression changes of Park7, Atg7 and Beclin1 as observed by qPCR in male and female OPCs post 24h hyperoxia. Da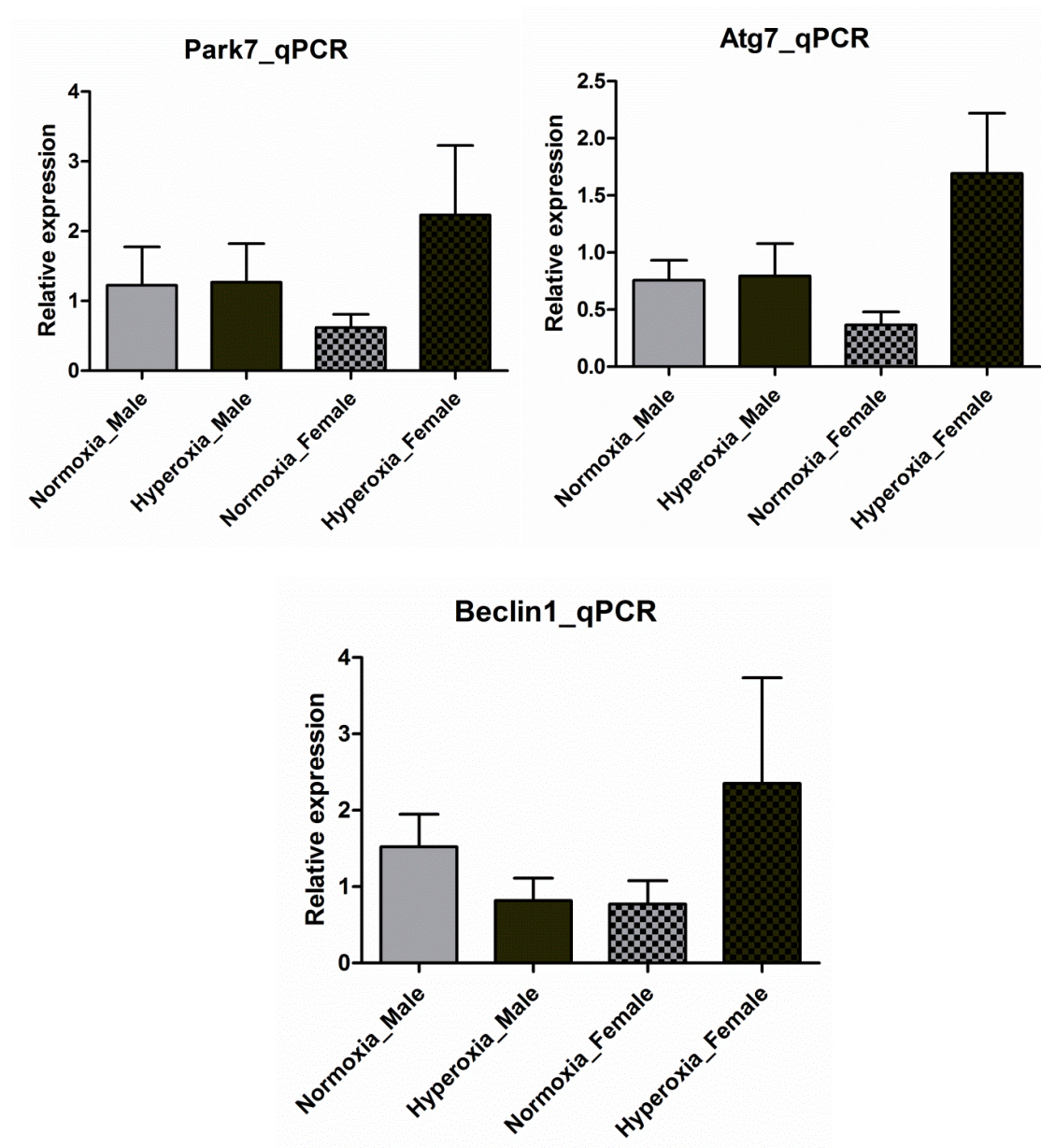ta are representative of three independent experiments. Bars and error represent mean ± SEM of replicate measurements. $*p < 0.05$, $**p < 0.01$, $***p < 0.001$, $****p < 0.0001$ (Student's t test).

However, the present results are not conclusive of this effect and therefore we intend to further investigate the effect of hyperoxia in male and female OPCs on the Pink1-Parkin pathway of mitophagy using Pink1 and Parkin knockout mice.

5.1.7 DISCUSSION

Hyperoxia is well known to hinder the maturation of OPCs, being a worrying cause of white matter damage in preterm brain[1, 25]. Considering the backdrop of clinical studies mentioning male sex as an independent associated risk factor [5-7, 26], it became evident that the male and female brains respond differently to hyperoxic insult.

These results show that there exists a very clear distinction between how the male and female derived OPCs respond to high oxygen. Although we observed a difference in the basal level expression of CNPase in both the groups, the effect of oxygen was very prominent on the male cells being highly vulnerable. Even after returning the cells to normal oxygen conditions, they remained in suspension with very few cells that attached to the surface of the plate. CNPase was seen to be significantly downregulated in these cells and also the number of CNPase positive differentiating cells was observed to be extremely few. Interestingly, the female OPCs could recover much better after the oxygen shock. Surprisingly, 24h treatment with 80% O_2 did not result in wide spread cell death in both the populations (data not shown).

The following global proteome analysis results revealed the severity of the effect on mitochondrial proteins as well as on the NRF mediated oxidative stress response pathway in the male derived OPCs. However, the most striking observation was the alteration in nuclear envelope proteins in the male derived cells. Like any other cell, differentiation of OPCs into mature oligodendrocytes require extensive chromatin reorganization and programmed gene repositioning which is achieved by the aid of nuclear envelope components including the nuclear lamina, nuclear membrane and the nuclear pore complex proteins [66, 124, 137-139]. In the male cells, hyperoxia lead to the downregulation of lamin and NPC proteins which disrupts the fine-tuned chromatin reorganization and gene repositioning, resulting in a delay in their maturation. Since the NPCs are the primary channels for communication between the nucleus and the cytoplasm, it is very likely that they have an impact on nearly every cellular process. This could also mean that in a developing brain, such an imbalance of NPC proteins in the OPCs can result in altered cell division capability producing an abnormal pool of OPCs compromised on their ability to give rise to mature oligodendrocytes. Thereby, these facts might explain why the brain fails to recover after hyperoxic injury even though it is known

that there is an apparent replenishment of OPCs [140, 141]. Their subsequent failure to differentiate might lead to long term effects in the male subjects. Hence, a more detailed study into the compositional changes in NPC and the functional significance of these variations in brain development could be useful for understanding the underlying pathologies of various developmental issues.

Nup133 targeted ChIP-Seq study results support the above mentioned argument of NPC components being responsible for a delay in OPC maturation in male derived cells due to hyperoxia. We show that it is involved in regulating the expression of a number of oligodendrocyte differentiation related genes in both male and female OPCs. Since Nup133 occupancy was found at the transcription start sites of these genes, it might act as a transcription factor or transcription factor activator/repressor, hence directly regulating gene expression. Alternatively, it may also indirectly induce differentiation by gating the expression of other transcription factors, for instance, Olig1, Egr2 and Hes5 etc. Hence, a downregulation of this important NPC component in the male cells as a result of hyperoxia leads to disruption of the programmed regulation of these genes required during OPC differentiation. Moreover, the involvement of Nup133 in regulating mitochondrial and oxidative stress response functions through its direct downstream target Nrf1 illustrates that it could be involved in a myriad of overlapping mechanisms not only during cell differentiation but also other important cellular functions. Hence, further studies on Nup133 functions will provide insight into its role in additional cellular processes and regulatory networks. This will be particularly beneficial for fully understanding the role of NPC components in various disease models.

To conclude, this data provides direct evidence that there exists a sex based difference in oxidative stress response of OPCs. This observation itself conveys a strong message supporting the need to study how complex cellular processes are regulated differently in male and female brains during development and for a better understanding of how the brain copes up with different forms of stress after preterm birth. Even though we have uncovered the reasons behind the susceptibility of male OPCs towards oxidative stress, this study also very strongly advocates that there may exist unknown novel mechanisms in the female cells that help them to resist oxidative stress. These mechanisms involving steroid hormones and their receptors have been explained in the second part. At functional level, our findings on Nup133 playing a key role in regulating cell differentiation as well as cellular stress response provides insight into a new mechanism of hyperoxia induced damage in OPCs and thereby reveals a

new function of Nup133 that has not been described before; opening up new avenues for understanding the molecular mechanisms behind hyperoxia induced white matter damage in the developing brain.
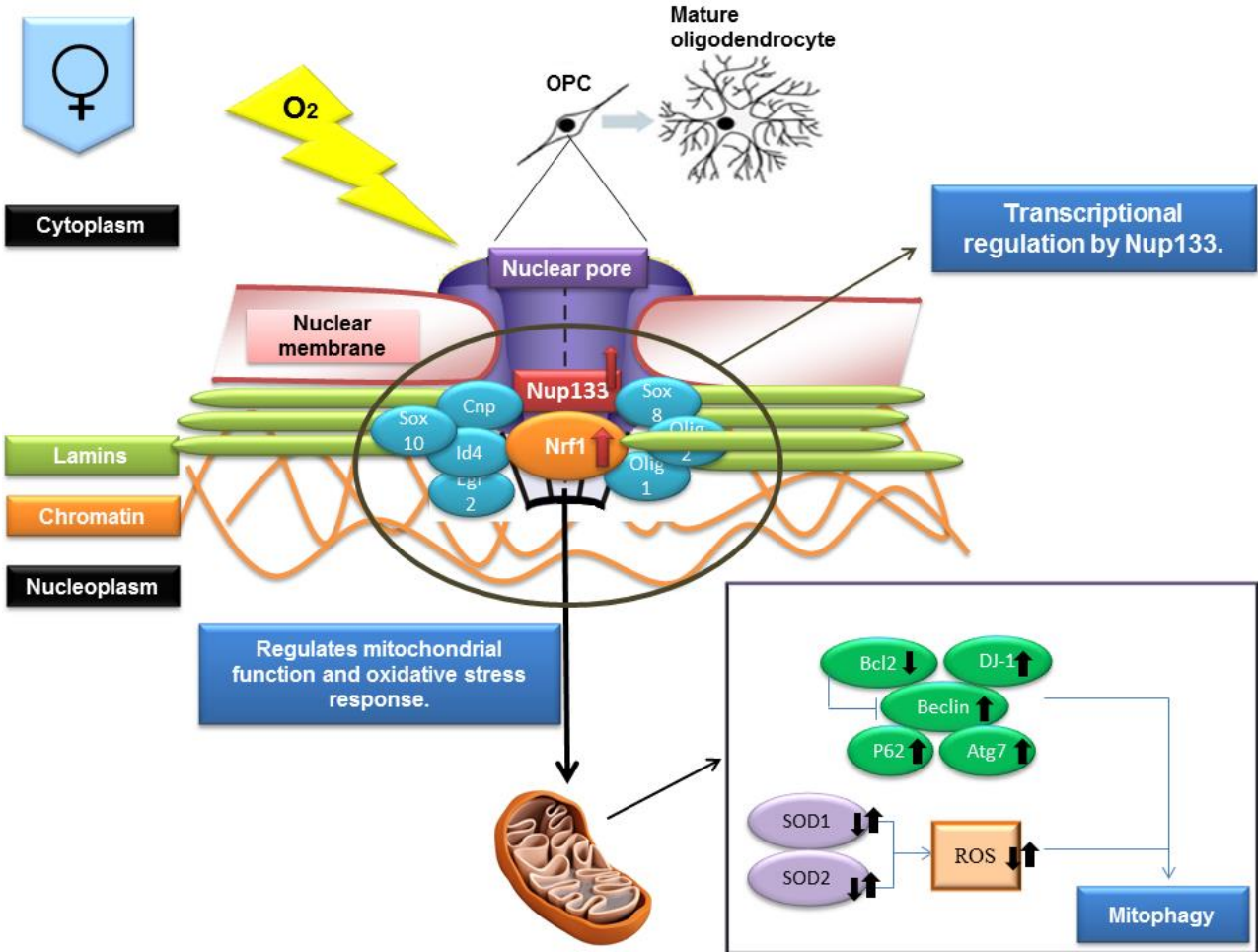
Figure 26. Summary of hyperoxia induced mechanism in female OPCs.
Figure showing an upregulation in Nup133 as a result of hyperoxia in female cells leading to normal transcriptional regulation of differnetiation related genes and an upregulation in Nrf1 expression positively regulating mitochondrial function and oxidative stress response. Another mechansim with an upregulation in mitophagy related genes indicating efficient mitophagy in female cells to combat oxidative stress related damage.
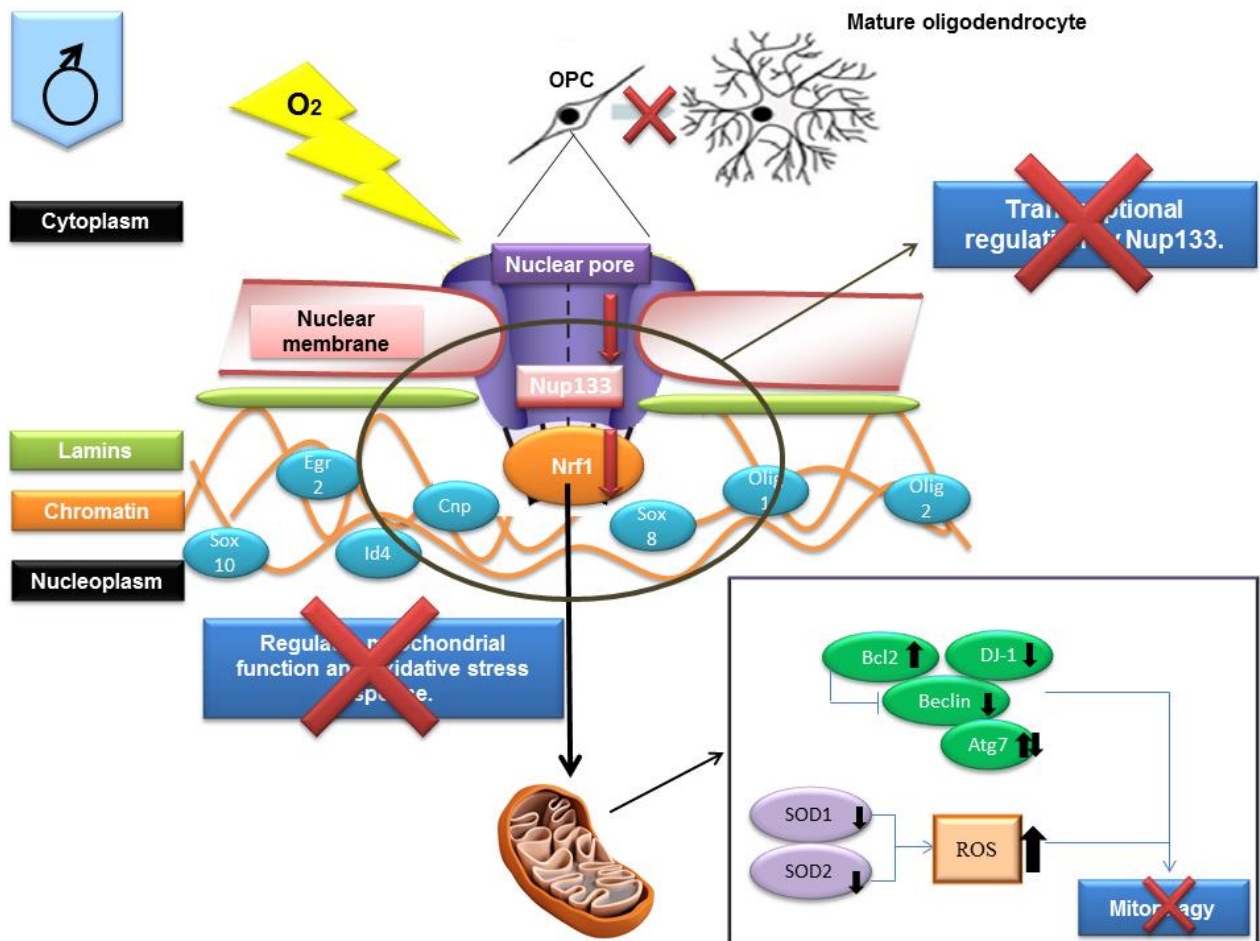
Figure 27. Summary of hyperoxia induced mechanism in male OPCs.
Figure showing a downregulation in Nup133 and Lamin proteins as a result of hyperoxia in male cells leading to disruption in the transcriptional regulation of differnetiation related genes and a downregulation in Nrf1 expression disrupting the normal regulation of mitochondrial function and oxidative stress response. Another mechansim with a downregulation in SOD isoforms indicating increased ROS production and downregulation in mitophagy related genes indicating inefficient mitophagy in male cells leaving them vulnerable to oxidative stress related damage.

5.2. PART II (EFFECT OF ESTROGEN AND FETAL ZONE STEROIDS)

5.2.1 Nup133 directly interacts with Estrogen receptor alpha and together control Nrf1 expression.

Our experiments with oxygen treatment showed a significant upregulation in the expression of estrogen receptor alpha (ERα) in the female derived mouse OPCs indicating a possible role of ERα in oxidative stress response in female cells (Figure 28-A). It was notable that even though the estrogen receptor beta (ERβ) is known to be more prominently expressed in brain tissue [158], we did not observe any notable changes in its expression levels post hyperoxic treatment in both male and female derived cells (Figure 28-A). A number of previous studies have shown that ERα controls Nrf1 expression [159-162]. Hence, to decipher the interaction between Nup133 and ERα in these cells, we performed co-immunoprecipitation experiments using Nup133 antibody and found ERα to be co-precipitated with Nup133, indicating a direct interaction between the two (Figure 28-B). Treatment with the ERα specific agonist PPT (1,3,5-tris(4-hydroxyphenyl)-4-propyl-1H-pyrazole) increased Nup133 expression in male cells under normal conditions whereas in the presence of the ER antagonist ICI 182,780 (7α,17β-[9-[(4,4,5,5,5-Pentafluoropentyl)sulfinyl]nonyl]estra-1,3,5(10)-triene-3,17-diol), Nup133 abundance decreased in the female cells (Figure 28-C). These results indicate towards the possibility of ERα being an upstream regulator of Nup133 in the female cells.
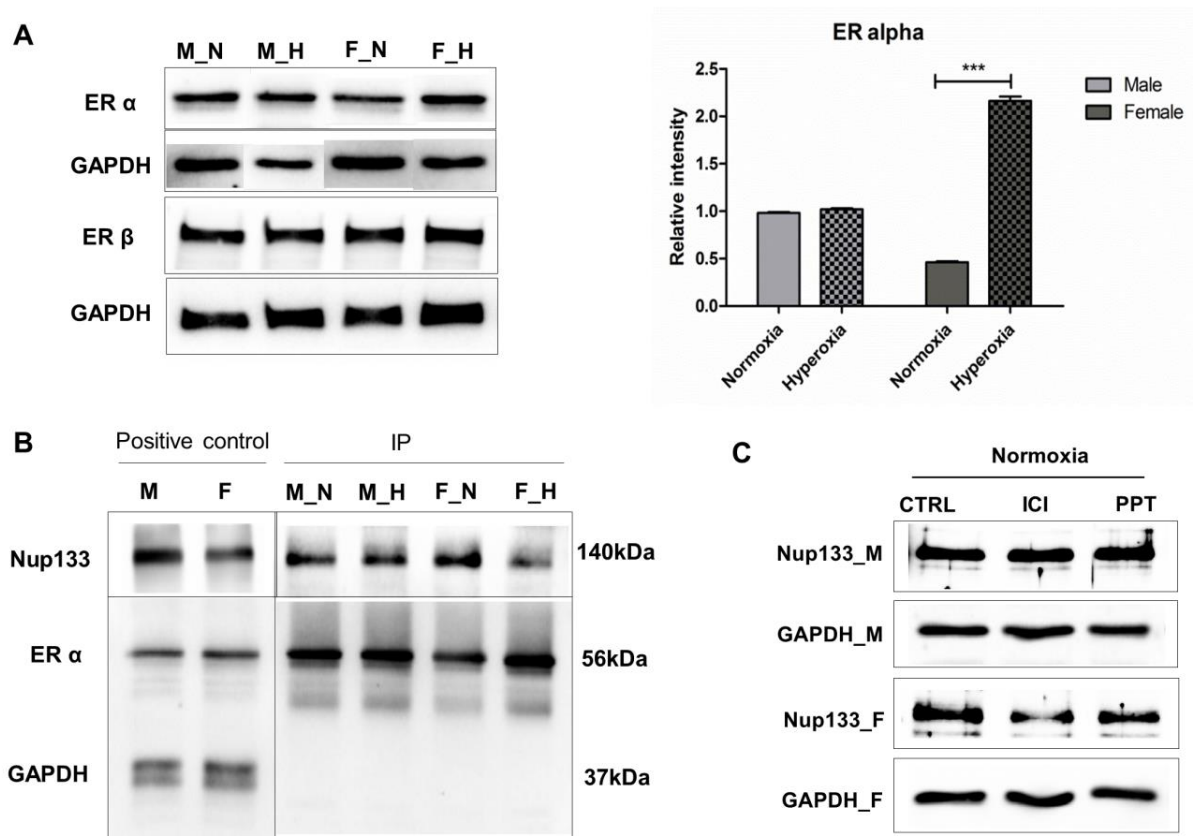
Figure 28. Nup133 directly interacts with ERα.
(A) Western blot analysis of male and female OPCs with anti-ERα and anti-ERβ antibodies at normal ($3\%O_2$) conditions and 24h post $80\%O_2$ shock, showing a significant increase in ERα expression in the female OPCs.
(B) Western blot results of co-immunoprecipitation performed using anti-Nup133 antibody showing the interaction between ERα and Nup133 in male and female OPCs under normoxia and hyperoxia.
(C) Western blot results showing Nup133 expression post treatment of male and female OPCs with 4,4',4''-(4-Propyl-[1H]-pyrazole-1,3,5-triyl)trisphenol (PPT) and ICI 182,780 (ICI) under normoxia and 24h hyperoxia.

Treatment with 17β-estradiol (E2) showed an exact similar trend in Nup133 and Nrf1 mRNA expression (Figure 29-A,B) rendering a positive effect especially on the male cells post hyperoxia by bringing back Nup133 and Nrf1 expressions comparable to normal. Proteome analysis of the cells post treatment with E2 under hyperoxia also showed that the mitochondrial dysfunction was significantly reduced in male cells (Figure 29-C). These findings along with the observation that treatment with E2 increased the Nrf1 mRNA levels significantly in female cells post hyperoxia (Figure 29-B), suggest that steroid hormones and their receptors do contribute to a difference in how Nrf1 is regulated in male and female cells. In female cells, there possibly exists a stronger regulation via ERα whereas in male cells Nrf1 seems to be regulated mainly by Nup133.
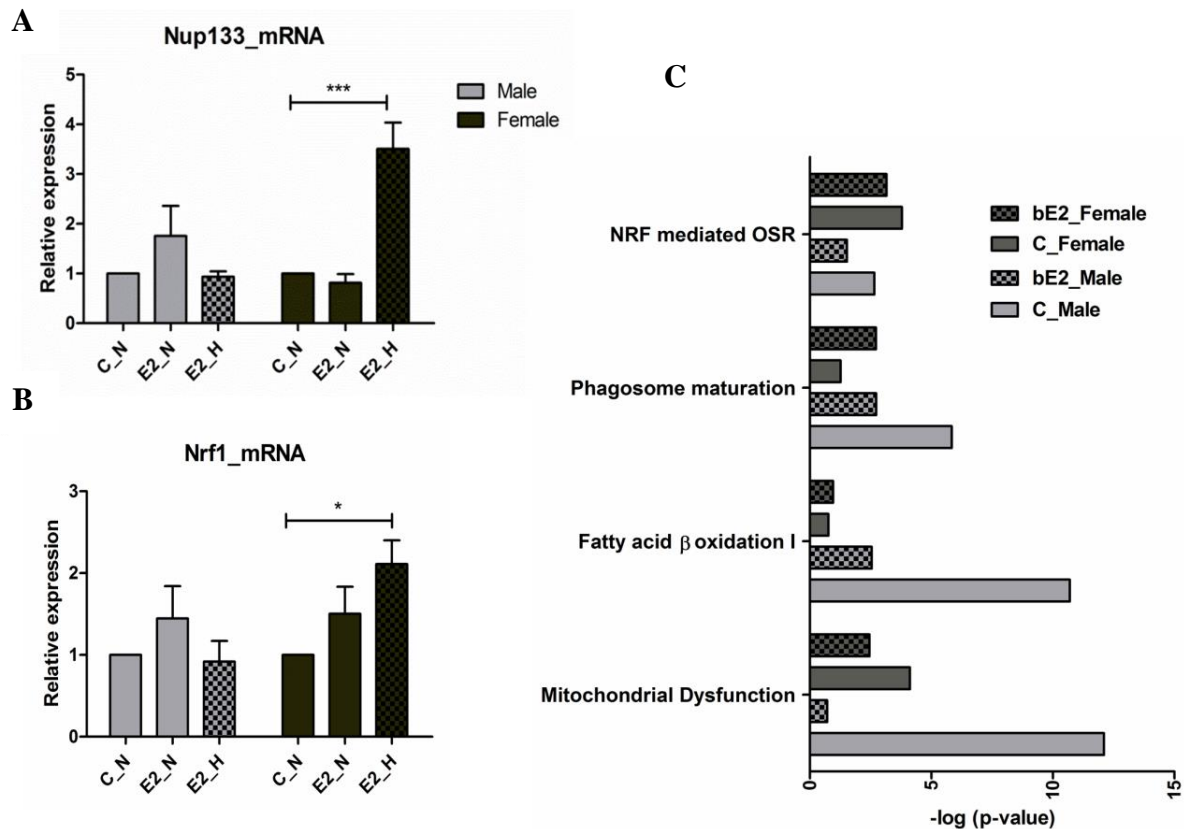
Figure 29. Nup133 directly interacts with ERα.

(A) RT-qPCR results showing Nup133 mRNA expression changes post 17-β estradiol (E2) treatment in male and female OPCs under normoxia and hyperoxia.

(B) RT-qPCR results showing NRF1 mRNA expression changes post 17-β estradiol (E2) treatment in male and female OPCs under normoxia and hyperoxia.

(C) Functional categorization of significantly enriched proteins in male and female OPCs post 24h 80%O_2 and E2 treatment using IPA. Bar graphs depict the most extensively enriched biological processes among the altered proteins. Cut off p value < 0.05 (Fisher's exact test). 'C' represents control. Data is representative of five independent experiments.

All other data are representative of three independent experiments. Bars and error represent mean $\pm$ SEM of replicate measurements. $*p < 0.05$, $**p < 0.01$, $***p < 0.001$, $****p < 0.0001$ (Student's t test).

5.2.2 FZSs can act as potent ligands to human steroid hormone receptors: *In silico* analysis.

Apart from estrogen, since the FZSs are present in high concentrations during human fetal development and since not much is known about the poteintal role of these molecules in brain development, we first investigated their ability to interact with the conventional steroid hormone receptors using an *in silico* method of analysis.

The chemical structures of the FZSs as well as the structures of the receptor molecules were docked together using the softwares as mentioned in the methods part. For each docking, the negative score that was generated by the software based on the chemical affinity of the ligand and receptor structures was then plotted to compare the affinity of the ligand to specific receptor molecules. A higher negative docking score predicts a stronger interation between the ligand and the receptor. We chose the ligand molecules based on their concentraions observed in the human urine sample data with 16a-OH-DHEA being especially found in very high concentraion. Upon comparison between the probability of interaction of the chosen ligand molecules with the estrogen receptors alpha and beta, we found that 16a-OH-DHEA and 16a-OH-Pregnanalone had a sepcific high affinity scores towards ERα whereas, only 16a-OH-Pregnanalone showed a particularly high affinity interaction with the ERβ (Figure 30). Considering this high binding probability of 16a-OH-DHEA to the ERα, we later performed experiments on our model system by giving specific treatments with 16a-OH-DHEA.
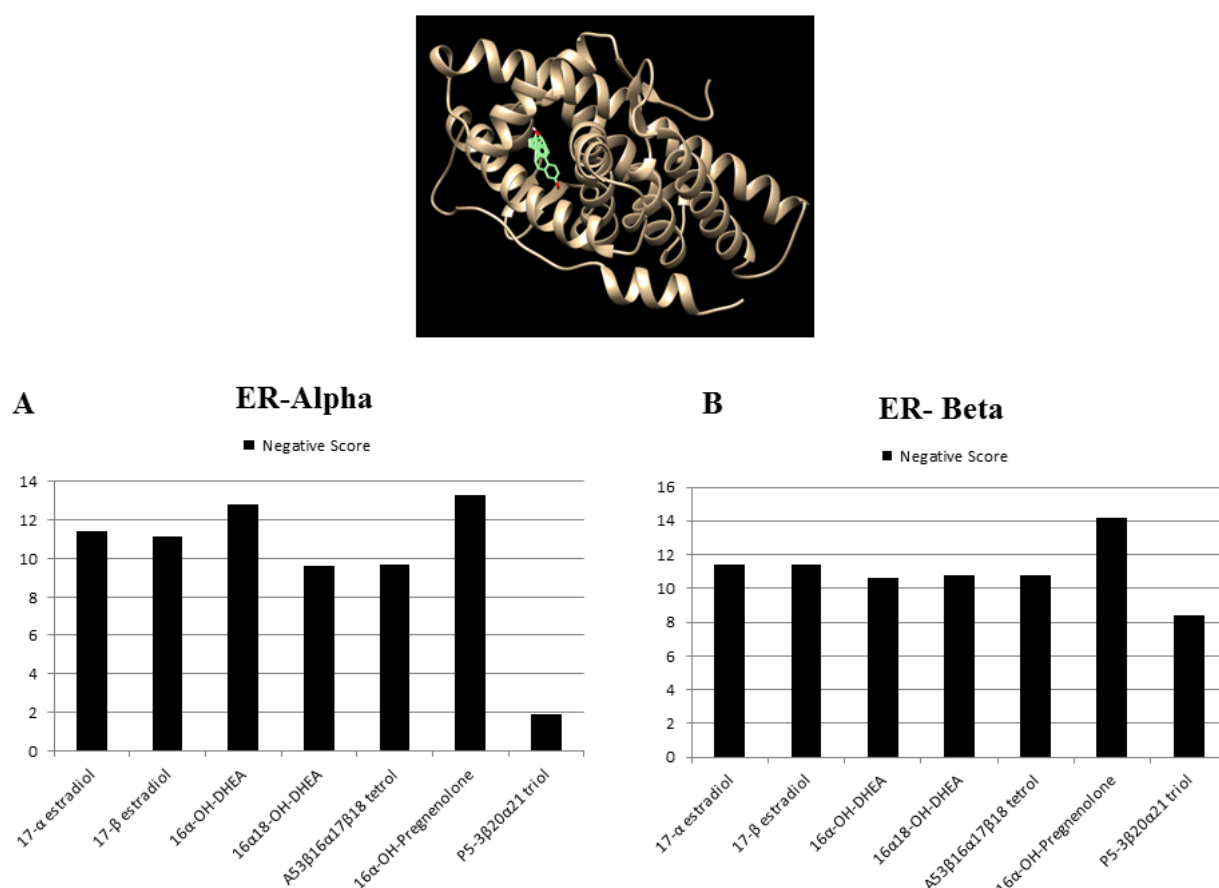
Figure 30.Molecular docking results showing the probability of interaction between FZS molecules with the estrogen receptors alpha and beta.
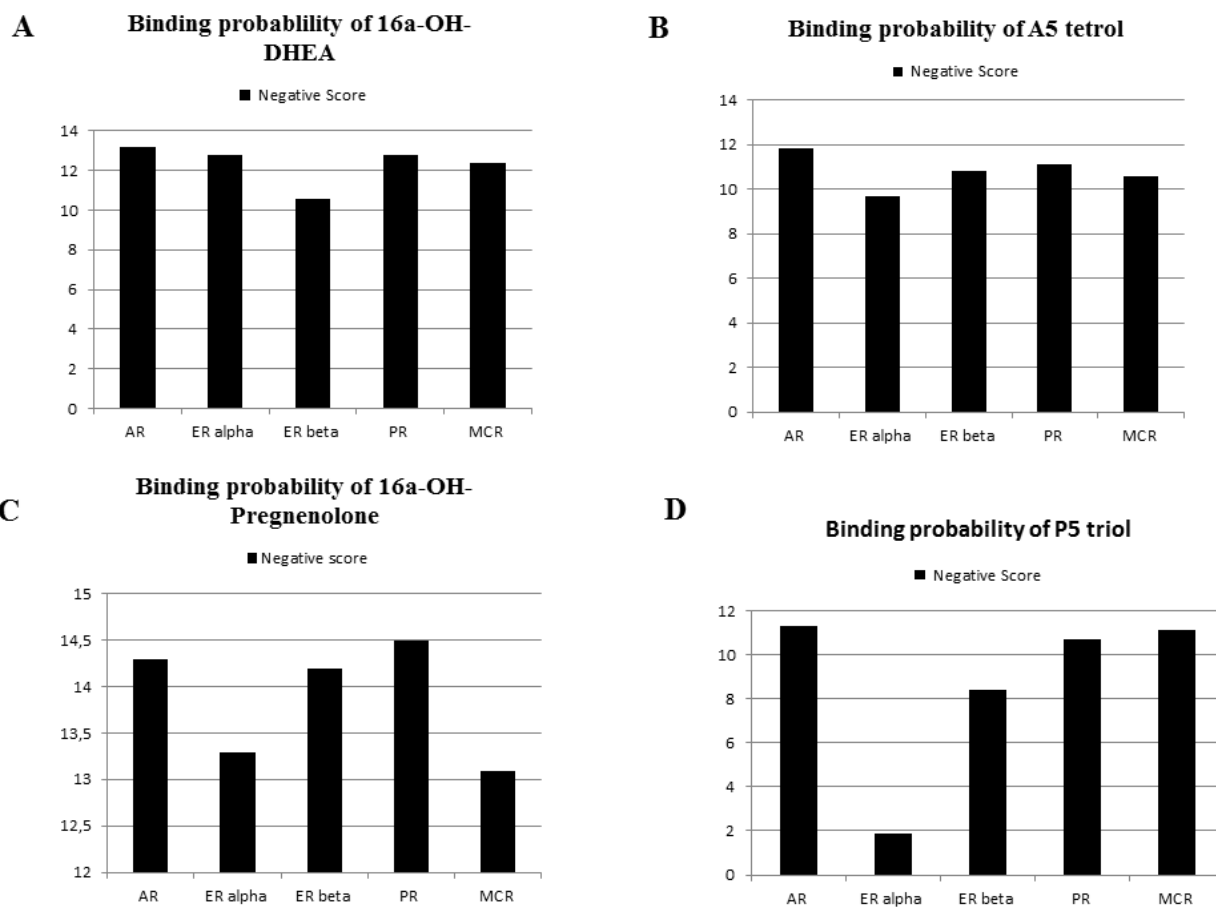
Figure 31. Binding probability of specific FZSs to the classical steroid hormone receptors.

We also analysed the specific binding probability of a few selected FZSs to the human androgen receptor (AR), estrogen receptors alpha and beta, progesterone receptor (PR) and the metallocorticoid receptor (MCR) (Figure 31). The results showed varied affinity towards the different receptors indicating that each of these molecules had the probability of binding to multiple steroid hormone receptors.

5.2.3 Fetal zone steroid amounts differ in the urine of preterm male and female infants.

As mentioned earlier, in case of humans, it is not only E2 but also a number of other steroid hormone precursors that can play potential roles in brain development and combating stress [9-11] which can contribute to a differential outcome in preterm infants. We analyzed urine samples collected from human preterm and term infants along a period of time starting from day 1 to day 3 after birth using gas chromatography-mass spectrometry. The urinary steroid profile showed high level of total FZSs in the urine of healthy preterm infants when compared to healthy term infants (Figure 32-A). On analyzing the profiles in male and female preterm infants, we found that the total concentration of FZSs was significantly higher in sick female infants as compared to males (Figure 32-B). Since the sick infants were exposed to longer hyperoxia, this increase in the FZS concentration in female infants is notable considering their potential role as neuroprotective agents. 16α-OH-DHEA was found to be present in very high concentrations when compared to the other detected metabolites in the preterm group (Figure 32-C) and significantly higher in the healthy preterm group than in the terms (Figure 32-D).

A Total concentration

B Total concentration

C

D 16α-OH-DHEA

E 16α-OH-DHEA

F 16α-OH-DHEA_Early preterms

G Adiol

H 21-OH-P5-olon
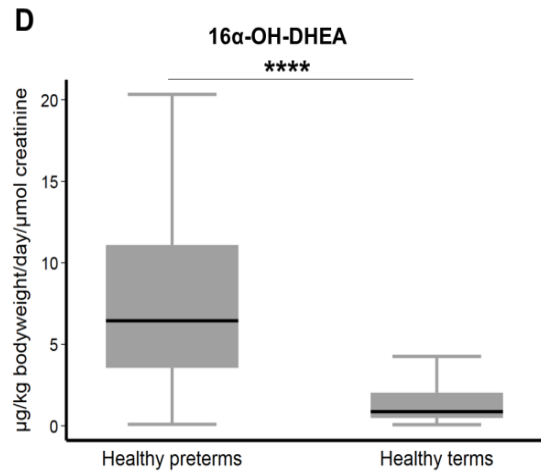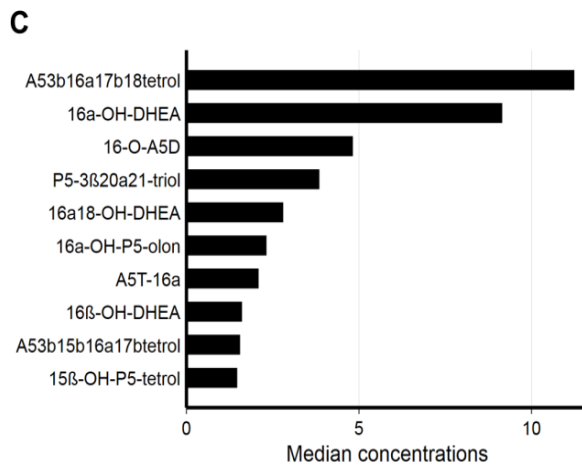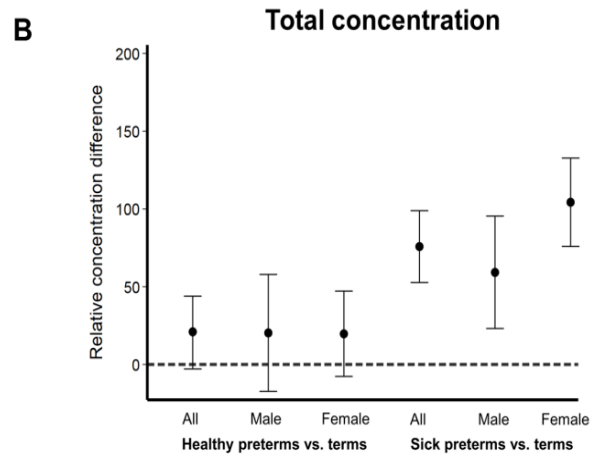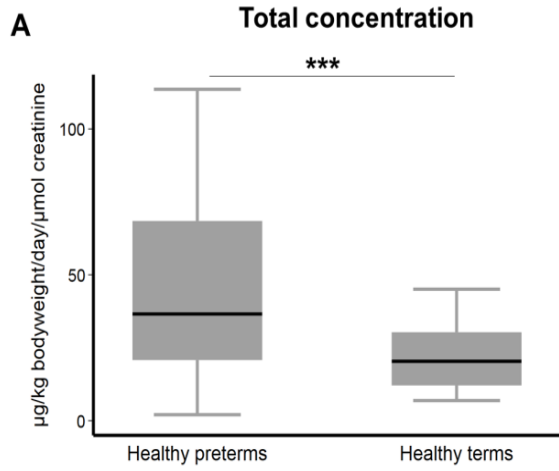
Figure 32. Fetal zone steroids are excreted in high amounts in preterm infant urine.
(A) Total FZS excretion in healthy term (>36 weeks gestational age, n=42) and healthy preterm (<36 weeks gestational age, n=71) infants during the first three days after birth measured in µg/kg bodyweight/day/µmol creatinine. ∗∗∗p < 0.001 as determined by Wilcoxon–Mann–Whitney test.
(B) A comparison of the total FZS excretion in healthy male preterm (<36 weeks gestational age, n=42) and healthy female preterm (<36 weeks gestational age, n=29) infants compared to sick male preterm (<36 weeks gestational age, n=38) and sick female preterm (<36 weeks gestational age, n=26) infants during the first three days after birth.
(C) Graph showing the concentrations of the highest ten analyzed FZSs over a period of first 3 days after birth in all preterm infants (healthy and sick, n=135).
(D) 16α-OH-DHEA concentration in preterm (n=135) and term (n=63) infants. ∗∗∗∗p < 0.0001 as determined by Wilcoxon–Mann–Whitney test.
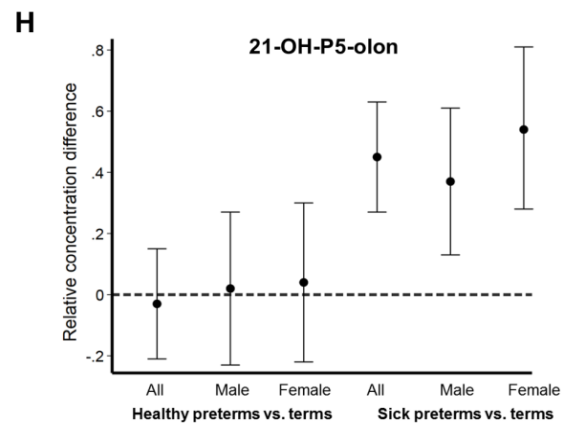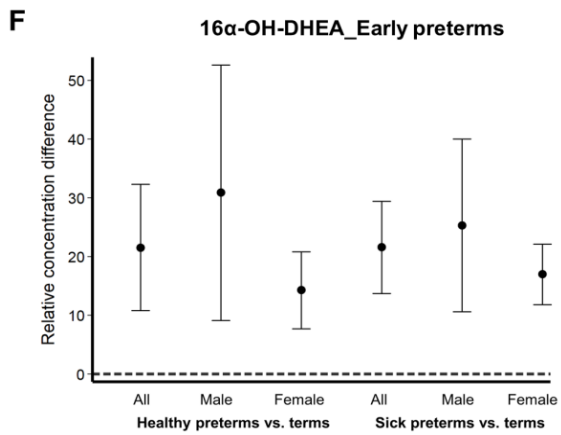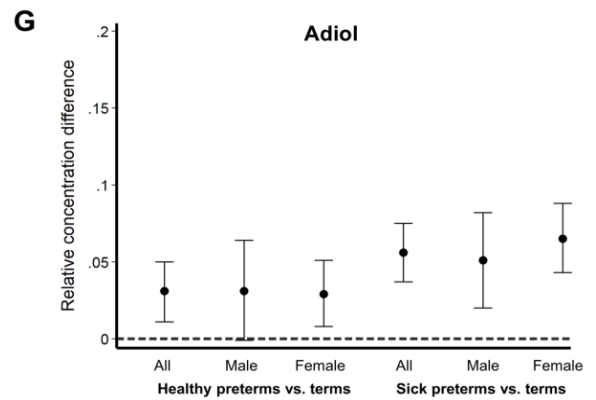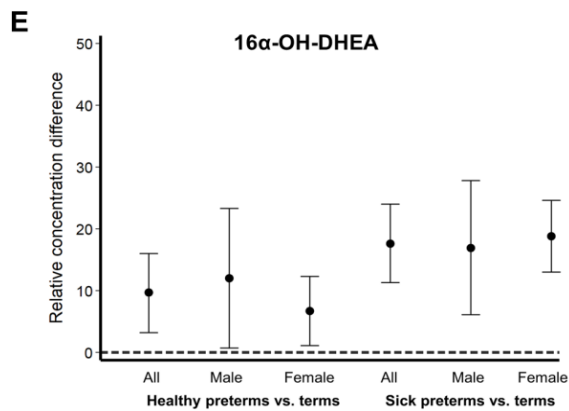 (E) Comparison of 16α-OH-DHEA excretion in healthy male preterm (<36 weeks gestational age, n=42) and healthy female preterm (<36 weeks gestational age, n=29) infants compared to sick male preterm (<36 weeks gestational age, n=38) and sick female preterm (<36 weeks gestational age, n=26) infants during the first three days after birth.
(F) Comparison of Adiol excretion in healthy male preterm (<36 weeks gestational age, n=42) and healthy female preterm (<36 weeks gestational age, n=29) infants compared to sick male preterm (<36 weeks gestational age, n=38) and sick female preterm (<36 weeks gestational age, n=26) infants during the first three days after birth.
(G) Comparison of 16α-OH-DHEA excretion in healthy male early preterm (<30 weeks gestational age, n=7) and healthy female early preterm (<30 weeks gestational age, n=10) infants compared to sick male early preterm (<30 weeks gestational age, n=23) and sick female early preterm (<30 weeks gestational age, n=21) infants during the first three days after birth.
(H) Comparison of 21-OH-P5 olon (a pregnane derivative) excretion in healthy male preterm (<36 weeks gestational age, n=42) and healthy female preterm (<36 weeks gestational age, n=29) infants compared to sick male preterm (<36 weeks gestational age, n=38) and sick female preterm (<36 weeks gestational age, n=26) infants during the first three days after birth.
Concentration in term infants is considered as the baseline control for all regression analysis plots.

Further comparison based on gender and wellness showed that 16α-OH-DHEA was present in a higher concentration in healthy preterm males than females and was found to be increased in the sick female preterm infants (Figure 32-E). Upon considering only the early preterm infants (<30 weeks gestational age) we saw that 16α-OH-DHEA was significantly higher in the healthy as well as sick male infants with a slight drop in concentration in the sick males (Figure 32-F). Androstene-3β, 17α-diol (Adiol) at the same time was found to be similar in healthy female and male preterms and a greater increase was observed in the sick female group (Figure 32-G). The pregnane derivative 21-OH-P5 olon in healthy pretrms was seen to be almost similar to term group and showed a significant higher concentration in the sick female group (Figure 32-H). Hence, in order to understand the consequences of these observed differences in FZS concentrations, we tested a few on the mouse OPCs.

5.2.4 FZSs have a protective effect on both male and female cells.

We tested the effect of 16α-OH-DHEA along with adiol and allopregnenalone on the maturation of OPCs and found that all the three FZSs had a positive effect on the maturation of male and female OPCs post hyperoxia (Figure 33-A) as seen by changes in MAG levels, especially in the male cells. We also found that FZSs upregulate the expression of NRF1 post hyperoxia in the female cells and maintained it to the normoxic control level in the male cells (Figure 33-B). Considering the otherwise drastic drop of NRF1 in male cells post hyperoxia, it can be clearly seen that the FZSs have a significant protective effect. On looking at the expressions of Nup133 and ERα, it becomes clear that this observed NRF1 upregulation is mediated by both ERα and Nup133 in female cells. Whereas in male cells, this effect seems to be mediated mainly by Nup133 (Figure 33-C,D). Hence, we show that the FZSs have a positive effect on stress response and maturation post hyperoxia in the male cells.

Figure 33. FZSs and E2 show protective effects on male and female OPCs.
(A) Western blot results showing the expression of MAG in OPCs after treatment with 100nM Adiol (AD), 100nM Allopregnanolone (AL) and 100nM 16α-OH-DHEA under normoxia and hyperoxia.
(B) Western blot results showing the expression of NRF1 in OPCs after treatment with 100nM Adiol (AD), 100nM Allopregnanolone (AL) and 100nM 16α-OH-DHEA under normoxia and hyperoxia.
(C) Western blot results showing the expression of Nup133 in OPCs after treatment with 100nM Adiol (AD), 100nM Allopregnanolone (AL) and 100nM 16α-OH-DHEA under normoxia and hyperoxia.
(D) Western blot results showing the expression of ERα in OPCs after treatment with 100nM Adiol (AD), 100nM Allopregnanolone (AL) and 100nM 16α-OH-DHEA under normoxia and hyperoxia.

These results also illustrate that the FZSs are potential ligands of ERα and can protect the OPCs against oxidative stress. Considering that the basal FZS levels in healthy preterm females are higher than in male infants and get further increased in case of illness (Figure 32-B), we propose that the presence of these FZSs render the female cells more resistant towards oxidative stress compared to the males. This also makes it worth to investigate in detail any changes in the concentration of these FZSs in male and female infants under specific disease conditions. An overall combination effect as mentioned above must also be considered.

5.2.5 Estradiol in presence of 16αOH-DHEA exerts a negative effect on the maturation of male derived cells.

Since preterm birth is associated with a drop in estrogen levels, it has been advocated that substituting estrogen to intrauterine levels can be beneficial [163-165]. But considering the high amounts of circulating FZSs, it is important to investigate the effect of E2 substitution in presence of FZSs in male and female infants. Hence, we chose 16α-OH-DEHA since it is the second most abundant FZS found in preterm infant urine (Figure 32-C) and checked its effect on differentiation of OPCs in the presence of E2. We treated male and female OPCs with 100nM 17-ß-estradiol alone and in combination with 100nM 16α-OH-DHEA. On giving high oxygen treatment for 24h, we found that the co-treatment resulted in downregulation of CNPase and myelin associated glycoprotein (MAG) expression in the male cells (Figure 34-A). We checked the expression of Nup133 and ERα under the same treatment conditions and found that both were downregulated in the E2+16α-OH-DHEA group in male cells. Same was observed with Nup50 and LaminB1 expression too (Figure 34-D). Whereas in the female cells, an upregulation was seen in both Nup133 and ERα (Figure 34-B,C). This observation coincides with significant higher levels of 16α-OH-DHEA in the urine of early (<30 weeks gestational age) male preterm infants and in both healthy and sick group (Figure 32-F).
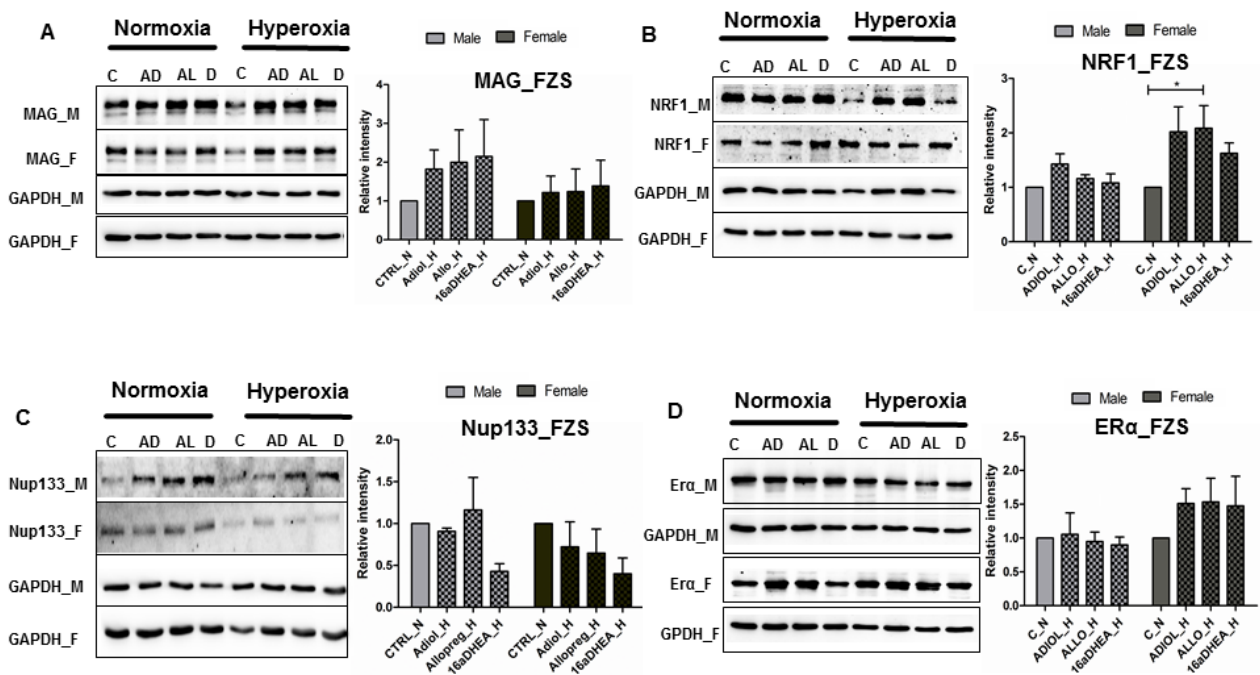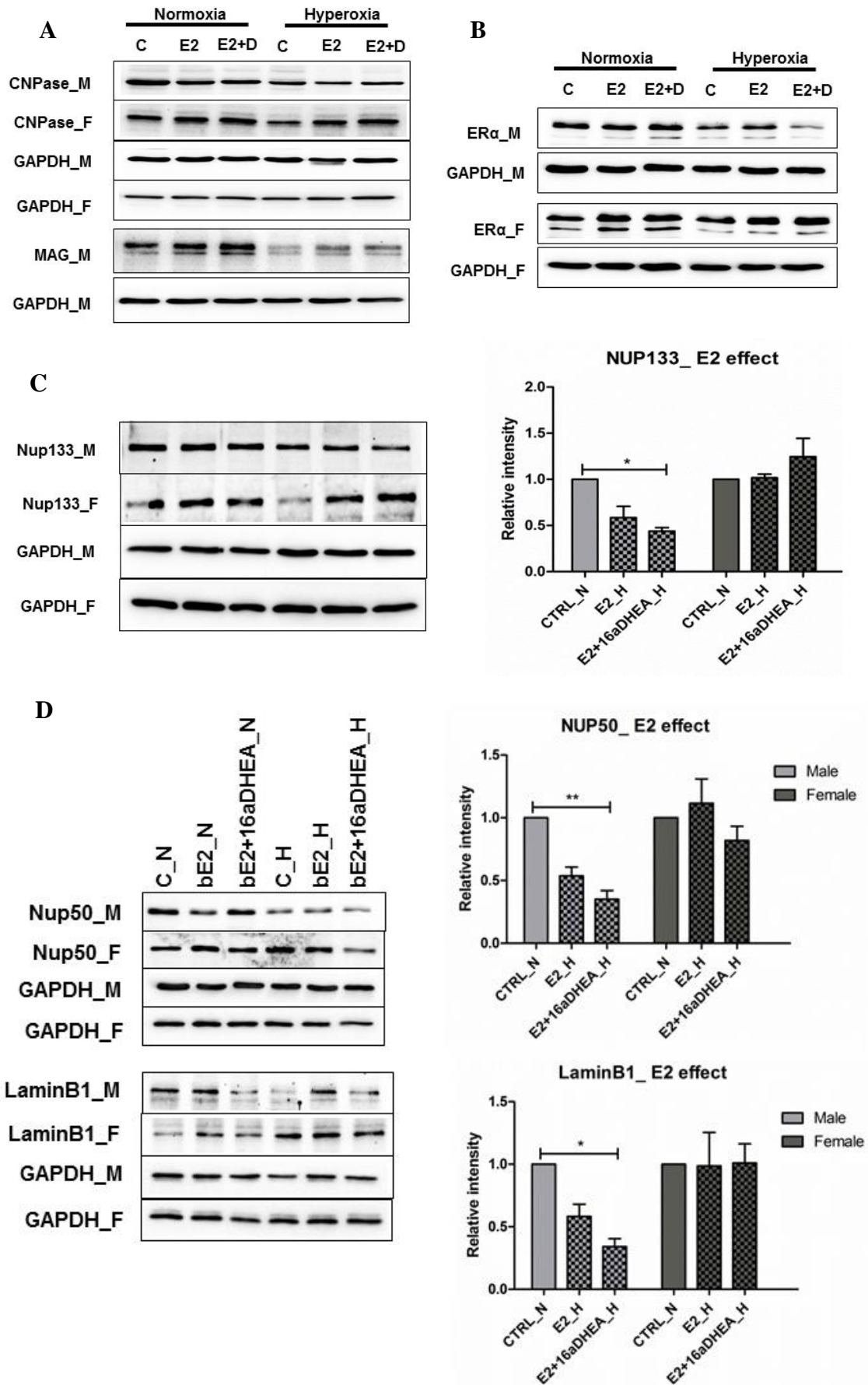
Figure 34. FZSs and E2 show discrete effects on male and female OPCs

.
(A) Western blot results showing the expression of CNPase and MAG in OPCs after treatment with 100nM 17-β estradiol (E2) alone and E2 in combination with 100nM 16α-OH-DHEA (E2+D) under normoxia and hyperoxia.
(B) Western blot results showing the expression of ERα in OPCs after treatment with 100nM 17-β estradiol (E2) alone and E2 in combination with 100nM 16α-OH-DHEA (E2+D) under normoxia and hyperoxia.
(C) Western blot results showing the expression of Nup133 in OPCs after treatment with 100nM 17-β estradiol (E2) alone and E2 in combination with 100nM 16α-OH-DHEA (E2+D) under normoxia and hyperoxia.
(D) Western blot results showing the expression of Nup50 and LaminB1 in OPCs after treatment with 100nM 17-β estradiol (E2) alone and E2 in combination with 100nM 16α-OH-DHEA (E2+D) under normoxia and hyperoxia.
Data are representative of three independent experiments. Bars and error represent mean ± SEM of replicate measurements. ∗p < 0.05, ∗∗p < 0.01, ∗∗∗p < 0.001, ∗∗∗∗p < 0.0001 (Student's t test).

5.2.6 16α-OH-DHEA activates different mechanisms in male and female cells.

A co-treatment of 16α-OH-DHEA with ICI 182, 780 (ICI) which is an estrogen receptor antagonist resulted in a significant upregulation of Nup133 as well as MAG in the male cells post 24h hyperoxia (Figure 35-A,B). A similar trend in upregulation was also observed in Nup50 and LaminB1 (Figure 35-C). In the female cells on the contrary, no such upregulation was seen in Nup133 but MAG (Figure 35-A, B). However, Nup50 and LaminB1 showed upregulation in the female cells post hyperoxia (Figure 35-C). This shows that it potentially activates other steroid hormone receptors apart from ERα and ERβ and that it has possibly different interactions in the male and female cells. These results also show the importance of considering FZSs and their effect on male and female brain development separately, especially for E2 substitution as a therapy.
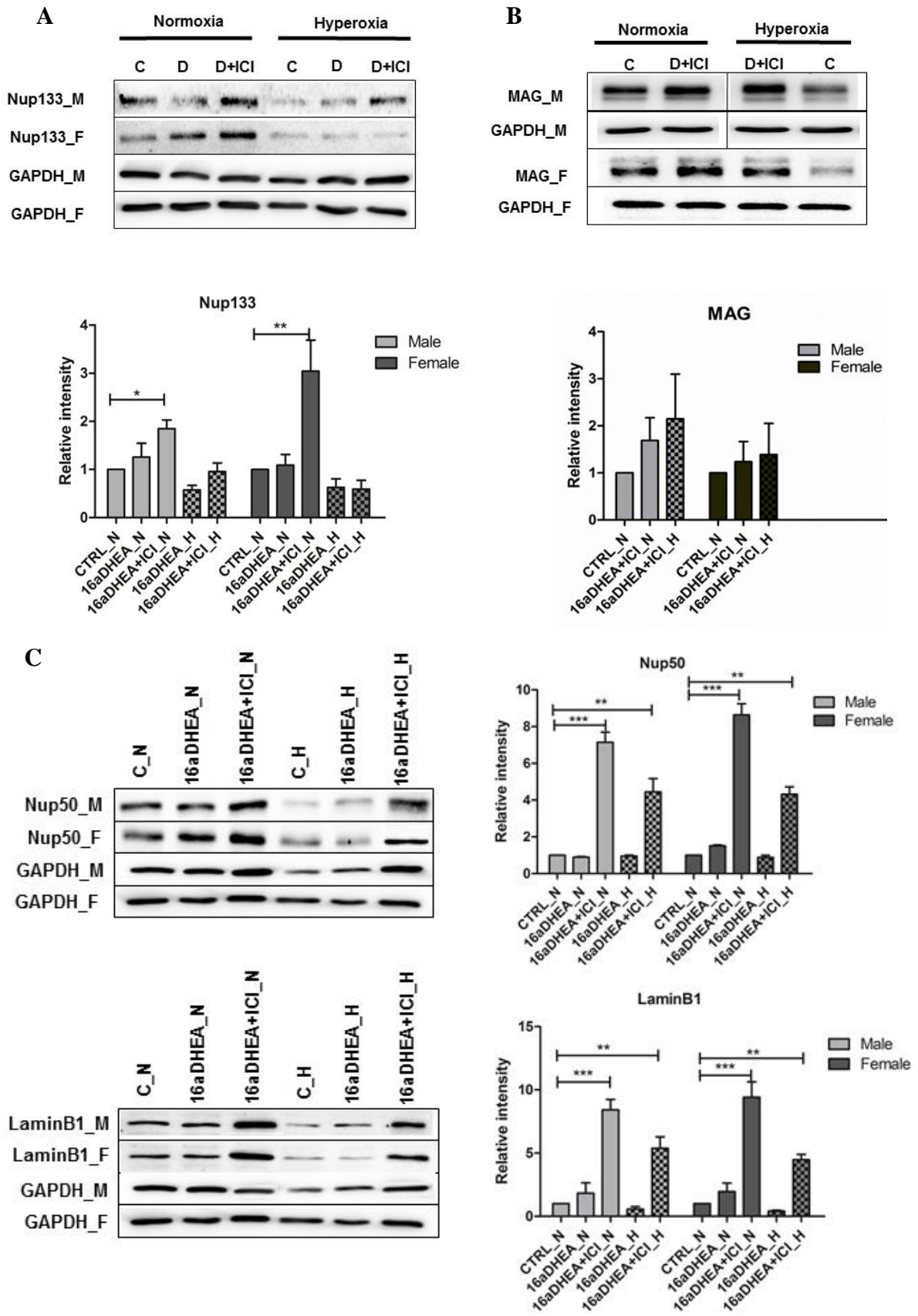
Figure 35. 16α-OH-DHEA activates different mechanisms in male and female cells.

(A) Western blot results showing the expression of Nup133 in OPCs after treatment with 100nM 16α-OH-DHEA alone and 16α-OH-DHEA in combination with 100nM ICI (D+ICI) under normoxia and hyperoxia.
(B) Western blot results showing the expression of MAG in OPCs after treatment with 100nM 16α-OH-DHEA in combination with 100nM ICI (D+ICI) under normoxia and hyperoxia.
(C) Western blot results showing the expression of Nup50 and LaminB1 in OPCs after treatment with 100nM 16α-OH-DHEA alone and 16α-OH-DHEA in combination with 100nM ICI (D+ICI) under normoxia and hyperoxia.
Data are representative of three independent experiments. Bars and error represent mean ± SEM of replicate measurements. ∗p < 0.05, ∗∗p < 0.01, ∗∗∗p < 0.001, ∗∗∗∗p < 0.0001 (Student's t test).

5.2.7 DISCUSSION

Steroid hormones have been long implicated in neuroprotection and we have also observed the same effect of neuroprotection by estradiol and FZSs in our previous study on female derived immature oligodendroglial cell line (OLN93) [10]. However, the exact mechanisms how these hormones and their precursors act on the cells to rescue them under conditions of stress is yet to be completely deciphered. Our results show how differentiation and Nrf1- oxidative stress responses are mediated by Nup133 in the male cells and the involvement of the classical estrogen receptor alpha (ERα) as a possible upstream regulator of Nup133. It also suggests that there exists a difference in the extent of regulation via ERα in the male and female cells with a possible stronger regulation in the female cells allowing them to better cope up with the oxidative stress. By means of this mechanism, we have explained how the FZSs and E2 can have a differential effect on the male and female cells. Addition of estradiol alone protects the cells from oxidative stress but it was the addition of FZSs that allowed both the male and female cells to mature to a greater extend post hyperoxia expressing late stage oligodendrocyte differentiation markers such a mylein associated glycoprotein (MAG).

Previous works from Heckmann et al. and other working groups [166] had shown that fetal zonal steroids are synthesized in persistant high concentrations in premature babies until a considerably long duration. However, a gender based analysis on the concentration differences in individual FZS molecules in preterm and term infants and also in sick and healthy preterm infants revealed a striking difference between the male and female groups. We strongly believe that this could be linked to the gender based difference in the neurological outcome that has been observed over various clinical studies. The experimental results with FZSs performed on male and female cells completely supports this hypothesis

and shows that this differential effect can be crucial for designing clinically effective neuroprotective strategies. As our results show that these FZSs can activate different mechanisms in male and female cells, more detailed studies would be still required to uncover the role of these FZSs as potential pleotrophic molecules that can interact with a number of steroid hormone receptors activating a myraid of distintct or overlapping signalling and mechanisms.

This study also throws light on the possible consequences of substituting estrogen in preterm infants without considering the presence of high amounts of circulating FZSs and that these consequences can be largely influenced by gender. The experimental results very clearly show a negative impact of co-treatment on the described mechanism in the male cells. Even though in a human system the situation is much more complex, these results point towards the first clues that demand futher detailed studies using various model systems to understand these complex interactions and their subsequent consequences without ignoring the gender aspect.

Taken together, we have uncovered the reasons behind the susceptibility of male OPCs towards oxidative stress and at the same time show that the presence of FZSs renders resistance to the female cells against oxidative stress. At functional level, our findings on Nup133 playing a key role in regulating cell differentiation as well as cellular stress response provides insight into a new mechanism of hyperoxia induced damage in OPCs and thereby reveals a new function of Nup133; opening up new avenues for understanding the molecular mechanisms behind hyperoxia induced white matter damage in the developing brain.

6. SUMMARY

Hyperoxia is a well-known cause of cerebral white matter injury in preterm infants with male sex being an independent and critical risk factor for poor neurodevelopmental outcome. We investigated the underlying mechanisms behind such a sex dependent difference in oligodendrocyte progenitor cells (OPCs). Our findings demonstrate that oxidative stress severely affects cellular functions related to energy metabolism, stress response, and maturation in male derived oligodendrocyte progenitor cells (OPCs) whereas the female cells remain largely unaffected. This impairment of maturation is accompanied by the downregulation of nucleoporin and nuclear lamina proteins. We identify Nup133, which regulates OPC maturation as a major target protein affected by hyperoxia in male cells and that this differential response is mediated by an inverse Nup133 regulation in the male and female cells. It also regulates mitochondrial function and oxidative stress response through its downstream target Nuclear respiratory factor 1 (Nrf1). Additionally, the presence of 17-β estradiol and higher amounts of fetal zone steroids (precursors for maternal estrogen synthesis during fetal development) confer resistance to the female cells mediated by the estrogen receptor alpha (ERα) along with Nup133. Both Nup133 and ERα regulate mitochondrial function and oxidative stress response by transcriptional regulation of Nrf1. These findings establish prominent sex based differences and the molecular mechanisms involved in differential response of OPCs towards oxidative stress and the important role of Nup133 in mediating a severe negative outcome in the male cells.

7. ZUSAMMENFASSUNG

Sauerstoffüberversorgung (Hyperoxie) ist eine bekannte Ursache für zerebrale Verletzungen der weißen Substanz bei Frühgeborenen männlichen Geschlechts, die ein unabhängiger und kritischer Risikofaktor für eine unzureichende neuronale Entwicklung ist. Wir untersuchten die zugrunde liegenden Mechanismen hinter einem solchen geschlechtsabhängigen Unterschied in Oligodendrozyten-Progenitorzellen (OPCs). Unsere Ergebnisse zeigen, dass oxidativer Stress die Zellfunktionen im Zusammenhang mit dem Energiestoffwechsel, der Stressreaktion und der Reifung in männlichen Oligodendrozyten-Vorläuferzellen (OPCs) stark beeinflusst, während die weiblichen Zellen weitgehend unbeeinflusst bleiben. Diese Beeinträchtigung der Reifung geht einher mit der Herunterregulierung von Nukleoporin und nuklearen Lamina-Proteinen. Wir identifizieren Nup133, das die OPC-Reifung als ein wichtiges Zielprotein regelt, das von Hyperoxie in männlichen Zellen betroffen ist und diese differentielle Reaktion durch eine inverse Nup133-Regulation in männlichen und weiblichen Zellen vermittelt. Es reguliert auch die mitochondriale Funktion und die Reaktion auf oxidativen Stress durch sein Downstream-Ziel Nuclear respiratory factor 1 (Nrf1). Darüber hinaus verleihen das Vorhandensein von 17-β Östradiol und höhere Mengen an Steroiden der fetalen Zone (Vorläufer für die mütterliche Östrogensynthese während der fetalen Entwicklung) Resistenz gegenüber weiblichen Zellen, die durch den Östrogenrezeptor alpha (ERα) zusammen mit Nup133 vermittelt werden. Sowohl Nup133 als auch ERα regulieren die mitochondriale Funktion und die Reaktion auf oxidativen Stress durch transkriptionelle Regulation von Nrf1. Diese Ergebnisse zeigen markante geschlechtsspezifische Unterschiede und die molekularen Mechanismen, die an der differenzierten Reaktion von OPCs auf oxidativen Stress beteiligt sind, und die wichtige Rolle von Nup133 bei der Vermittlung eines schwerwiegenden negativen Ergebnisses in den männlichen Zellen.

8. REFERENCES

1. Gerstner, B. et al. Hyperoxia causes maturation-dependent cell death in the developing white matter. The Journal of neuroscience : the official journal of the Society for Neuroscience 28, 1236-1245 (2008).

2. Felderhoff-Mueser, U. et al. Oxygen causes cell death in the developing brain. Neurobiology of disease 17, 273-282 (2004).

3. Collins, M.P., Lorenz, J.M., Jetton, J.R. & Paneth, N. Hypocapnia and other ventilation-related risk factors for cerebral palsy in low birth weight infants. Pediatric research 50, 712-719 (2001).

4. Gerstner, B. et al. Maturation-dependent oligodendrocyte apoptosis caused by hyperoxia. Journal of neuroscience research 84, 306-315 (2006).

5. Hintz, S.R., Kendrick, D.E., Vohr, B.R., Kenneth Poole, W. & Higgins, R.D. Gender differences in neurodevelopmental outcomes among extremely preterm, extremely-low-birthweight infants. Acta Paediatr 95, 1239-1248 (2006).

6. Ingemarsson, I. Gender aspects of preterm birth. BJOG : an international journal of obstetrics and gynaecology 110 Suppl 20, 34-38 (2003).

7. Mayoral, S.R., Omar, G. & Penn, A.A. Sex differences in a hypoxia model of preterm brain damage. Pediatric research 66, 248-253 (2009).

8. Nunez, J.L. & McCarthy, M.M. Sex differences and hormonal effects in a model of preterm infant brain injury. Annals of the New York Academy of Sciences 1008, 281-284 (2003).

9. Hubner, S., Reich, B. & Heckmann, M. Role of sex steroids and their receptors in human preterm infants: Impacts on future treatment strategies for cerebral development. Biochemical pharmacology 98, 556-563 (2015).

10. Hubner, S. et al. Protective Effects of Fetal Zone Steroids Are Comparable to Estradiol in Hyperoxia-Induced Cell Death of Immature Glia. Endocrinology 158, 1419-1435 (2017).

11. Heckmann, M. et al. Persistent high activity of the fetal adrenal cortex in preterm infants: is there a clinical significance? Journal of pediatric endocrinology & metabolism : JPEM 19, 1303-1312 (2006).

12. Heckmann, M. et al. Cortisol production rates in preterm infants in relation to growth and illness: a noninvasive prospective study using gas chromatography-mass spectrometry. The Journal of clinical endocrinology and metabolism 90, 5737-5742 (2005).

13. Chang, E. Preterm birth and the role of neuroprotection. BMJ 350, g6661 (2015).

14. Penn, A.A., Gressens, P., Fleiss, B., Back, S.A. & Gallo, V. Controversies in preterm brain injury. Neurobiology of disease 92, 90-101 (2016).

15. Back, S.A. et al. Selective vulnerability of late oligodendrocyte progenitors to hypoxia-ischemia. The Journal of neuroscience : the official journal of the Society for Neuroscience 22, 455-463 (2002).

16.   Back, S.A. et al. Late oligodendrocyte progenitors coincide with the developmental window of vulnerability for human perinatal white matter injury. The Journal of neuroscience : the official journal of the Society for Neuroscience 21, 1302-1312 (2001).

17.   Levison, S.W. & Goldman, J.E. Both oligodendrocytes and astrocytes develop from progenitors in the subventricular zone of postnatal rat forebrain. Neuron 10, 201-212 (1993).

18.   Volpe, J.J. Neurobiology of periventricular leukomalacia in the premature infant. Pediatric research 50, 553-562 (2001).

19.   Volpe, J.J., Kinney, H.C., Jensen, F.E. & Rosenberg, P.A. Reprint of "The developing oligodendrocyte: key cellular target in brain injury in the premature infant". International journal of developmental neuroscience : the official journal of the International Society for Developmental Neuroscience 29, 565-582 (2011).

20.   Back, S.A. & Miller, S.P. Brain injury in premature neonates: A primary cerebral dysmaturation disorder? Annals of neurology 75, 469-486 (2014).

21.   Buser, J.R. et al. Arrested preoligodendrocyte maturation contributes to myelination failure in premature infants. Annals of neurology 71, 93-109 (2012).

22.   Saugstad, O.D. Chronic lung disease: oxygen dogma revisited. Acta Paediatr 90, 113-115 (2001).

23.   Felderhoff-Mueser, U. et al. Caspase-1-processed interleukins in hyperoxia-induced cell death in the developing brain. Annals of neurology 57, 50-59 (2005).

24.   Gerstner, B. et al. Estradiol attenuates hyperoxia-induced cell death in the developing white matter. Annals of neurology 61, 562-573 (2007).

25.   Saugstad, O.D. Is oxygen more toxic than currently believed? Pediatrics 108, 1203-1205 (2001).

26.   Sutton, P.S. & Darmstadt, G.L. Preterm birth and neurodevelopment: a review of outcomes and recommendations for early identification and cost-effective interventions. Journal of tropical pediatrics 59, 258-265 (2013).

27.   Wood, C.E. Estrogen/hypothalamus-pituitary-adrenal axis interactions in the fetus: The interplay between placenta and fetal brain. Journal of the Society for Gynecologic Investigation 12, 67-76 (2005).

28.   Ishida, T. et al. [Changes in placental enzymatic activities in relation to estrogen production during pregnancy]. Nihon Sanka Fujinka Gakkai zasshi 37, 547-554 (1985).

29.   Gerstner, B. et al. 17beta-estradiol protects against hypoxic/ischemic white matter damage in the neonatal rat brain. Journal of neuroscience research 87, 2078-2086 (2009).

30.   Lustig, R.H. Sex hormone modulation of neural development in vitro. Hormones and behavior 28, 383-395 (1994).

31.   Weaver, C.E., Jr., Park-Chung, M., Gibbs, T.T. & Farb, D.H. 17beta-Estradiol protects against NMDA-induced excitotoxicity by direct inhibition of NMDA receptors. Brain research 761, 338-341 (1997).

32.   Sawada, H. et al. Estradiol protects mesencephalic dopaminergic neurons from oxidative stress-induced neuronal death. Journal of neuroscience research 54, 707-719 (1998).

33.   Zhao, L. & Brinton, R.D. Select estrogens within the complex formulation of conjugated equine estrogens (Premarin) are protective against neurodegenerative insults: implications for a composition of estrogen therapy to promote neuronal function and prevent Alzheimer's disease. BMC neuroscience 7, 24 (2006).

34.   Diczfalusy, E. Endocrine Functions of the Human Fetoplacental Unit. Federation proceedings 23, 791-798 (1964).

35.   Ishimoto, H. & Jaffe, R.B. Development and function of the human fetal adrenal cortex: a key component in the feto-placental unit. Endocrine reviews 32, 317-355 (2011).

36.   Hata, K. et al. Ultrasonographic evaluation of adrenal involution during antenatal and neonatal periods. Gynecologic and obstetric investigation 26, 29-32 (1988).

37.   Grueters, A. & Korth-Schutz, S. Longitudinal study of plasma dehydroepiandrosterone sulfate in preterm and fullterm infants. The Journal of clinical endocrinology and metabolism 55, 314-320 (1982).

38.   Ben-David, S. et al. Parturition itself is the basis for fetal adrenal involution. The Journal of clinical endocrinology and metabolism 92, 93-97 (2007).

39.   Lathe, R. & Kotelevtsev, Y. Steroid signaling: ligand-binding promiscuity, molecular symmetry, and the need for gating. Steroids 82, 14-22 (2014).

40.   Maninger, N., Wolkowitz, O.M., Reus, V.I., Epel, E.S. & Mellon, S.H. Neurobiological and neuropsychiatric effects of dehydroepiandrosterone (DHEA) and DHEA sulfate (DHEAS). Frontiers in neuroendocrinology 30, 65-91 (2009).

41.   Mellon, S.H. Neurosteroid regulation of central nervous system development. Pharmacology & therapeutics 116, 107-124 (2007).

42.   Wang, J.M. et al. Allopregnanolone reverses neurogenic and cognitive deficits in mouse model of Alzheimer's disease. Proceedings of the National Academy of Sciences of the United States of America 107, 6498-6503 (2010).

43.   Schumacher, M. et al. Revisiting the roles of progesterone and allopregnanolone in the nervous system: resurgence of the progesterone receptors. Progress in neurobiology 113, 6-39 (2014).

44.   Hill, M. et al. Neuroactive steroids, their precursors, and polar conjugates during parturition and postpartum in maternal and umbilical blood: 1. Identification and simultaneous determination of pregnanolone isomers. The Journal of steroid biochemistry and molecular biology 75, 237-244 (2000).

45.   Yawno, T., Yan, E.B., Walker, D.W. & Hirst, J.J. Inhibition of neurosteroid synthesis increases asphyxia-induced brain injury in the late gestation fetal sheep. Neuroscience 146, 1726-1733 (2007).

46.   Yawno, T., Hirst, J.J., Castillo-Melendez, M. & Walker, D.W. Role of neurosteroids in regulating cell death and proliferation in the late gestation fetal brain. Neuroscience 163, 838-847 (2009).

47.   Kelleher, M.A., Palliser, H.K., Walker, D.W. & Hirst, J.J. Sex-dependent effect of a low neurosteroid environment and intrauterine growth restriction on foetal guinea pig brain development. The Journal of endocrinology 208, 301-309 (2011).

48.   Hirst, J.J., Kelleher, M.A., Walker, D.W. & Palliser, H.K. Neuroactive steroids in pregnancy: key regulatory and protective roles in the foetal brain. The Journal of steroid biochemistry and molecular biology 139, 144-153 (2014).

49.   Brunton, P.J., Russell, J.A. & Hirst, J.J. Allopregnanolone in the brain: protecting pregnancy and birth outcomes. Progress in neurobiology 113, 106-136 (2014).

50.   Parker, C.R., Jr., Azziz, R., Potter, H.D. & Boots, L.R. Adrenal androgen production in response to adrenocorticotropin infusions in men. Endocrine research 22, 717-722 (1996).

51.   Regelson, W., Loria, R. & Kalimi, M. Dehydroepiandrosterone (DHEA)--the "mother steroid". I. Immunologic action. Annals of the New York Academy of Sciences 719, 553-563 (1994).

52.   Miller, K.K. et al. DHEA metabolites activate estrogen receptors alpha and beta. Steroids 78, 15-25 (2013).

53.   Auci, D. et al. Anti-inflammatory and immune regulatory properties of 5-androsten-3beta, 17beta-diol (HE2100), and synthetic analogue HE3204: implications for treatment of autoimmune diseases. Annals of the New York Academy of Sciences 1051, 730-742 (2005).

54.   Nicoletti, F. et al. 5-androstenediol ameliorates pleurisy, septic shock, and experimental autoimmune encephalomyelitis in mice. Autoimmune diseases 2010, 757432 (2010).

55.   Suzuki, T. et al. Androstenediol ameliorates alterations in immune cells cytokine production capacity in a two-hit model of trauma-hemorrhage and sepsis. Cytokine 34, 76-84 (2006).

56.   Szalay, L. et al. Androstenediol administration after trauma-hemorrhage attenuates inflammatory response, reduces organ damage, and improves survival following sepsis. American journal of physiology. Gastrointestinal and liver physiology 291, G260-266 (2006).

57.   Kiang, J.G. et al. Androstenediol inhibits the trauma-hemorrhage-induced increase in caspase-3 by downregulating the inducible nitric oxide synthase pathway. J Appl Physiol (1985) 102, 933-941 (2007).

58.   Hanna, D.M., Tadros, M.G. & Khalifa, A.E. ADIOL protects against 3-NP-induced neurotoxicity in rats: Possible impact of its anti-oxidant, anti-inflammatory and anti-apoptotic actions. Progress in neuro-psychopharmacology & biological psychiatry 60, 36-51 (2015).

59.   Saijo, K., Collier, J.G., Li, A.C., Katzenellenbogen, J.A. & Glass, C.K. An ADIOL-ERbeta-CtBP transrepression pathway negatively regulates microglia-mediated inflammation. Cell 145, 584-595 (2011).

60.   Pettersson, H., Lundqvist, J., Oliw, E. & Norlin, M. CYP7B1-mediated metabolism of 5alpha-androstane-3alpha,17beta-diol (3alpha-Adiol): a novel pathway for potential regulation of the cellular levels of androgens and neurosteroids. Biochimica et biophysica acta 1791, 1206-1215 (2009).

61.   Raices, M. & D'Angelo, M.A. Nuclear pore complex composition: a new regulator of tissue-specific and developmental functions. Nature reviews. Molecular cell biology 13, 687-699 (2012).

62.   Wente, S.R. & Rout, M.P. The nuclear pore complex and nuclear transport. Cold Spring Harbor perspectives in biology 2, a000562 (2010).

63.   Alber, F. et al. The molecular architecture of the nuclear pore complex. Nature 450, 695-701 (2007).

64.   D'Angelo, M.A. & Hetzer, M.W. Structure, dynamics and function of nuclear pore complexes. Trends in cell biology 18, 456-466 (2008).

65.   Rabut, G., Doye, V. & Ellenberg, J. Mapping the dynamic organization of the nuclear pore complex inside single living cells. Nature cell biology 6, 1114-1121 (2004).

66.   Talamas, J.A. & Capelson, M. Nuclear envelope and genome interactions in cell fate. Frontiers in genetics 6, 95 (2015).

67.   Weberruss, M. & Antonin, W. Perforating the nuclear boundary - how nuclear pore complexes assemble. Journal of cell science 129, 4439-4447 (2016).

68.   Capelson, M. & Hetzer, M.W. The role of nuclear pores in gene regulation, development and disease. EMBO reports 10, 697-705 (2009).

69.   Dauer, W.T. & Worman, H.J. The nuclear envelope as a signaling node in development and disease. Developmental cell 17, 626-638 (2009).

70.   Mekhail, K. & Moazed, D. The nuclear envelope in genome organization, expression and stability. Nature reviews. Molecular cell biology 11, 317-328 (2010).

71.   Casolari, J.M. et al. Genome-wide localization of the nuclear transport machinery couples transcriptional status and nuclear organization. Cell 117, 427-439 (2004).

72.   Taddei, A. et al. Nuclear pore association confers optimal expression levels for an inducible yeast gene. Nature 441, 774-778 (2006).

73.   Brown, C.R., Kennedy, C.J., Delmar, V.A., Forbes, D.J. & Silver, P.A. Global histone acetylation induces functional genomic reorganization at mammalian nuclear pore complexes. Genes & development 22, 627-639 (2008).

74.   Capelson, M. et al. Chromatin-bound nuclear pore components regulate gene expression in higher eukaryotes. Cell 140, 372-383 (2010).

75.   Kalverda, B., Pickersgill, H., Shloma, V.V. & Fornerod, M. Nucleoporins directly stimulate expression of developmental and cell-cycle genes inside the nucleoplasm. Cell 140, 360-371 (2010).

76.   Vaquerizas, J.M. et al. Nuclear pore proteins nup153 and megator define transcriptionally active regions in the Drosophila genome. PLoS genetics 6, e1000846 (2010).

77.   Ikegami, K. & Lieb, J.D. Integral nuclear pore proteins bind to Pol III-transcribed genes and are required for Pol III transcript processing in C. elegans. Molecular cell 51, 840-849 (2013).

78.   Liang, Y., Franks, T.M., Marchetto, M.C., Gage, F.H. & Hetzer, M.W. Dynamic association of NUP98 with the human genome. PLoS genetics 9, e1003308 (2013).

79.   Ptak, C., Aitchison, J.D. & Wozniak, R.W. The multifunctional nuclear pore complex: a platform for controlling gene expression. Current opinion in cell biology 28, 46-53 (2014).

80.   Sood, V. & Brickner, J.H. Nuclear pore interactions with the genome. Current opinion in genetics & development 25, 43-49 (2014).

81.   Woulfe, J.M. Abnormalities of the nucleus and nuclear inclusions in neurodegenerative disease: a work in progress. Neuropathology and applied neurobiology 33, 2-42 (2007).

82.   Gomez-Cavazos, J.S. & Hetzer, M.W. Outfits for different occasions: tissue-specific roles of Nuclear Envelope proteins. Current opinion in cell biology 24, 775-783 (2012).

83.   Hetzer, M.W., Walther, T.C. & Mattaj, I.W. Pushing the envelope: structure, function, and dynamics of the nuclear periphery. Annual review of cell and developmental biology 21, 347-380 (2005).

84.   Boehmer, T. & Schwartz, T.U. Purification, crystallization and preliminary X-ray analysis of a Nup107-Nup133 heterodimeric nucleoporin complex. Acta crystallographica. Section F, Structural biology and crystallization communications 63, 816-818 (2007).

85.   Harel, A. et al. Removal of a single pore subcomplex results in vertebrate nuclei devoid of nuclear pores. Molecular cell 11, 853-864 (2003).

86.   Orjalo, A.V. et al. The Nup107-160 nucleoporin complex is required for correct bipolar spindle assembly. Molecular biology of the cell 17, 3806-3818 (2006).

87.   Vasu, S. et al. Novel vertebrate nucleoporins Nup133 and Nup160 play a role in mRNA export. The Journal of cell biology 155, 339-354 (2001).

88.   Walther, T.C. et al. The conserved Nup107-160 complex is critical for nuclear pore complex assembly. Cell 113, 195-206 (2003).

89.   Zuccolo, M. et al. The human Nup107-160 nuclear pore subcomplex contributes to proper kinetochore functions. The EMBO journal 26, 1853-1864 (2007).

90.   Xu, L. & Massague, J. Nucleocytoplasmic shuttling of signal transducers. Nature reviews. Molecular cell biology 5, 209-219 (2004).

91.   Lupu, F., Alves, A., Anderson, K., Doye, V. & Lacy, E. Nuclear pore composition regulates neural stem/progenitor cell differentiation in the mouse embryo. Developmental cell 14, 831-842 (2008).

92.   Berke, I.C., Boehmer, T., Blobel, G. & Schwartz, T.U. Structural and functional analysis of Nup133 domains reveals modular building blocks of the nuclear pore complex. The Journal of cell biology 167, 591-597 (2004).

93.   Kouzarides, T. Chromatin modifications and their function. Cell 128, 693-705 (2007).

94.   Greber, U.F., Senior, A. & Gerace, L. A major glycoprotein of the nuclear pore complex is a membrane-spanning polypeptide with a large lumenal domain and a small cytoplasmic tail. The EMBO journal 9, 1495-1502 (1990).

95.   Wozniak, R.W., Bartnik, E. & Blobel, G. Primary structure analysis of an integral membrane glycoprotein of the nuclear pore. The Journal of cell biology 108, 2083-2092 (1989).

96.   Stavru, F., Nautrup-Pedersen, G., Cordes, V.C. & Gorlich, D. Nuclear pore complex assembly and maintenance in POM121- and gp210-deficient cells. The Journal of cell biology 173, 477-483 (2006).

97.   Doucet, C.M., Talamas, J.A. & Hetzer, M.W. Cell cycle-dependent differences in nuclear pore complex assembly in metazoa. Cell 141, 1030-1041 (2010).

98.   Bodoor, K. et al. Sequential recruitment of NPC proteins to the nuclear periphery at the end of mitosis. Journal of cell science 112 (Pt 13), 2253-2264 (1999).

99.   Olsson, M., Ekblom, M., Fecker, L., Kurkinen, M. & Ekblom, P. cDNA cloning and embryonic expression of mouse nuclear pore membrane glycoprotein 210 mRNA. Kidney international 56, 827-838 (1999).

100.   Olsson, M., Scheele, S. & Ekblom, P. Limited expression of nuclear pore membrane glycoprotein 210 in cell lines and tissues suggests cell-type specific nuclear pores in metazoans. Experimental cell research 292, 359-370 (2004).

101.   D'Angelo, M.A., Gomez-Cavazos, J.S., Mei, A., Lackner, D.H. & Hetzer, M.W. A change in nuclear pore complex composition regulates cell differentiation. Developmental cell 22, 446-458 (2012).

102.   Fan, F. et al. cDNA cloning and characterization of Npap60: a novel rat nuclear pore-associated protein with an unusual subcellular localization during male germ cell differentiation. Genomics 40, 444-453 (1997).

103.   Buchwalter, A.L., Liang, Y. & Hetzer, M.W. Nup50 is required for cell differentiation and exhibits transcription-dependent dynamics. Molecular biology of the cell 25, 2472-2484 (2014).

104.   Smitherman, M., Lee, K., Swanger, J., Kapur, R. & Clurman, B.E. Characterization and targeted disruption of murine Nup50, a p27(Kip1)-interacting component of the nuclear pore complex. Molecular and cellular biology 20, 5631-5642 (2000).

105.   Prokocimer, M. et al. Nuclear lamins: key regulators of nuclear structure and activities. Journal of cellular and molecular medicine 13, 1059-1085 (2009).

106.   Ho, C.Y. & Lammerding, J. Lamins at a glance. Journal of cell science 125, 2087-2093 (2012).

107.   Snider, N.T. & Omary, M.B. Post-translational modifications of intermediate filament proteins: mechanisms and functions. Nature reviews. Molecular cell biology 15, 163-177 (2014).

108.   Dittmer, T.A. & Misteli, T. The lamin protein family. Genome biology 12, 222 (2011).

109.   Rober, R.A., Weber, K. & Osborn, M. Differential timing of nuclear lamin A/C expression in the various organs of the mouse embryo and the young animal: a developmental study. Development 105, 365-378 (1989).

110.   Worman, H.J., Lazaridis, I. & Georgatos, S.D. Nuclear lamina heterogeneity in mammalian cells. Differential expression of the major lamins and variations in lamin B phosphorylation. The Journal of biological chemistry 263, 12135-12141 (1988).

111. Zuo, B. et al. Influences of lamin A levels on induction of pluripotent stem cells. Biology open 1, 1118-1127 (2012).

112. Guelen, L. et al. Domain organization of human chromosomes revealed by mapping of nuclear lamina interactions. Nature 453, 948-951 (2008).

113. Ikegami, K., Egelhofer, T.A., Strome, S. & Lieb, J.D. Caenorhabditis elegans chromosome arms are anchored to the nuclear membrane via discontinuous association with LEM-2. Genome biology 11, R120 (2010).

114. Peric-Hupkes, D. & van Steensel, B. Role of the nuclear lamina in genome organization and gene expression. Cold Spring Harbor symposia on quantitative biology 75, 517-524 (2010).

115. Peric-Hupkes, D. et al. Molecular maps of the reorganization of genome-nuclear lamina interactions during differentiation. Molecular cell 38, 603-613 (2010).

116. Broers, J.L. et al. Both lamin A and lamin C mutations cause lamina instability as well as loss of internal nuclear lamin organization. Experimental cell research 304, 582-592 (2005).

117. Kind, J. et al. Single-cell dynamics of genome-nuclear lamina interactions. Cell 153, 178-192 (2013).

118. Kind, J. & van Steensel, B. Stochastic genome-nuclear lamina interactions: modulating roles of Lamin A and BAF. Nucleus 5, 124-130 (2014).

119. Legartova, S. et al. Nuclear structures surrounding internal lamin invaginations. Journal of cellular biochemistry 115, 476-487 (2014).

120. Padeken, J. & Heun, P. Nucleolus and nuclear periphery: velcro for heterochromatin. Current opinion in cell biology 28, 54-60 (2014).

121. Constantinescu, D., Gray, H.L., Sammak, P.J., Schatten, G.P. & Csoka, A.B. Lamin A/C expression is a marker of mouse and human embryonic stem cell differentiation. Stem Cells 24, 177-185 (2006).

122. Eckersley-Maslin, M.A., Bergmann, J.H., Lazar, Z. & Spector, D.L. Lamin A/C is expressed in pluripotent mouse embryonic stem cells. Nucleus 4, 53-60 (2013).

123. Kim, Y. et al. Mouse B-type lamins are required for proper organogenesis but not by embryonic stem cells. Science 334, 1706-1710 (2011).

124. Amendola, M. & van Steensel, B. Mechanisms and dynamics of nuclear lamina-genome interactions. Current opinion in cell biology 28, 61-68 (2014).

125. Luperchio, T.R., Wong, X. & Reddy, K.L. Genome regulation at the peripheral zone: lamina associated domains in development and disease. Current opinion in genetics & development 25, 50-61 (2014).

126. Kohwi, M., Lupton, J.R., Lai, S.L., Miller, M.R. & Doe, C.Q. Developmentally regulated subnuclear genome reorganization restricts neural progenitor competence in Drosophila. Cell 152, 97-108 (2013).

127.   Le Bras, B. et al. Oligodendrocyte development in the embryonic brain: the contribution of the plp lineage. The International journal of developmental biology 49, 209-220 (2005).

128.   Sunny, D.E., Muzzio, D.O. & Heckmann, M. Method for generating highly pure culture of mouse derived Oligospheres under hypoxic conditions. Protocol Exchange doi:10.1038/protex.2015.092 (2015).

129.   Richter-Landsberg, C. & Heinrich, M. OLN-93: a new permanent oligodendroglia cell line derived from primary rat brain glial cultures. Journal of neuroscience research 45, 161-173 (1996).

130.   Grofer, B., Bodeker, R.H., Gortner, L. & Heckmann, M. Maturation of adrenal function determined by urinary glucocorticoid steroid excretion rates in preterm infants of more than 30 weeks of gestational age. Neonatology 98, 200-205 (2010).

131.   Heckmann, M., Wudy, S.A., Haack, D. & Pohlandt, F. Reference range for serum cortisol in well preterm infants. Archives of disease in childhood. Fetal and neonatal edition 81, F171-174 (1999).

132.   Papile, L.A., Burstein, J., Burstein, R. & Koffler, H. Incidence and evolution of subependymal and intraventricular hemorrhage: a study of infants with birth weights less than 1,500 gm. The Journal of pediatrics 92, 529-534 (1978).

133.   Heckmann, M. et al. Assessing cortisol production in preterm infants: do not dispose of the nappies. Pediatric research 57, 412-418 (2005).

134.   Klinger, G., Beyene, J., Shah, P. & Perlman, M. Do hyperoxaemia and hypocapnia add to the risk of brain injury after intrapartum asphyxia? Archives of disease in childhood. Fetal and neonatal edition 90, F49-52 (2005).

135.   Evans, M.J. & Scarpulla, R.C. NRF-1: a trans-activator of nuclear-encoded respiratory genes in animal cells. Genes & development 4, 1023-1034 (1990).

136.   Tiranti, V. et al. The gene (NFE2L1) for human NRF-1, an activator involved in nuclear-mitochondrial interactions, maps to 7q32. Genomics 27, 555-557 (1995).

137.   Akhtar, A. & Gasser, S.M. The nuclear envelope and transcriptional control. Nature reviews. Genetics 8, 507-517 (2007).

138.   Arib, G. & Akhtar, A. Multiple facets of nuclear periphery in gene expression control. Current opinion in cell biology 23, 346-353 (2011).

139.   Van de Vosse, D.W., Wan, Y., Wozniak, R.W. & Aitchison, J.D. Role of the nuclear envelope in genome organization and gene expression. Wiley interdisciplinary reviews. Systems biology and medicine 3, 147-166 (2011).

140.   Billiards, S.S. et al. Myelin abnormalities without oligodendrocyte loss in periventricular leukomalacia. Brain Pathol 18, 153-163 (2008).

141.   Volpe, J.J., Kinney, H.C., Jensen, F.E. & Rosenberg, P.A. The developing oligodendrocyte: key cellular target in brain injury in the premature infant. International journal of developmental neuroscience : the official journal of the International Society for Developmental Neuroscience 29, 423-440 (2011).

142.	Kuiper, G.G. et al. Comparison of the ligand binding specificity and transcript tissue distribution of estrogen receptors alpha and beta. Endocrinology 138, 863-870 (1997).

143.	Ivanova, M.M. et al. Estradiol and tamoxifen regulate NRF-1 and mitochondrial function in mouse mammary gland and uterus. Journal of molecular endocrinology 51, 233-246 (2013).

144.	Klinge, C.M. Estrogens regulate life and death in mitochondria. Journal of bioenergetics and biomembranes 49, 307-324 (2017).

145.	Papa, L. & Germain, D. Estrogen receptor mediates a distinct mitochondrial unfolded protein response. Journal of cell science 124, 1396-1402 (2011).

146.	Preciados, M., Yoo, C. & Roy, D. Estrogenic Endocrine Disrupting Chemicals Influencing NRF1 Regulated Gene Networks in the Development of Complex Human Brain Diseases. International journal of molecular sciences 17 (2016).

147.	Trotter, A. et al. Follow-up examination at the age of 15 months of extremely preterm infants after postnatal estradiol and progesterone replacement. The Journal of clinical endocrinology and metabolism 86, 601-603 (2001).

148.	Trotter, A., Maier, L. & Pohlandt, F. Management of the extremely preterm infant: is the replacement of estradiol and progesterone beneficial? Paediatric drugs 3, 629-637 (2001).

149.	Trotter, A. & Pohlandt, F. The replacement of oestradiol and progesterone in very premature infants. Annals of medicine 32, 608-614 (2000).

150.	Ballabh, P. Pathogenesis and prevention of intraventricular hemorrhage. Clinics in perinatology 41, 47-67 (2014).

151.	Lutzmann, M., Kunze, R., Buerer, A., Aebi, U. & Hurt, E. Modular self-assembly of a Y-shaped multiprotein complex from seven nucleoporins. The EMBO journal 21, 387-397 (2002).

152.	Silver, I. & Erecinska, M. Oxygen and ion concentrations in normoxic and hypoxic brain cells. Advances in experimental medicine and biology 454, 7-16 (1998).

153.	Stacpoole, S.R. et al. Derivation of neural precursor cells from human ES cells at 3% O(2) is efficient, enhances survival and presents no barrier to regional specification and functional differentiation. Cell death and differentiation 18, 1016-1023 (2011).

154.	Stacpoole, S.R. et al. Neural precursor cells cultured at physiologically relevant oxygen tensions have a survival advantage following transplantation. Stem cells translational medicine 2, 464-472 (2013).

155.	Rosova, I., Dao, M., Capoccia, B., Link, D. & Nolta, J.A. Hypoxic preconditioning results in increased motility and improved therapeutic potential of human mesenchymal stem cells. Stem Cells 26, 2173-2182 (2008).

156.	Studer, L. et al. Enhanced proliferation, survival, and dopaminergic differentiation of CNS precursors in lowered oxygen. The Journal of neuroscience : the official journal of the Society for Neuroscience 20, 7377-7383 (2000).

157. Cerghet, M. et al. Proliferation and death of oligodendrocytes and myelin proteins are differentially regulated in male and female rodents. The Journal of neuroscience : the official journal of the Society for Neuroscience 26, 1439-1447 (2006).

158. Kuiper, G.G. et al. Comparison of the ligand binding specificity and transcript tissue distribution of estrogen receptors alpha and beta. Endocrinology 138, 863-870 (1997).

159. Ivanova, M.M. et al. Estradiol and tamoxifen regulate NRF-1 and mitochondrial function in mouse mammary gland and uterus. Journal of molecular endocrinology 51, 233-246 (2013).

160. Klinge, C.M. Estrogens regulate life and death in mitochondria. Journal of bioenergetics and biomembranes 49, 307-324 (2017).

161. Papa, L. & Germain, D. Estrogen receptor mediates a distinct mitochondrial unfolded protein response. Journal of cell science 124, 1396-1402 (2011).

162. Preciados, M., Yoo, C. & Roy, D. Estrogenic Endocrine Disrupting Chemicals Influencing NRF1 Regulated Gene Networks in the Development of Complex Human Brain Diseases. International journal of molecular sciences 17 (2016).

163. Trotter, A. et al. Follow-up examination at the age of 15 months of extremely preterm infants after postnatal estradiol and progesterone replacement. The Journal of clinical endocrinology and metabolism 86, 601-603 (2001).

164. Trotter, A., Maier, L. & Pohlandt, F. Management of the extremely preterm infant: is the replacement of estradiol and progesterone beneficial? Paediatric drugs 3, 629-637 (2001).

165. Trotter, A. & Pohlandt, F. The replacement of oestradiol and progesterone in very premature infants. Annals of medicine 32, 608-614 (2000).

166. Midgley, P.C., Russell, K., Oates, N., Shaw, J.C. & Honour, J.W. Activity of the adrenal fetal zone in preterm infants continues to term. Endocrine research 22, 729-733 (1996).

9. APPENDICES

APPENDIX I – Preparation of media, buffers and other solutions.

Medium, Buffers und Solutions

Dissection buffer for OPC culture

5ml   Penicillin Streptomycin solution
1.5ml 45% Glucose solution
in 500ml sterile HBSS

Store at 4°C.

Neurosphere growth medium (100ml)

94.3ml	DMEM/F12 (with NaHCO3)
1.332ml	45% Glucose solution
500ul	1M HEPES
100ul	Progesterone (1000x stock)
1ml	Putrescine (100x stock)
2ml	B-27 supplement
100ul	ITSS
7.32ul	Heparin
20ul	EGF (100ug/ml)
5ul	FGF (100ug/ml)

Prepare sterile and store at 4°C.
Stable for 1 week.

Oligosphere medium (100ml)

69.2ml	DMEM/F12 (with NaHCO$_3$)
70ul	Progesterone (1000x stock)
700ul	Putrescine (100x stock)
70ul	ITSS
30ml	B104 Conditioned medium

Prepare sterile.
Sotre at 4°C. Stable for 1 week.

Trypan blue solution

7,5ml   0,4% Trypanblue solution
7,5ml   DPBS
Mix and centrifuge for 5min at 3000rpm.
Transfer supernatant to fresh tubes.
Aliquote and store at
RT.

B104 culture medium (200ml)

	180ml	DMEM/F12 (wo NaHCO$_3$)
45%	602ul	Glucose solution
	20ml	FCS

Store at 4°C for maximum 1 week.

N2 medium (200ml)

	198ml	DMEM/F12
100x	2ml	N2-supplement
45%	602ul	Glucose solution

Prepare fresh before use.

Hormone solutions

A stock solution of 0,1M or 0,01M was
prepared in DMSO
Note: 0,01M Adiol Stock solution prepared
in DMSO:EtOH 1:1 ratio.
Working solution: 100uM in DMSO
Aliquote and store at -20°C.
Note: Final conc. 100nM requires 1:1.000
dilutions in the medium.

FACS-Buffer

0,5%	2,5g	BSA
2mM	0,405g	EDTA

Dissolve in 500ml DPBS
pH-7,2
Filter and store at 4°C.

Propidium Iodide

0,05%   5mg   PI
Dissolve in 10ml DPBS
Store at 4°C.
Note: Light sensitive. Store protected from

light.

Hoechst

0,1%   10mg   Hoechst
in 10ml DMSO
Store at -20°C.

Poly-L-Lysin

0,01%   5mg   Poly-L-Lysin
in 50ml Aqua Ad Iniectabilia
Filter sterilize and store at -20°C.

4% PFA

40g   PFA
800ml   1x PBS
Warm to 60°C on a magnetic stirrer.
Add NaOH till the solution becomes clear.
pH-7,25
Filter, aliquote and store at -20°C or at 4°C
for maximum 2 days.

Blocking for IF

5%   500µl   NGS
0,3%   300µl   10% Triton
     9,2ml   1x PBS

Antibody dilution for IF

3%   300µl   NGS
0,3%   300µl   10% Triton
     9,4ml   1x PBS

2% Agarose gel

2g   Agarose
100ml   1x TAE-Puffer
Heat in a microwave till the agarose is
completely dissolved.
Cool upto 60°C and the add 5µl RedSafe
DNA dye.

Mix and immediately pour into the mould.
Allow it to set for at least 30 mins.

Running gel buffer

1,5M   45,41g   Tris
in 100ml ddH$_2$O
pH-8,8
Make up the volume to 250ml with ddH$_2$O
Store at 4°C.

Stacking gel buffer

1M   30,28g   Tris
in 100ml ddH$_2$O lösen
pH- 6,8
Make up the volume to 250ml with ddH2O
Store at 4°C.

Ponceau S staining buffer

0,2% (w/v)   Ponceau S
5% Glacial acetic acid
Store at RT.

10% SDS solution

10g   SDS
in 100ml ddH$_2$O
Store at RT.

12% Resolving gel for 10ml, 1.5mm thick gels

3,2ml   ddH$_2$O
2,6ml   Resolving gel buffer
0,1ml   10% SDS
4ml   Rotiphorese 30 Acrylamide solution
Mix on a magnetic stirrer.
100µl   10% APS
10µl   TEMED
Mix on magnetic stirrer and pour
immediately between the glass plates.
Cover with 2ml absolute Ethanol.
30-60min polymerisation time.

Stacking gel for 2 Gels 1.5mm thick

6,1ml   ddH$_2$O

2,6ml	Stacking gel buffer	
104μl	10% SDS	
1,3ml	Rotiphorese 30 Acrylamide solution	

Mix on a magnetic stirrer.

100μl	10% APS
20μl	TEMED

Mix on magnetic stirrer and pour immediately between the glass plates.
Insert the comb.
10-40min polymerization time.

Running buffer Gel electrophoresis

100ml	Rotiphorese 10x SDS Page
900ml	ddH$_2$O

Store at RT.

Transfer buffer Western Blot (1x)

3,028g	Tris (25mM)
14,411g	Glycine (192mM)
2,5ml (10% stock solution)	SDS (0.025%)
200ml	Methanol

mit ddH$_2$O auf 1l auffüllen
bei 4°C lagern

Blocking buffer for WB

3g	BSA
100ml	TBST (1x)

Filter and store at 4°C.

8% Resolving gel for 10ml, 1.5mm thick gels

4,6ml	ddH$_2$O
2,6ml	Resolving gel buffer
0,1ml	10% SDS
2,6ml	Rotiphorese 30 Acrylamide solution

Mix on a magnetic stirrer.

100μl	10% APS
10μl	TEMED

Mix on magnetic stirrer and pour immediately between the glass plates.
Cover with 2ml absolute Ethanol.
30-60min polymerisation time.

Stripping Buffer

15g	Glycin
1g	SDS
10ml	Tween 20

Dissolve in 800ml ddH$_2$O
Adjust the pH to 2.2

1x TBS + 0,3% Tween 20 (TBST)

997ml	1x TBS
3ml	Tween 20
bei RT lagern	

Make up the volume to 1L with ddH$_2$O and filter-
Store at 4°C.

OLN-93 Growth Medium

	443,75ml	DMEM (Biochrom)
10%	50ml	FCS
1%	5ml	P/S
0,05%	1,25ml	20% HSA

Prepare sterile. Can be stored at 4°C for maximum upto 2 weeks.

OLN-93 Treatment Medium

	46,875ml	DMEM (Biochrom)
5%	2,5ml	FCS

FACS Buffer

0,5%	2,5g	BSA
0,1%	0,5g	NaN$_3$

Dissolve in 500ml DPBS
Filter and store at 4°C.

1%	0,5ml	P/S
0,05%	0,125ml	20% HSA

Prepare sterile. Can be stored at 4°C for maximum upto 2 weeks.

APPENDIX II – List of primers and sequences.

Primer	Sequence (5'-> 3')	Working dilution
Gapdh_Mouse_F	GTGTTCCTACCCCCAATGTGT	5µmol/l
Gapdh_Mouse_R	ATTGTCATACCAGGAAATGAGCTT	5µmol/l
Hprt1_Mouse_F	CCTAAGATGAGCGCAAGTTGAA	5µmol/l
Hprt1_Mouse_R	CCACAGGACTAGAACACCTGCTAA	5µmol/l
Nup210_Mouse_F	GCCTCCTGTCACACTTCCTG	5µmol/l
Nup210_Mouse_R	TGAAAGCAGCCGGAGATGAG	5µmol/l
Nup50_Mouse_F	CAAAGCGCAGAAACGTTGGA	5µmol/l
Nup50_Mouse_R	GGGCTCTGCTGCTGTCTTTA	5µmol/l
Esr1_Mouse_F	ATTCTTCTCAAGCAGGTGGC	5µmol/l
Esr1_Mouse_R	CCCTCTCCATGGGCATCTTG	5µmol/l
Nup133_Mouse_F	GTTTCCGAGCGTCTCCTCTC	5µmol/l
Nup133_Mouse_R	CGAGTTAACCGCAGATCCCA	5µmol/l
Esr1_F_Ms_ChIP_A	**TCGGGTTGAGCACTTTTGGT**	**5µmol/l**
Esr1_R_Ms_ChIP_A	CTGTGTTCTTGCCGTCCTCA	5µmol/l
Esr1_F_Ms_ChIP_B	CTTACTGCCACGGAGAGAGC	5µmol/l
Esr1_R_Ms_ChIP_B	CCAAGTTAACAGAGCACCGC	5µmol/l
Sirt2_F_Ms_ChIP	GAGGGTGGTGAGGTAGGGAA	5µmol/l
Sirt2_R_Ms_ChIP	TGCTCCCAGTCCCCATACTA	5µmol/l
Lamb2_F_Ms_ChIP	ACTATGACCTGCTACTGCGCT	5µmol/l
Lamb2_R_Ms_ChIP	TTCCACACCCAGAATGTCAGC	5µmol/l
Mag_F_Ms_ChIP Female	TCCTCTGCTTGCTGGCATAC	5µmol/l
Mag_R_Ms_ChIP Female	TAGGGTGAAAGACCCCCAGG	5µmol/l
Mag_F_Ms_ChIP Male	TGACCCTGGCTGGAACACA	5µmol/l
Mag_R_Ms_ChIP Male	CAACCTGTCTGTGGAGTGTGA	5µmol/l
Cnp_F_Ms_ChIP Female_A	GGAGGGTGGTAGGTACCAAGA	5µmol/l
Cnp_R_Ms_ChIP Female_A	GCTTTGCCAGAGCAGGAGAT	5µmol/l
Olig1_F_Ms_ChIP	TGCGCGAAGTTATCCTACCC	5µmol/l
Olig1_R_Ms_ChIP	GCAATCTTGGAGAGCTTGCG	5µmol/l
Egr2_F_Ms_ChIP	CTCGTCGGTGACCATCTTCC	5µmol/l
Egr2_R_Ms_ChIP	GAAGACACGCGGCTTACCTC	5µmol/l

Hes5_F_Ms_ChIP	TAATCGCCTCCAGAGCTCCA	5μmol/l	
Hes5_R_Ms_ChIP	GCGAGTTGCACTTACTCGGT	5μmol/l	
Nrf1_F_Ms_ChIP	CTGCAGGTCCTGTGGGAAT	5μmol/l	
Nrf1_R_Ms_ChIP	CATCCAACGTGGCTCTGAGT	5μmol/l	
Nup133_Rat_F	GATGGCTGAGGCTGACGAC	5μmol/l	
Nup133_Rat_R	CAGTGCCACCAAATCAGCAC	5μmol/l	

APPENDIX III- List of chemicals and other materials.

1. Chemicals and Reagents

Name	Company	Catalog number	Country
100x TE-Puffer, pH 8	Merck Millipore	57493	Germany
10x TAE-Puffer	Carl Roth	T845.2	Germany
17β-Estradiol (E2)	Sigma-Aldrich	E2758	Germany
2-Propanol (Isopropanol)	Carl Roth	6752.1	Germany
3,3',5-Triiodo-L-Thyronin (T3)	Sigma-Aldrich	T6397	Germany
(3α,5α)-3-Hydroxy-pregnan-20-one (Allopregnanolone)	Tocris	3653	UK
5-Androsten-3β, 16α-diol-17-one (16-OH-DHEA)	Steraloids Inc.	A7900-000	USA
(±)-1-[(3aR*,4S*,9bS*)-4-(6-Bromo-1,3-benzodioxol-5-yl)-3a,4,5,9b-tetrahydro-3H-cyclopenta[c]quinolin-8-yl]- ethanon (G1)	Tocris	3577	UK
4,4',4''-(4-Propyl-[1H]-pyrazole-1,3,5-triyl)trsiphenol (PPT)	Tocris	1426	UK
2,3-bis(4-Hydroxyphenyl)-propionitrile (DPN)	Tocris	1494	UK
(±)-(3aR*,4S*,9bS*)-4-(6-Bromo-1,3-benzodioxol-5-yl)-3a,4,5,9b-tetrahydro-8-(1-methylethyl)-3H-cyclopenta[c]quinolin (G36)	Tocris	4759	UK
5-Androsten-3β, 17β-diol (Adiol)	Steraloids Inc.	A7830-000	USA
Acetic acid	Sigma-Aldrich	45731	Germany
Acrylan	Antiseptica chem. Pharm. Gmbh	ACR-1L	Germany
Ammoniumperoxodisulfat (APS)	Merck Millipore	1.01201	Germany
Aqua Ad Iniectabilia	Alleman Pharma	PZN:	Germany

		8771010	
B-27 Supplement (50x)	Life Technologies	12587-010	Germany
BAPTA AM	Tocris	2787	UK
Bovines Albumin, Fraktion V (BSA)	MP Biomedicals	810033	USA
Cell Tracker REd CMTPX	Life Technologies	C34552	Germany
Corning Matrigel Basement membrane matrix (GFR-phenol red free)	Corning	356231	USA
Chloroform	Merck Millipore	1.02445.250	Germany
Dehydroepiandrosteron (DHEA)	Sigma-Aldrich	D4000	Germany
DEPC-Wasser	Thermo Fisher	AM9906	Germany
Dimethylsulfoxid (DMSO)	Sigma-Aldrich	D5879	Germany
Disodiumhydrogen-phosphate (Na2HPO4)	Merck Millipore	1.06580.1000	Germany
dNTP Mix (je 10mM)	Thermo Fisher	R0192	Germany
Donor Horse Serum (Pferdeserum, DHS)	Merck Millipore	S9135	Germany
DMEM/F12 (1:1) Medium	Life Technologies	11330-032	Germany
Dulbecco's Phosphate-Buffered Saline (DPBS)	PAN Biotech	P04-36500	Germany
Ethanol (EtOH)	Th. Geier	2246.1000	Germany
Ethylenediaminetertaacetic-acid (EDTA)	Merck Millipore	8190400025	Germany
Fetal Bovine Serum (FBS)	Merck Millipore	S0615	Germany
Forskolin	Sigma-Aldrich	F6886	Germany
GlutaMax	Life Technologies	35050-038	Germany
Guanidinium-Hydrochloride	Sigma-Aldrich	G3272	Germany
Gylcine	Acros Organics	56-40-6	Belgium
Halt Protease & Phosphatase Single-use inhibitor cocktail (100x)	Thermo Fisher	78442	Germany
Hank's Balanced Salt Solution (HBSS) w Calcium and Magnesium	Life Technologies	14025-100	Germany
Heparin	Sigma-Aldrich	H3149	Germany
HEPES buffer (1M)	Sigma-Aldrich	H0887	Germany
Human Merosin Purified Protein	Merck Millipore	CC085	Germany
Hyaluronidase	Sigma-Aldrich	H3884	Germany
Hydrochloric acid (HCl)	Carl Roth	4625.1	Germany
ICI 182,780 (Fulvestrant, ICI)	Sigma-Aldrich	I4409	Germany
Insulin-Transferrin-Sodium-Selenite supplement	Roche	11074547001	Germany
Kynurenic acid	Sigma-Aldrich	K3375	Germany

Methanol	Mallinckrodt Baker	8402	Germany
M-PER Mammalian Protein Extraction Reagent	Thermo Fisher	78501	Germany
N2 Supplement (100x)	Life Technologies	17502-048	Germany
Normal Goat Serum (Ziegenserum, NGS)	Jackson ImmunoResearch	005-000-121	USA
NuPAGE® Sample Reducing Agent	Thermo Fischer	NP0004	Germany
NuPAGE® LDS Sample Buffer	Thermo Fischer	NP0007	Germany
O'Gene Ruler DNA-Leiter	Thermo Fisher	SM1203	Germany
Paraformaldehyd (PFA)	Sigma-Aldrich	158127	Germany
Penicillin-Streptomycin (10,000 U/mL) (P/S)	Life Technologies	15140122	Germany
Phenylmethylsulfonyl fluoride	Sigma-Aldrich	P7626	Germany
Pierce™ Protein-Free (TBS) Blocking Buffer	Thermo Fisher	37570	Germany
Platelet-Derived Growth Factor-AA (PDGF-AA)	Peprotech	100-13A	Germany
Poly-D,L-Ornithin Hydrobromid (Poly-Ornithin)	Sigma-Aldrich	P0421	Germany
PowerUp™ SYBR™ Green Master Mix	Thermo Fischer	A25742	Germany
Poly-L-Lysin Hydrobromid (PLL)	Sigma-Aldrich	P9155	Germany
Potasiumchloride (KCl)	Carl Roth	P017.2	Germany
Potasiumdihydrogen-phosphate (KH2PO4)	Carl Roth	P018.2	Germany
Propidiumiodide (PI)	Sigma-Aldrich	P4170	Germany
Progesterone	Sigma-Aldrich	P8783	Germany
Putrescine dihydrochloride	Sigma-Aldrich	P5780	Germany
Recombinant Rat Ciliary Neurotrophic Factor (CNTF)	PeproTech	450-50	Germany
Recombinant human NRG-1-beta-1	PeproTech	100-03	Germany
Recombinat human FGF-basic (bFGF)	PeproTech	100-18B	Germany
Recombinant Human EGF	PeproTech	AF-100-15	Germany
Recombinant Human Heregulinβ-1	PeproTech	100-03	Germany
RedSafe	Intron Biotechnology	21141	Korea
10x *SDS Page*	Carl Roth	3060.2	Germany
Rotiphorese 30 Acrylamidlösung	Carl Roth	3029.2	Germany
Sodium bicarbonate (NaHCO$_3$)	Sigma-Aldrich	S5761	Germany
Sodiumchloride (NaCl)	Carl Roth	3957.1	Germany
Sodiumdodecylsulfate (SDS)	Serva	151-21-3	Germany
Sodiumhydroxide (NaOH)	Sigma-Aldrich	71692	Germany

SuperSignal™ West Femto Maximum Sensitivity Substrate	Thermo Fischer	34095	Germany
Tetramethylethylenedi-amine (TEMED)	Carl Roth	2367.1	Germany
Tris(hydroxymethyl)-aminomethan (Tris)	Carl Roth	0188.2	Germany
Triton X-100	Sigma-Aldrich	T8787	Germany
TRIzol Reagent	Life Technologies	15596-026	Germany
Trypanblue 0,4%	Sigma-Aldrich	93595	Germany
TrypLE Express	Life Technologies	12604-021	Germany
Trypsin	Sigma-Aldrich	T5266	Germany
Trypsin Inhibitor from Glycine max	Sigma-Aldrich	T6522	Germany
Tween 20	Sigma-Aldrich	P137-9	Germany
Vectashield Mounting Medium with Dapi	Vector Laboratories	H-1500	UK
β-Mercaptoethanol (β-ME)	Sigma-Aldrich	M-6250	Germany

2. Kits

Name	Company	Catalog-number	Country
MAGnify Chromation Immunoprecipitation System	Life Technologies	49-2024	Germany
High Pure RNA Isolation Kit	Roche	11828665001	Germany
CellEvent Caspase-3/7 Green Flow Cytometry Assay Kit	Life Technologies	C10427	Germany
QuantiTect Reverse Transcription Kit	QIAGEN	205313	Germany
RNeasy Plus Mini Kit	QIAGEN	74134	Germany
Pierce Classic Magnetic IP/Co-IP Kit	Thermo Fischer Scientific	88804	Germany
Pierce Direct Magnetic IP/Co-IP Kit	Thermo Fischer Scientific	88828	Germany
Nuclear Extraction Kit	Abcam	ab113474	UK
Cell Proliferation ELISA, BrdU	Roche	11647229001	Germany
ER Stress-induced Autophagy Antibody Sampler Kit	Cell Signaling Technology	89947	USA

Actin Nucleation and Polymerization Antibody Sampler Kit	Cell Signaling Technology	8606	USA
Rho-GTPase Antibody Sampler Kit	Cell Signaling Technology	9968	USA
Cofilin Activation Antibody Sampler Kit	Cell Signaling Technology	8354	USA
PDGF Receptor Activation Antibody Sampler Kit	Cell Signaling Technology	12651	USA
CytoSelect 96-Well Cell Invasion Assay	Cell Biolabs	CBA-112	USA
Ion PGM™ Hi-Q™ View OT2 Kit	Thermo Fischer Scientific	A29900	Germany
Ion 316™ Chip Kit v2 BC	Thermo Fischer Scientific	4488145	Germany
Ion PGM™ Hi-Q™ View Sequencing Kit	Thermo Fischer Scientific	A30044	Germany
QIAamp DNA Kit Mini	QIAGEN	51304	Germany

3. Other materials

Name	Company	Catalog-number	Country
0,22μm Syringe-filter	Carl Roth	P666.1	Germany
15ml tubes, PP 17x120mm	Sarstedt	62554502	Germany
50ml tubes, PP 30x115mm	BD Bioscience	352070	Germany
40μm Cell strainer	BD Bioscience	352340	Germany
60x15mm Petridishes	Sarstedt	83.3901	Germany
0.22μm Vaccum Filter	Sarstedt	83.1822.001	Germany
8-well on PCA detachable	Sarstedt	94.6140.802	Germany
μ-slide 8-well	ibidi	80826/80821	Germany
Amersham Protran 0.45μm NC Western Blotting Membrane	GE Healthcare	10600012	Germany
Cell culture plates (6-well; 24-well; 96-well), cell+ for adherent cultures	Sarstedt	83.XXXX.300	Germany
Cell scraper	Greiner BioOne	541070	Germany
Coverslip round, 12mm	Carl Roth	P231.1	Germany
Coverslip 24x60mm	Carl Roth	H878	Germany
Criterion blotter Filter paper	Bio-Rad Laboratories	1704085	Germany

Eppendorf tubes (0,5ml; 1,5ml; 2ml und 5ml)	Eppendorf	0030.119.401	Germany
FACS-tubes	Falcon, Corning	352008	Germany
Glaspasteurpipette	John Poulten	D812	UK
Glass slides	R. Langenbrinck	03-0040	Germany
MicroAmp Fast 96-well Reaction plate (0.1ml)	Thermo Fischer	4346907	Germany
Optical Adhesive covers	Thermo Fischer	4360954	Germany
Petridishes, cell+ for adherent cultures	Sarstedt	82.1473	Germany
Pipette tips	Eppendorf	0030.000.XXX	Germany
Pipette tips with Filter	Biozym	VT0210/VT0260	Germany
PVDF-Membrane	Bio-Rad Laboratories	162-0177	Germany
Quali-PCR-Tube-Streifen	Kisker Biotech	G003-SF	Germany
Scalpel blade No.10	Feather	0201500010	Japan
Syringe (10ml)	BD Bioscience	309110	Germany
T75- cell culture flasks, Red cap	Sarstedt	83.1813.002	Germany
Stericup-GP, 0,22 µm, Polyethersulfon, 250 ml Filter	Merck Millipore	SCGPU02RE	Germany
T-75 cell culture flasks, Green cap (suspension culture)	Sarstedt	83.3911.502	Germany

4. Softwares

Name	Company	Country
Ingenuity Pathway Analysis	Qiagen	Germany
ChemSketch	Advanced Chemistry Development (ACD/Labs)	Canada
Endnote	Thomson Reuters	USA
FACSDIVA	BD Bioscience	Germany
FlowJo	FlowJo	USA
Graphpad Prism 5	GraphPad Software	USA
ImageLab	Bio-Rad Laboratories	Germany
LAS AF	Leica	Germany
Microsoft Office	Microsoft Corporation	USA
ImageJ	National Institutes of Health	USA
STRING (Version 10.5)	Swiss Institute of Bioinformatics	EU

PANTHER (Version 13.0)	University of Southern California	USA	
UCSF Chimera (1.10.2)	California University	USA	
Maestro 10.4	Schroedinger	Germany	
UCSC Genome Viewer	California University	USA	
Integrative Genomics Viewer	University of California	USA	
StepOne Software (Version 2.0.2)	Thermo Fischer Scientific	Germany	

APPENDIX IV- List of antibodies.

Antibodies

Name	Company	Catalog number	Country
Anti-A2B5-APC mAb conjugate (Clone- 105-HB29)	Miltenyi Biotec	130-093-582	Germany
Anti-Caspase 3 (Rabbit polyclonal)	Abcam	ab13847	UK
Anti-Estrogen Receptor alpha (Mouse monolclonal- TE111.5D11)	Thermo Fischer Scientific	MA5-13065	Germany
Anti-Fas Ligand (Rabbit polyclonal)	Abcam	ab15285	UK
Anti-Nucleoporin p62 (E-4) Mouse mAb	Santa Cruz Biotechnology	Sc-48389	Germany
Anti-rabbit IgG, HRP-linked Antibody	Cell Signaling Technology	7074P2	USA
Anti-Rabbit NUP133 Polyclonal	Proteintech	12405-1-AP	UK
Goat Anti-Mouse IgG (H+L) Alexa Fluor 488 Conjugate	Life Technologies	A-11029	Germany
Goat Anti-Mouse IgG (H+L) Alexa Fluor 594 Conjugate	Life Technologies	A-11005	Germany
Goat Anti-Rabbit IgG (H+L) Alexa Fluor 594 Conjugate`	Life Technologies	A-11012	Germany
Mouse Anti-CNPase (Clone 11-5B)	Abcam	ab6319	UK
Mouse Anti-Estrogen receptor alpha (33) mAb	Thermo Fischer Scientific	MA1-310	Germany
Mouse IgM-APC Isotype control antibody	Miltenyi Biotec	130-099-085	Germany
PE Anti-Mouse CD140a (Clone- APA5)	Biolegend	135906	USA
PE Rat IgG2a, k Isotype Ctrl (Clone- RTK2758)	Biolegend	400508	USA

Peroxidase AffiniPure F(ab')2 Fragment Goat Anti-Mouse IgG (H+L)	Jackson ImmunoResearch	115-036-146	USA
Rabbit Anti-ATG7 mAb (D12B11)	Cell Signaling Technology	8558	USA
Rabbit Anti-Estrogen receptor beta polyclonal	Thermo Fischer Scientific	PA1-311	Germany
Rabbit Anti-GAPDH (D16H11) mAb	Cell Signaling Technology	5174	USA
Rabbit Anti-GPER/GPR30	Abcam	ab39742	UK
Rabbit Anti-Lamin B1 mAb (D9V6H)	Cell Signaling Technology	13435	USA
Rabbit Anti-LC3B polyclonal	Cell Signaling Technology	2775	USA
Rabbit Anti-MAG mAb (D4G3)	Cell Signaling Technology	9043	USA
Rabbit Anti-NCOA5 polyclonal	Novus Biologicals	NB100-2571	USA
Rabbit Anti-NUP133 mAb (EPR10809)	Abcam	ab181355	UK
Rabbit Anti-NUP50 polyclonal	Novus Biologicals	NB100-93324	USA

10. ACKNOWLEDGEMENT

Last but not the least; I thank God, my almighty Father for guiding me throughout, giving me the courage, motivation and endurance to accomplish my goal.

Eidesstattliche Erklärung

Hiermit erkläre ich, dass ich die vorliegende Dissertation selbständig verfasst und keine anderen als die angegebenen Hilfsmittel benutzt habe.

Die Dissertation ist bisher keiner anderen Fakultät, keiner anderen wissenschaftlichen Einrichtung vorgelegt worden.

Ich erkläre, dass ich bisher kein Promotionsverfahren erfolglos beendet habe und dass eine Aberkennung eines bereits erworbenen Doktorgrades nicht vorliegt.

Greifswald, 8.4.2020

(Ort, Datum)

(Donna Elizabeth Sunny)